UNIVERSITY OF CALIFORNIA, SAN DIEGO

Extreme DNA Content Variation in the Mammalian Central Nervous System

A dissertation submitted in partial satisfaction of the requirements for the degree Doctor of Philosophy

in

Biomedical Sciences

by

Diane M. Bushman

Committee in charge:

Professor Jerold Chun, Chair
Professor Joan Heller-Brown, Co-chair
Professor Don Cleveland
Professor Edward Koo
Professor Kun Zhang

2013

The Dissertation of Diane M. Bushman is approved, and it is acceptable in quality and form for publication on microfilm and electronically:

Co-chair

Chair

University of California, San Diego

2013

DEDICATION

To chromosomes and cocktails, late nights and laughter, and friends with whom to share all the frustrations and delights that life has in store; to the thrilling intensity of truly engaging the mind, and the spark of pleasure from sharing hard-earned knowledge with the world; to striving for success in the face of failure; and to my family, for their loving support through it all.

EPIGRAPH

We are all walking repositories of neuronal genomic diversity.

-Tom Curran,
The Scientist

TABLE OF CONTENTS

LIST OF ABBREVIATIONS

AD	Alzheimer's disease
ANOVA	Analysis of variance
APP	Amyloid precursor protein
Aβ	Amyloid beta
bFGF	Basic fibroblast growth factor
$CaCl_2$	Calcium chloride
CBL	Cerebellum
CCL18	Chemokine (C-C motif) ligand 18
CDK1	Cyclin-dependent kinase 1
CEN	Chicken erythrocyte nuclei
CGH	Comparative genomic hybridization
CI	Confidence interval
CNS	Central nervous system
CNV	Copy number variation
CO_2	Carbon dioxide
Ct	Crossing threshold
CTX	Cortex
CV	Coefficient of variation
DAPI	4',6-diamidino-2-phenylindole
DCV	DNA content variation
DI	DNA index
DNA	Deoxyribonucleic acid
DS	Down syndrome
E	Embryonic
EGTA	Ethylene glycol tetraacetic acid
FACS	Fluorescence activated cell sorting
FASD	Fetal alcohol spectrum disorders
FCM	Flow cytometry
FCTX	Frontal cortex
FISH	Fluorescence *in situ* hybridization
FSC	Forward Scatter
gDNA	Genomic DNA
GFP	Green fluorescent protein
H_2O	Water

H_2O_2	Hydrogen peroxide
HCl	Hydrochloric acid
hESC	Human embryonic stem cell
ICS-MCB	Interphase chromosome-specific multicolor banding
IFC	Integrated fluidic circuitry
iPSC	Induced pluripotent stem cell
LYM	Lymphocyte
MAP	Microtubule associated protein
Mb	Megabases
MDA	Multiple displacement amplification
MDMA	Methylenedioxymethamphetamine
MGB	Major groove binding
$MgCl_2$	Magnesium chloride
MOMPs	Mitochondril outer membrane proteins
MVA	Mosaic variegated aneuploidy
ND	Non-diseased
NeuN	Neuronal nuclear marker
NHEJ	Non-homologous end joining
NP-40	Nonidet P 40
NPC	Neural progenitor cell
PBS	Phosphate buffered saline
PBSE	Phosphate buffered saline containing 2mM ethylene glycol tetraacetic acid
PCD	Programmed cell death
PCDH11X	Protocadherin 11 X linked
PI	Propidium iodide
PMI	Postmortem interval
PSEN1	Presenilin 1
PSEN2	Presenilin 2
qPCR	Quantitative polymerase chain reaction
RCN	Relative copy number
ROS	Reactive oxygen species
$\mathbf{S}\bar{x}$	Standard error of the mean
SEM	Standard error of the mean
SEMA4A	Semaphorin 4A
SKY	Spectral karyotyping

SSC	Side Scatter
SSC	Saline-sodium citrate buffer
zVAD-fmk	N-Benzyloxycarbonyl-Val-Ala-Asp(O-Me) fluoromethylketone

LIST OF FIGURES

LIST OF TABLES

ACKNOWLEDGEMENTS

I would like to thank Professor Jerold Chun for his enthusiasm and drive in my thesis project – admirably, you are always overflowing with new ideas, and encouraging me to expand on mine. I would also like to thank the entire Chun lab, past and present, for their support and guidance in navigating the tough aspects of successful research. I would especially like to thank Alycia Mosely Austin, my aneuploidy sister, who led the way with poise and dedication; Keira Herr, for making sure science and fun were mixed in just the right ratio; Hope Mirendil, for our challenging lunch-time conversations; Rich Rivera for the extent of his scienctific knowledge and his willingness to lend a hand to any problem; and Danielle Jones for her support in all things, administrative and otherwise, and her wonderful sense of humor.

Thank you to my committee members, Professors Joan Heller-Brown, Don Cleveland, Kun Zhang, and Eddie Koo, for their suggestions and guidance on this dissertation work – your suggestions, offered from such different areas of scientific expertise, were invaluable for developing and expanding the scope of these projects.

I would like to thank Professors Deborah Lycan and Gary Reiness at Lewis and Clark College for helping me as a young scientist to develop the critical thinking skills necessary for good scientific enquiry, and for their continuing support of my professional scientific career.

I would like to thank the following agencies that have provided my funding: the NIH Pharmacology Training grant and the NIDA Neuroscience of Drugs of Abuse Training grant.

Finally, I extend my deepest thanks to the passel of folks who have stood beside me, cheering me on without fail, especially: the Bushman clan – Robert, Linda, Charles, Karen, Helen, and Robert Langendoerfer; my best friend, Benjamin Z. Connealy; the Faces – Julie Bemski, Jenn Smith, Matty Shepard, Gale Orcutt, Tessa Dardani and Arianna Trott; and Erilynn Heinrichsen, Rebecca Jimenez, Emily Witham, Bethany Sotak, Margaret Butko, Ariana Lorenzana, Julianne McCall and Kevin West.

The Introduction section, in part, is currently in press as an invited review: **Bushman, D.M**. & J. Chun. *The genomically mosaic brain: aneuploidy and more in neural diversity and disease*. Seminars in Cell and Developmental Biology. The dissertation author was the primary author of this material under the supervision of Dr. Jerold Chun.

Chapter 1, in full, is currently being prepared for submission for publication of this material. The dissertation author was the primary investigator and author of this material. Willem Westra and Yun C. Yung assisted with the design of the project, performed flow cytometric data collection and analysis, and FISH analyses. Jerold Chun supervised the project and provided advice.

Chapter 2, in full, is a reprint of the material as it appearsin the Journal of Neuroscience. Peterson, S.E.*, Yang, A.H.*, **Bushman, D.M.** *, Westra, J.W., Yung, Y.C., Barral, S., Mutoh, T., Rehen, S.K. & J. Chun. *Aneuploid cells are differentially susceptible to caspase-mediated death during embryonic cerebral cortical development*. Journal of Neuroscience. 2012 Nov 14; 32 (46): 16213-22. The dissertation author was a co-primary author of this material.

Chapter 3, in full, is currently being prepared for submission for publication of this material. The dissertation author was the primary investigator and author of this material. Hope Mirendil assisted with the design of the project, performed animal injections and tissue isolation, and assisted with metaphase chromosome spread counts and deconvolution microscopy sample preparation. Sidney Perez assisted with metaphase chromosome spread quantitation and deconvolution microscopy sample preparation, and performed all lagging chromosome data collection. Claudia Martinez assisted with metaphase chromosome spread quantitation. Jerold Chun supervised the project and provided advice.

VITA

2006 Bachelor of Arts, Lewis and Clark College

2013 Doctor of Philosophy, University of California, San Diego

PUBLICATIONS

Bushman, D.M., Westra, J.W. & J. Chun. Somatic genomic mosaicism via increased DNA content and APP locus amplification in single Alzheimer's disease neurons. (In preparation)

Bushman, D.M., Mirendil, H.E., Perez, S.O. & J. Chun. *Alterations in neural aneuploidy by drugs of abuse during fetal brain development*. (In preparation)

Bushman, D.M. & J. Chun. *The genomically mosaic brain: aneuploidy and more in neural diversity and disease*. Seminars in Cell and Developmental Biology. (In press)

Peterson, S.E.*, Yang, A.H.*, **Bushman, D.M.** *, Westra, J.W., Yung, Y.C., Barral, S., Mutoh, T., Rehen, S.K. & J. Chun. *Aneuploid cells are differentially susceptible to caspase-mediated death during embryonic cerebral cortical development*. Journal of Neuroscience. 2012 Nov 14; 32 (46): 16213-22. (* co-first author)

Peterson, S.E., Westra, J.W., Rehen, S.K., Young, H., **Bushman, D.M.**, Paczkowski, C.M., Yung, Y.C., Lynch, C.L., Tran, H.T., Nickey, K.S., Wang, Y., Laurent, L.C., Loring, J.F., Carpenter, M.K. & J. Chun. *Normal human pluripotent stem cell lines exhibit pervasive mosaic aneuploidy*. PLoS One. 2011; 6 (8): e23018. Epub 2011 Aug 16.

Chun, J., Westra, J.W., **Bushman, D.M.** *A reply to Iourov I, et al.* Neurodegenerative Disease. 2011 8, 38-40.

Westra, J.W., Rivera, R.R., **Bushman, D.M**., Yung, Y.C., Peterson, S.E., Barral, S. & J. Chun. *Neuronal DNA content variation (DCV) with regional and individual differences in the human brain*. Journal of Comparative Neurology. 2010 Oct 1; 518 (19): 3981-4000.

Martin, S.L., **Bushman, D.M.**, Wang, F., Li, P.W., Walker, A., Cummiskey, J., Branciforte, D. & M.C. Williams. *A single amino acid substitution in ORF1 dramatically decreases L1 retrotransposition and provides insight into nucleic acid chaperone activity*. Nucleic Acids Research. 2008 Oct; 36 (18): 5845-54. Epub 2008 Sept 12.

ABSTRACT OF THE DISSERTATION

Extreme DNA Content Variation in the Mammalian Central Nervous System

by

Diane M. Bushman

Doctor of Philosophy in Biomedical Sciences

University of California, San Diego, 2013

Professor Jerold Chun, Co-Chair

Professor Joan Heller-Brown, Co-chair

Genomically identical cells have long been assumed to comprise the human brain, with post-genomic mechanisms giving rise to its enormous diversity, complexity, and disease susceptibility. However, the identification of neural cells containing somatically generated mosaic aneuploidy – loss and/or gain of chromosomes from a euploid complement – and other genomic variations including LINE1 retrotransposons and regional patterns of DNA content variation (DCV), demonstrate that the brain is genomically heterogeneous. The effects of constitutive aberrations, as observed in Down syndrome, implicate roles for defined mosaic genomes relevant to cellular survival, differentiation potential, stem cell biology, brain organization, and neuropathological processes. Analyses of genomic mosaicism in sporadic Alzheimer's disease (AD) provide evidence for potential functional mosaic changes, as dramatic genomic alterations in the AD frontal cortex manifested via a significant increase in DCV. The resulting somatic locus-specific amplification of amyloid precursor protein supports mosaicism as a factor in AD pathogenesis,

while microfluidic quantitative (q)PCR analyses of single cortical AD neurons reveal the variability of somatic changes that occur within the brain of a single individual. Given the range of genomic variation that has been observed, understanding of the precise phenotypes and functions produced by genomic mosaicism in either diseased or normal brains is limited. However, the ablation of programmed cell death leading to increased observance of extreme karyotypes in cortical neural progenitor cells supports the functional non-equivalence of varied mosaic forms, as extremely aneuploid cells are targeted for elimination while cells with mild aneuploidies survive. Induction of increased neural mosaic aneuploidy through fetal exposure to substances of abuse demonstrates the fragility of the individual cellular genome and the vulnerability of the brain to induced mosaicism with pathogenic potential, highlighting the consequences of compromised somatic genomic integrity.

INTRODUCTION

Aneuploidy is a gain (hyperploidy) or loss (hypoploidy) of chromosomes such that the resulting chromosome number is not an exact multiple of the haploid complement. A related term, aneusomy, reflects specific chromosome gains (hypersomy) or loss (hyposomy) in a cell, although the full karyotype for that cell may be unknown relative to the germline chromosomal complement. Aneuploidies and aneusomies within an organism can be defined as either *constitutive*, meaning that changes begin in the germline or early embryogenesis, resulting in a conserved change in virtually all cells of an organism; or *mosaic*, which indicates somatic changes in individual cells that result in mixed aneuploid and euploid forms with varied prevalence throughout an organism. There are several well-known pathophysiological chromosomal disorders including Down (trisomy 21), Edwards (trisomy 18), and Patau (trisomy 13) syndromes, which are most commonly constitutive in >95% of cases [1-5], along with sex chromosome aneuploidies like Klinefelter's (XXY) and Turner's (monosomy of X) syndromes that also result in abnormal development and behavior [6-10]. Mosaic disorders affecting the brain have also been described, such as mosaic variegated aneuploidy (MVA) [11-15].

While such chromosomal aberrations have been long associated with neurogenetic disorders, chromosomal aneuploidies or aneusomies are also known to be a normal feature of the brain, manifesting as complex mosaics [16-28]. In the central nervous system (CNS), mosaic aneuploidies were first identified in the cerebral cortex of normal developing mice [23], a result that has been extended throughout the neuraxis and to all vertebrate species thus far examined [21, 22, 25], including non-diseased humans [19, 24, 25, 27, 28]. Moreover, these changes have been a harbinger for other genomic alterations, generally referred to as DNA content variation (DCV) [29] 2010).

Genomic diversity in cells of the normal brain: Mosaic aneuploidy and DNA content variation (DCV)

1. Detection techniques

As early as 1902, Theodor Boveri identified chromosome aberrations in cancerous tumors, demonstrating the existence of living, aneuploid cells [30]. The simplest evaluations of chromosome numbers merely count chromosomes in metaphase spreads, when the condensed state of the chromatids allows for visualization, as well as identification of balanced and unbalanced translocations by Giemsa staining [31]. Despite the simplicity of this assay, it is notable that the correct human complement of chromosomes was not established until 1956 [32], some three years after report of the double helix [33], underscoring ambiguities that are associated with chromosome counts. A definitive modern technique called spectral karyotyping, or SKY, relies on the hybridization of genomic fragments labeled with distinct fluorochromes to the metaphase spreads of single cells and the subsequent identification of each chromosome pair or sex chromosomes [34]. These strategies require condensed chromosomes, and as such cannot be definitively used on interphase or non-mitotic cells. Fluorescent *in situ* hybridization (FISH) also employs hybridization of a probe against a defined but limited chromosomal region ("point probes"), which can be used to assess aneusomies in single interphase cells using a fluorescent or enzymatic readout. Multicolor FISH allows for simultaneous evaluation of several chromosomes or different regions along a single chromosome, including quantification of FISH signal intensity [35]. However, there are technical limitations that can lead to false-positive and false-negative probe hybridization, which require careful controls to identify true aneuploidy versus artifactual hybridization, such as pairing of chromosome homologs that may lead to the incorrect interpretation of a "pseudo monosomy" [27]. A modification of point probe FISH is interphase chromosome-specific multicolor banding (ICS-MCB) wherein a set of specific paints derived from microdissected chromosomes labels the target chromosome with a distinct spectral pattern for the simultaneous visualization of several regions of the chromosome [36, 37]. This technique has not been widely used and may depend on the cell type and/or age of the

interrogated chromatin. An independent technique for chromosomal copy number analysis is comparative genomic hybridization (CGH) and array CGH [38, 39]. CGH requires the hybridization of test genomic samples to a representation of a standardized genome, and allows for copy number analyses from tissue samples or prenatal cytogenetic samples. Previously, the requirement of a relatively large, genomically homogenous set of cells limited the use of CGH in identifying mosaic aneuploidy. While Ballif and colleagues reported the detection of mosaicism even at levels of 10-20% [40], its effectiveness in CNS samples remains to be determined.

Single cell approaches that are currently in development will help to lower the detection threshold. The genome from single cells isolated by laser microdissection, flow cytometry, or other techniques could be amplified in a uniform and unbiased manner (*e.g.*, using multiple displacement amplification (MDA) [41]) for analysis by single-cell CGH or quantitative PCR for target genomic regions. Even more definitively, the resulting amplicons from single-cell MDA could serve as a template for genomic sequencing, an approach being pursued for cancer cells [42, 43], as well as partial sequencing from neurons [44]. The promise of these techniques is currently tempered by a range of factors including use of adequate control genomes, the current low throughput of the technique that is critical in view of the one trillion cells that make up the human brain, and sufficient information storage limitations for the terabytes of data produced by whole-genome sequencing.

A distinct approach to assessing genomic uniformity is DNA flow cytometry that has a long history of identifying cells with varying DNA content associated with phases of the cell cycle [45, 46]. The highly integrated and physically connected nature of the brain (*e.g.*, its synaptic neuropil) makes analyses of single cells difficult and incomplete, thus limiting prior flow cytometry efforts for studying the brain. Modifications of this approach to interrogate isolated nuclei rather than intact cells from the brain for DNA content has identified brain cell populations with a surprising range of DNA content. This was manifested as an overall increase in DNA content within cerebral cortical neurons compared to cerebellar neurons from the same individual, demonstrating the pervasive existence of normal human brain cells having DNA content variation

(DCV) [29]. DCV in the frontal cortex averages a gain of 250Mb, with NeuN-positive neurons showing significant increases compared to non-neuronal nuclei. Importantly, DCV appears to encompass myriad forms of mosaic aneuploidy that exist in both the cerebral cortex and cerebellum [24, 25, 27, 28]. By contrast, DCV also appears to be distinct from aneuploidy because of the expanded DNA content histograms in the cerebral cortex that are less prominent in the cerebellum, suggesting an independent mechanism for increased DNA content.

These technical approaches, along with others in development, have allowed assessments of single brain cells, demonstrating genomic mosaicism amongst cells of the brain – and likely other tissues and cells, including stem cell lines [47, 48] – thus redefining the genomic organization of the brain from homogenously uniform to a complex genomic mosaic. These data underscore a need to consider individual genomes in cellular function in the normal and diseased brain, as well as the effects of identified genes operating in varied genomic surroundings.

2. Mosaic aneuploidy in the non-diseased brain

The first report of widespread genomic mosaicism came from studies of aneuploidy in mice, which revealed that approximately 33% of proliferating cerebral cortical neural progenitor cells (NPCs), isolated from the ventricular zone of the embryonic brain [23], were aneuploid. A range of other neurogenic regions generate aneuploid cells, including cerebellar NPCs that represent ~15% of mitotic cells at postnatal day (P) P0 and ~21% at P7 [17, 25]. This somatically derived form of genomic variation is characterized by the apparently stochastic loss or gain of all chromosomes, creating a genomic mosaic that displays a predominance of hypoploidy over hyperploidy [23]. During periods of cell division, mosaic aneuploidy in NPCs results from chromosomal segregation defects (lagging chromosomes, non-disjunction and supernumerary centrosomes) during mitosis [26, 49]. Some mosaically aneuploid cells remain capable of differentiating into neuronal and glial lineages [17], and can survive into the adult brain [23], where they can be integrated into active neural circuitry [18]. In the mosaic landscape of the CNS, the genomic diversity of aneuploid cells, and the subsequent differences in gene expression

profiles [17, 50-52] suggest that a great deal of cellular variability and diversity exists without negatively impacting the high functionality of the system.

In the human CNS, the same trends have been reported: the genomic variation caused by aneuploidy in the developing brain reaches 30-35%, while most other tissues display low, albeit detectable, levels of aneuploidy [20, 28]. While the total amount of aneuploidy in the mature human brain remains unknown, reflecting both the size of the brain and the limitations of current evaluation techniques, several studies provide evidence that a significant population of aneuploid cells is also present in the adult human brain. Rehen and colleagues tracked chromosome 21 in neurons and non-neuronal cells from the frontal cortex and hippocampus of non-diseased human brains (aged 2 through 86), using dual-locus hybridization that combined a chromosome paint with a FISH point probe for increased specificity, reporting a rate of ~4% aneusomy for chr 21, with monosomy more frequent than trisomy [24]. Several subsequent studies have attempted to give a more complete analysis of the aneuploidy rate in non-diseased adult human brains by analyzing several chromosomes, including 21, using mixes of multiple enumeration probes or ICS-MCB. These studies reported lower frequencies of aneuploidy (0.1-0.8% on average) for an estimated total aneuploidy level of 10% [16, 53, 54]. It is critical to note that all of these studies suffer from: 1) an inability to objectively identify trisomy – subjectivity is inherent in scoring ambiguous hybridization patterns; 2) an inability to precisely compare the same cell types and brain regions between different individuals; and 3) severe limitations of sample size, as interrogation of even 10,000 cells represents less than 0.000001% of the more than 1 trillion cells in the human brain. The differences in total observed aneuploidy levels may be complicated by the precision of the techniques used to evaluate aneuploidy, discussed above. What can be concluded is that developmental aneuploidy amongst NPCs is robust, while aneusomies in adult brains unambiguously exist but at levels that require further clarification to determine aneusomy rates for all chromosomes simultaneously.

3. Functions of neural mosaic aneuploidy

The functional significance of neural mosaic aneuploidy is beginning to emerge. Aneuploidy has clear cellular and organismal consequences, as seen in analyses of genomically unstable cancers and constitutively aneuploid diseases like Down syndrome [55-57]. As noted above, aneuploidy in cells is known to affect gene expression compared to euploid counterparts in a range of organisms, from yeast to mammals [17, 50-52, 58-60]. Aneuploidy can affect a range of cellular processes including survival, proliferation potential, and protein imbalances [58, 61-64]. The integration of adult aneuploid neurons into the circuitry of the normal brain [18] therefore suggests the potential of these neurons to influence normal brain functions. However, proven consequences of mosaic aneuploidy in the CNS have been difficult to establish because of the difficulty in identifying the mechanistic link between a specific karyotype and an identified function in a living cell. Not only have aneuploidies been overwhelmingly studied on fixed, non-living cells therefore precluding functional studies, but the loss or gain of a chromosome affects the expression of all genes and regulatory regions therein, creating an intricate web of interconnected consequences. Use of GFP reporters integrated into a defined chromosome have enabled gene expression analyses on cells with defined aneusomy (with the associated loss of GFP) vs. normal cells, and this approach indicates that aneuploidies can alter gene expression profiles within seemingly homogenous populations of neural cells [17]. In light of these observations, it would be surprising if mosaic aneuploid cells within the brain did not have functional consequences. Moreover, it is notable that aneuploidies are species-specific by virtue of unique chromosome organization and number that in part define a species. Thus, gains and/or losses of identified chromosomes within one species would be expected to have non-identical, albeit possibly overlapping effects on the most closely related chromosome from another species (*i.e.*, based on the degree of synteny between chromosomes of the compared species).

The existence and prevalence of mosaic aneuploidies is proof of a normally mutable genome, and it would therefore be anticipated that other forms of genomic change could exist in

cells of the brain. Following the demonstration of mosaic aneuploidies, the identification of possibly amplified repeat elements like LINE1 retrotransposable elements was reported [65, 66] that have been proposed to "jump" amongst neurons. However, this mechanism may not occur sufficiently to account for increased diversity, at least within the human cerebral cortex [29, 44]. More broadly, the identification of DCV that is best manifested as DNA gains within the human cerebral cortex, encompasses aneuploidies, possible LINE retrotransposons, as well as other genomic changes. The actual origins of DCV are not known but could involve a range of reported structural variants that include not only aneuploidy, but also somatic versions of copy number variation (CNV) [67] and other alterations to the genome, in view of the evidence for genomic, rather than extragenomic, origins of the increases in DNA content [29].

4. Mosaic aneuploidy in pluripotent stem cell lines

Mosaic aneuploidy has been clearly demonstrated in NPCs in the CNS, but the effective study of its functional consequences is limited, as noted above, by available experimental paradigms. Human embryonic stem cells (hESCs) and induced pluripotent stem cells (iPSCs) offer an attractive *in vitro* system to examine cellular processes that could be affected by mosaic aneuploidy, including differentiation, development, and neurological models. This approach has been supported by the observation that stem cells also show genomic heterogeneity produced by aneuploidy or other genomic alterations like CNVs [47, 48, 68-72]. Culture-induced aneuploidies have been observed in hESCs [73, 74] – in particular, gains of chromosomes 12, 17, 1, or X have been reported, which may arise by imparting a selective growth or survival advantage to cells with these karyotypes; cells with these recurrent gains can overwhelm the culture, leading to a clonal constitutively aneuploid cell population (*i.e.*, all cells of the culture exhibit the same aberrant karyotype) [75]. In contrast, consistent with observations on mouse ES cells [72], a recent study found that ~18-35% of cells within a given hESC line show mosaic aneuploidy, suggesting that the stochastic loss and/or gain of chromosomes is an inherent characteristic of stem cell biology [48], and this is also consistent with results from analyzing NPCs. In this study, six commercially-

available hESC lines and an iPSC line derived from fibroblasts showed significant levels of mosaic aneuploidy, independent of passage number and cell culture conditions (varied media, supplements and substrates, and investigators) [48]. It is important to emphasize the difference between the stochastic generation of mosaic aneuploidy versus clonal constitutively aneuploid karyotypes in long-term culture, particularly with respect to stem cell usage as a therapeutic. Mosaic aneuploidy mimics the genomic variability observed *in vivo* and likely contributes to the normal phenotypic heterogeneity of gene expression patterns [76, 77]. Devalle and colleagues suggest that mosaicism in stem cell culture may be well tolerated as cells can respond divergently to a range of stimuli, but the low levels and the random nature of this aneuploidy does not impart a selective clonal advantage to cells. Conversely, inundation of a culture by cells with clonal constitutive changes, arising from adaptations to stressful or unhealthful environments [75], represents a challenge for stem cell safety and usage *in vivo*. Such changes have been correlated with cancers, such as the loss of chromosome 10, gain of chromosome 7 or chromosome 1p and 19q deletions in human gliomas [55, 57, 78-81], as well as the identification of cancer related genes on the most common aneuploid chromosomes in hESC culture [73, 82, 83]. The carcinogenic risks that mosaically aneuploid hESCs pose to transplantation therapies – as well as within mosaic populations in the developing and adult brain – remain to be determined, but raise the formal possibility of aneuploid progenitor cell populations as a source of cancer stem cells in the brain, as well as other tissues. These issues deserve further analyses, especially where transplantation is designed to incorporate cells for the lifetime of an individual, as would be desired for neurons.

Significance

Genomic mosaicism within the CNS represents a relatively new frontier towards understanding the development and function of the brain, as well as numerous pathological processes that afflict it. Certain aneuploidies, including extreme forms like MVA and Down syndrome (DS), are well recognized for influencing brain function, with clearly demonstrated

unambiguous consequences to altering genomic content; studies of mosaic aneuploidy and its consequences in other disease states is only just beginning. Changes observed in gene expression associated with specific aneusomies within a single cell type of normal brain cells implicate functional consequences for aneuploidy in the non-diseased CNS as well, and recent analyses of the developing brain support distinct functions based upon karyotype, with varied aneuploid forms differentially promoting cell survival or death. Studies of aneuploidy in the non-diseased CNS question the assumption that aneuploidy is in fact "abnormal" in the development and function of certain cell lineages, and that it is deleterious – views contradicted by the maintenance of aneuploid populations in the normal brain. Indeed, some forms of aneuploidy may have beneficial consequences for neural development and function; this intriguing hypothesis will be addressed in the future by analyses of living, aneuploid cells. Long-lived cells like post-mitotic neurons may be especially apt at utilizing genomic alterations to their advantage, since they would not be under genomic constraints of highly mitotic cell populations. The stable and seemingly permanent changes produced by genomic alterations in a single neuron could provide a mechanism for creating and stabilizing functional mosaic populations within the brain, such as those constituting a neural network.

Aneuploidies represent a major alteration to neural genomes, but they are certainly not unique in this. The term DNA content variation or "DCV" has been proposed to encompass all of the different forms of genomic changes that are likely to be present within cells of the brain, from aneuploidy to putative mobile LINE elements, de novo CNVs, and other forms of DCV as have been identified within the frontal cortex. DCV within the frontal cortex that is distinct from the pattern observed in the cerebellum from the same individual also demonstrates regional differences in mosaicism, and supports non-random mechanisms in the generation and/or maintenance of this variability. It is notable that types of genomic changes are not mutually exclusive: the genomic landscape could well be heterogeneous with DNA gains, losses, or coincident gains and losses from each of the known sources of DCV.

Our current understanding of the brain does not broadly integrate the existence of genomic mosaicism, but future studies of genomic mosaic alterations using DNA sequences from new single-cell technologies, and strategies that seek to define the cell types, intercellular relationships and global patterns of mosaicism within the brain would complement and expand our knowledge of CNS form and function. Similarly, the possible detection of alterations to normally occurring genomic variation in a disease could identify risk factors, biomarkers and/or new therapeutic targets for the treatment of neurological and psychiatric disorders, particularly for common disease forms that share etiology but not causitive gene associations with rarer familial disease forms. Genomic mosaicism places organizational uniqueness upon the brain, even within syngenic organisms, which could provide a basis for behavioral diversity within a population towards promoting its survival and optimal fitness.

We would like to thank Danielle Jones for the assistance with editing. The text of this section, in full, is currently in press as an invited review: Bushman, D.M. & J. Chun. *The genomically mosaic brain: aneuploidy and more in neural diversity and disease*. Seminars in Cell and Developmental Biology. The dissertation author was the primary author of this material under the supervision of Dr. Jerold Chun.

References

[1] Alberman E, Mutton D, Morris JK. Cytological and epidemiological findings in trisomies 13, 18, and 21: England and Wales 2004-2009. Am J Med Genet A 2012;158A:1145-50.

[2] Kalousek DK, Howard-Peebles PN, Olson SB, Barrett IJ, Dorfmann A, Black SH, et al. Confirmation of CVS mosaicism in term placentae and high frequency of intrauterine growth retardation association with confined placental mosaicism. Prenatal Diagn 1991;11:743-50.

[3] Benn P, Hsu LY, Perlis T, Schonhaut A. Prenatal diagnosis of chromosome mosaicism. Prenatal Diagn 1984;4:1-9.

[4] Jinawath N, Zambrano R, Wohler E, Palmquist MK, Hoover-Fong J, Hamosh A, et al. Mosaic trisomy 13: understanding origin using SNP array. J Med Genet 2011;48:323-6.

[5] Robinson WP, Binkert F, Bernasconi F, Lorda-Sanchez I, Werder EA, Schinzel AA. Molecular studies of chromosomal mosaicism: relative frequency of chromosome gain or loss and possible role of cell selection. Am J Hum Genet 1995;56:444-51.

[6] Cohen FL, Durham JD. Sex chromosome variations in school-age children. J Sch Health 1985;55:99-102.

[7] Visootsak J, Graham JM, Jr. Social function in multiple X and Y chromosome disorders: XXY, XYY, XXYY, XXXY. Dev Disabil Res Rev 2009;15:328-32.

[8] Abramsky L, Chapple J. 47,XXY (Klinefelter syndrome) and 47,XYY: estimated rates of and indication for postnatal diagnosis with implications for prenatal counselling. Prenatal Diagn 1997;17:363-8.

[9] Walter E, Mazaika PK, Reiss AL. Insights into brain development from neurogenetic syndromes: evidence from fragile X syndrome, Williams syndrome, Turner syndrome and velocardiofacial syndrome. Neuroscience 2009;164:257-71.

[10] Bishop DV, Canning E, Elgar K, Morris E, Jacobs PA, Skuse DH. Distinctive patterns of memory function in subgroups of females with Turner syndrome: evidence for imprinted loci on the X-chromosome affecting neurodevelopment. Neuropsychologia 2000;38:712-21.

[11] Garcia-Castillo H, Vasquez-Velasquez AI, Rivera H, Barros-Nunez P. Clinical and genetic heterogeneity in patients with mosaic variegated aneuploidy: delineation of clinical subtypes. Am J Med Genet A 2008;146A:1687-95.

[12] Kajii T, Kawai T, Takumi T, Misu H, Mabuchi O, Takahashi Y, et al. Mosaic variegated aneuploidy with multiple congenital abnormalities: homozygosity for total premature chromatid separation trait. Am J Med Genet 1998;78:245-9.

[13] Warburton D, Anyane-Yeboa K, Taterka P, Yu CY, Olsen D. Mosaic variegated aneuploidy with microcephaly: a new human mitotic mutant? Ann Genet 1991;34:287-92.

[14] Kajii T, Ikeuchi T, Yang ZQ, Nakamura Y, Tsuji Y, Yokomori K, et al. Cancer-prone syndrome of mosaic variegated aneuploidy and total premature chromatid separation: report of five infants. Am J Med Genet 2001;104:57-64.

[15] Matsuura S, Ito E, Tauchi H, Komatsu K, Ikeuchi T, Kajii T. Chromosomal instability syndrome of total premature chromatid separation with mosaic variegated aneuploidy is defective in mitotic-spindle checkpoint. Am J Hum Genet 2000;67:483-6.

[16] Iourov IY, Vorsanova SG, Liehr T, Yurov YB. Aneuploidy in the normal, Alzheimer's disease and ataxia-telangiectasia brain: differential expression and pathological meaning. Neurobiol Dis 2009;34:212-20.

[17] Kaushal D, Contos JJ, Treuner K, Yang AH, Kingsbury MA, Rehen SK, et al. Alteration of gene expression by chromosome loss in the postnatal mouse brain. J Neurosci 2003;23:5599-606.

[18] Kingsbury MA, Friedman B, McConnell MJ, Rehen SK, Yang AH, Kaushal D, et al. Aneuploid neurons are functionally active and integrated into brain circuitry. Proc Natl Acad Sci U S A 2005;102:6143-7.

[19] Kingsbury MA, Yung YC, Peterson SE, Westra JW, Chun J. Aneuploidy in the normal and diseased brain. Cell Mol Life Sci 2006;63:2626-41.

[20] Pack SD, Weil RJ, Vortmeyer AO, Zeng W, Li J, Okamoto H, et al. Individual adult human neurons display aneuploidy: detection by fluorescence in situ hybridization and single neuron PCR. Cell Cycle 2005;4:1758-60.

[21] Rajendran RS, Wellbrock UM, Zupanc GK. Apoptotic cell death, long-term persistence, and neuronal differentiation of aneuploid cells generated in the adult brain of teleost fish. Dev Neurobiol 2008;68:1257-68.

[22] Rajendran RS, Zupanc MM, Losche A, Westra J, Chun J, Zupanc GK. Numerical chromosome variation and mitotic segregation defects in the adult brain of teleost fish. Dev Neurobiol 2007;67:1334-47.

[23] Rehen SK, McConnell MJ, Kaushal D, Kingsbury MA, Yang AH, Chun J. Chromosomal variation in neurons of the developing and adult mammalian nervous system. Proc Natl Acad Sci U S A 2001;98:13361-6.

[24] Rehen SK, Yung YC, McCreight MP, Kaushal D, Yang AH, Almeida BS, et al. Constitutional aneuploidy in the normal human brain. J Neurosci 2005;25:2176-80.

[25] Westra JW, Peterson SE, Yung YC, Mutoh T, Barral S, Chun J. Aneuploid mosaicism in the developing and adult cerebellar cortex. J Comp Neurol 2008;507:1944-51.

[26] Yang AH, Kaushal D, Rehen SK, Kriedt K, Kingsbury MA, McConnell MJ, et al. Chromosome segregation defects contribute to aneuploidy in normal neural progenitor cells. J Neurosci 2003;23:10454-62.

[27] Yurov YB, Iourov IY, Monakhov VV, Soloviev IV, Vostrikov VM, Vorsanova SG. The variation of aneuploidy frequency in the developing and adult human brain revealed by an interphase FISH study. J Histochem Cytochem 2005;53:385-90.

[28] Yurov YB, Iourov IY, Vorsanova SG, Liehr T, Kolotii AD, Kutsev SI, et al. Aneuploidy and confined chromosomal mosaicism in the developing human brain. PLoS ONE 2007;2:e558.

[29] Westra JW, Rivera RR, Bushman DM, Yung YC, Peterson SE, Barral S, et al. Neuronal DNA content variation (DCV) with regional and individual differences in the human brain. J Comp Neurol 2010;518:3981-4000.

[30] Boveri T. Concerning the origin of malignant tumours by Theodor Boveri. Translated and annotated by Henry Harris. J Cell Sci 2008;121 Suppl 1:1-84.

[31] Barch MJ, Knutsen, T. & Spurbeck, J. L. The AGT Cytogenetics Laboratory Manual. Philadelphia: Lippincott; 1997.

[32] Tjio JH, Levan A. THE CHROMOSOME NUMBER OF MAN. . Hereditas 1956;42:1-6.

[33] Watson JD, Crick FH. Molecular structure of nucleic acids; a structure for deoxyribose nucleic acid. Nature 1953;171:737-8.

[34] Schrock E, du Manoir S, Veldman T, Schoell B, Wienberg J, Ferguson-Smith MA, et al. Multicolor spectral karyotyping of human chromosomes. Science 1996;273:494-7.

[35] Iourov IY, Soloviev IV, Vorsanova SG, Monakhov VV, Yurov YB. An approach for quantitative assessment of fluorescence in situ hybridization (FISH) signals for applied human molecular cytogenetics. J Histochem Cytochem 2005;53:401-8.

[36] Liehr T, Heller A, Starke H, Rubtsov N, Trifonov V, Mrasek K, et al. Microdissection based high resolution multicolor banding for all 24 human chromosomes. Int J Mol Med 2002;9:335-9.

[37] Iourov IY, Vorsanova SG, Yurov YB. Chromosomal variation in mammalian neuronal cells: known facts and attractive hypotheses. Int Rev Cytol 2006;249:143-91.

[38] Gorman P, Roylance R. Fluorescence in situ hybridization and comparative genomic hybridization. Methods Mol Med 2006;120:269-95.

[39] Pinkel D, Albertson DG. Comparative genomic hybridization. Annu Rev Genomics Hum Genet 2005;6:331-54.

[40] Ballif BC, Rorem EA, Sundin K, Lincicum M, Gaskin S, Coppinger J, et al. Detection of low-level mosaicism by array CGH in routine diagnostic specimens. Am J Med Genet A 2006;140:2757-67.

[41] Spits C, Le Caignec C, De Rycke M, Van Haute L, Van Steirteghem A, Liebaers I, et al. Whole-genome multiple displacement amplification from single cells. Nat Protoc 2006;1:1965-70.

[42] Navin N, Hicks J. Future medical applications of single-cell sequencing in cancer. Genome Med 2011;3:31.

[43] Navin N, Kendall J, Troge J, Andrews P, Rodgers L, McIndoo J, et al. Tumour evolution inferred by single-cell sequencing. Nature 2011;472:90-4.

[44] Evrony GD, Cai X, Lee E, Hills LB, Elhosary PC, Lehmann HS, et al. Single-neuron sequencing analysis of l1 retrotransposition and somatic mutation in the human brain. Cell 2012;151:483-96.

[45] Johnson LA. Sex preselection by flow cytometric separation of X and Y chromosome-bearing sperm based on DNA difference: a review. Reprod Fertil Dev 1995;7:893-903.

[46] Laerum OD, Farsund T. Clinical application of flow cytometry: a review. Cytometry 1981;2:1-13.

[47] Peterson SE, Chun J, Loring J. FISH analysis of human pluripotent stem cells. Methods Mol Biol 2011;767:191-200.

[48] Peterson SE, Westra JW, Rehen SK, Young H, Bushman DM, Paczkowski CM, et al. Normal human pluripotent stem cell lines exhibit pervasive mosaic aneuploidy. PLoS ONE 2011;6:e23018.

[49] Hassold T, Hunt P. To err (meiotically) is human: the genesis of human aneuploidy. Nat Rev Genet 2001;2:280-91.

[50] Hughes TR, Roberts CJ, Dai H, Jones AR, Meyer MR, Slade D, et al. Widespread aneuploidy revealed by DNA microarray expression profiling. Nat Genet 2000;25:333-7.

[51] Sheltzer JM, Torres EM, Dunham MJ, Amon A. Transcriptional consequences of aneuploidy. Proc Natl Acad Sci U S A 2012;109:12644-9.

[52] Torres EM, Williams BR, Amon A. Aneuploidy: cells losing their balance. Genetics 2008;179:737-46.

[53] Yurov YB, Iourov IY, Monakhov VV, Soloviev IV, Vostrikov VM, Vorsanova SG. The variation of aneuploidy frequency in the developing and adult human brain revealed by an interphase FISH study. J Histochem Cytochem 2005;53:385-90.

[54] Iourov IY, Liehr T, Vorsanova SG, Kolotii AD, Yurov YB. Visualization of interphase chromosomes in postmitotic cells of the human brain by multicolour banding (MCB). Chromosome Res 2006;14:223-9.

[55] Lengauer C, Kinzler KW, Vogelstein B. Genetic instabilities in human cancers. Nature 1998;396:643-9.

[56] Antonarakis SE, Lyle R, Dermitzakis ET, Reymond A, Deutsch S. Chromosome 21 and down syndrome: from genomics to pathophysiology. Nat Rev Genet 2004;5:725-38.

[57] Duesberg P, Rasnick D. Aneuploidy, the somatic mutation that makes cancer a species of its own. Cell Motil Cytoskeleton 2000;47:81-107.

[58] Torres EM, Sokolsky T, Tucker CM, Chan LY, Boselli M, Dunham MJ, et al. Effects of aneuploidy on cellular physiology and cell division in haploid yeast. Science 2007;317:916-24.

[59] Sheltzer JM, Blank HM, Pfau SJ, Tange Y, George BM, Humpton TJ, et al. Aneuploidy drives genomic instability in yeast. Science 2011;333:1026-30.

[60] Humpherys D, Eggan K, Akutsu H, Hochedlinger K, Rideout WM, 3rd, Biniszkiewicz D, et al. Epigenetic instability in ES cells and cloned mice. Science 2001;293:95-7.

[61] Williams BR, Prabhu VR, Hunter KE, Glazier CM, Whittaker CA, Housman DE, et al. Aneuploidy affects proliferation and spontaneous immortalization in mammalian cells. Science 2008;322:703-9.

[62] Pavelka N, Rancati G, Zhu J, Bradford WD, Saraf A, Florens L, et al. Aneuploidy confers quantitative proteome changes and phenotypic variation in budding yeast. Nature 2010;468:321-5.

[63] Torres EM, Dephoure N, Panneerselvam A, Tucker CM, Whittaker CA, Gygi SP, et al. Identification of aneuploidy-tolerating mutations. Cell 2010;143:71-83.

[64] Sheltzer JM, Amon A. The aneuploidy paradox: costs and benefits of an incorrect karyotype. Trends Genet 2011;27:446-53.

[65] Muotri AR, Chu VT, Marchetto MC, Deng W, Moran JV, Gage FH. Somatic mosaicism in neuronal precursor cells mediated by L1 retrotransposition. Nature 2005;435:903-10.

[66] Muotri AR, Gage FH. Generation of neuronal variability and complexity. Nature 2006;441:1087-93.

[67] Sebat J, Lakshmi B, Troge J, Alexander J, Young J, Lundin P, et al. Large-scale copy number polymorphism in the human genome. Science 2004;305:525-8.

[68] Hussein SM, Batada NN, Vuoristo S, Ching RW, Autio R, Narva E, et al. Copy number variation and selection during reprogramming to pluripotency. Nature 2011;471:58-62.

[69] Gore A, Li Z, Fung HL, Young JE, Agarwal S, Antosiewicz-Bourget J, et al. Somatic coding mutations in human induced pluripotent stem cells. Nature 2011;471:63-7.

[70] Longo L, Bygrave A, Grosveld FG, Pandolfi PP. The chromosome make-up of mouse embryonic stem cells is predictive of somatic and germ cell chimaerism. Transgenic Res 1997;6:321-8.

[71] Cervantes RB, Stringer JR, Shao C, Tischfield JA, Stambrook PJ. Embryonic stem cells and somatic cells differ in mutation frequency and type. Proc Natl Acad Sci U S A 2002;99:3586-90.

[72] Eggan K, Rode A, Jentsch I, Samuel C, Hennek T, Tintrup H, et al. Male and female mice derived from the same embryonic stem cell clone by tetraploid embryo complementation. Nat Biotechnol 2002;20:455-9.

[73] Draper JS, Smith K, Gokhale P, Moore HD, Maltby E, Johnson J, et al. Recurrent gain of chromosomes 17q and 12 in cultured human embryonic stem cells. Nat Biotechnol 2004;22:53-4.

[74] Buzzard JJ, Gough NM, Crook JM, Colman A. Karyotype of human ES cells during extended culture. Nat Biotechnol 2004;22:381-2; author reply 2.

[75] Devalle S, Sartore RC, Paulsen BS, Borges HL, Martins RA, Rehen SK. Implications of aneuploidy for stem cell biology and brain therapeutics. Front Cell Neurosci 2012;6:36.

[76] Chang HH, Hemberg M, Barahona M, Ingber DE, Huang S. Transcriptome-wide noise controls lineage choice in mammalian progenitor cells. Nature 2008;453:544-7.

[77] Graf T, Stadtfeld M. Heterogeneity of embryonic and adult stem cells. Cell Stem Cell 2008;3:480-3.

[78] Lengauer C, Kinzler KW, Vogelstein B. Genetic instability in colorectal cancers. Nature 1997;386:623-7.

[79] Rajagopalan H, Lengauer C. Aneuploidy and cancer. Nature 2004;432:338-41.

[80] Takeuchi H, Kubota T, Kitai R, Matsuda K, Hashimoto N, Sato K. Chromosome 1p and 19q deletions in malignant glioneuronal tumors with oligodendroglioma-like component. J Neurooncol 2009;91:33-8.

[81] Thiel G, Losanowa T, Kintzel D, Nisch G, Martin H, Vorpahl K, et al. Karyotypes in 90 human gliomas. Cancer Genet Cytogenet 1992;58:109-20.

[82] Baker DE, Harrison NJ, Maltby E, Smith K, Moore HD, Shaw PJ, et al. Adaptation to culture of human embryonic stem cells and oncogenesis in vivo. Nat Biotechnol 2007;25:207-15.

[83] Hovatta O, Jaconi M, Tohonen V, Bena F, Gimelli S, Bosman A, et al. A teratocarcinoma-like human embryonic stem cell (hESC) line and four hESC lines reveal potentially oncogenic genomic changes. PLoS ONE 2010;5:e10263.

CHAPTER 1

Somatic genomic mosaicism via increased DNA content and APP locus amplification in single Alzheimer's disease neurons

Abstract

Sporadic Alzheimer's disease (AD), comprising >90% of all AD cases, is not clearly linked to known germline variations that characterize familial AD, yet patients show the same neuropathology and cognitive impairment. Here we report analyses of genomic mosaicism in sporadic AD. Analyses for aneuploidy produced by mosaic trisomy 21 did not identify linkage to disease. By contrast a robust and significant increase in neuronal DNA content variation (DCV) occurs in neurons of the frontal cortex of sporadic AD brains, with an average gain of ~330 Mb and ranging beyond 1500 Mb. Quantitative PCR of fewer than 100 cells for amyloid precursor (APP) copy number variation (CNV) identified APP gains in 3 of 7 sporadic AD paired frontal cortex and cerebellar samples, consistent with mosaic locus amplification. Single-cell genomic analyses by microfluidic qPCR confirmed mosaic alterations of APP CNVs, compared to normal and trisomy 21 controls: specific amplification of the APP locus ranged beyond 12 copies, within single AD cortical neurons, and averaged ~3 copies/neuron overall. These data demonstrate the existence of altered genomic mosaicism in sporadic AD resulting in somatic amplification of pathogenic AD loci, and raise the possibility that DCV may underlie the etiology of sporadic AD.

Introduction

Alzheimer's Disease is the most common dementia, impacting an estimated 26.7 million people worldwide [1]. AD neuropathology includes the accumulation of plaques composed of amyloid (A) β, neurofibrillary tangles containing microtubule-associated protein (MAP) Tau, synaptic loss and neuronal death particularly in the hippocampus, and frontal and entorhinal cortices, leading to progressive cognitive decline. Familial AD is characterize by its early onset (<60 years) and makes up ~5% of all cases through inherited autosomal dominant mutations in

any one of 3 genes that by definition are transmitted through the germline to all cells. The genes are amyloid precursor protein (*APP*) on chromosome 21, which is cleaved to form the Aβ peptide found in amyloid plaques; and presenilin 1 (*PSEN1*) on chromosome 14 or presenilin 2 (*PSEN2*) on chromosome 1, both of which contribute to the catalytic activity of the Aβ-cleaving enzyme ɣ-secretase [1-3]. Sporadic AD, characterized by its late-onset (>60 years), arises from a less understood set of genetic, epigenetic, and environmental risk factors [4-6], yet shares the same neuropathology and cognitive impairment seen with familial cases.

The location of *APP* on chromosome 21 [7-9] – trisomic in Down syndrome – provides a strong link between *APP* gene dosage and AD neuropathogenesis, as individuals with Down syndrome develop identical neuropathology [3, 10-12]. The pathogenicity of *APP* locus amplification in familial AD has been validated by autosomal dominant duplications of the *APP* locus that are sufficient to cause familial early-onset AD [13-16]. Conversely, the locus-specific loss in a partial trisomy 21 Down syndrome case provided AD-protective effects [17], as does a familial APP loss-of-function mutation [18]. In stark contrast, >90% of AD cases are sporadic and not clearly linked to a known germline mutation, including APP gene duplications [7, 19-21].

The discovery of somatic mosaic genomic variability in normal brains revealed that cells within single brains can have distinct genomes [6, 22-32]. Non-diseased human brain exhibits a surprising range of heterogeneity produced by aneuploidy and additional forms of genomic variation, referred to as DNA content variation (DCV) [27]. DCV in the human brain was most notably characterized by gains of ~250 Mb within cerebral cortical neurons, and moreover showed neuroanatomical regionality in comparison to cerebellar neurons of the same brain [27]. This regionality of DCV roughly paralleled that seen for amyloid plaque accumulation in AD [33, 34], suggesting that alterations in DCV might contribute to sporadic AD, perhaps through the amplification of disease-related loci. This possibility was explored here on clinically validated AD brains, utilizing the heightened sensitivity of a state-of-the-art microfluidic qPCR system to track the specific amplification of the *APP* locus within single AD cortical neurons. These data indicate that the genomic mosaicism produced by DCV may in part underlie the etiology of sporadic AD.

Materials and Methods

Human tissue samples

All protocols requiring human tissue usage were approved by the Human Subject Committee at The Scripps Research Institute, and conform to National Institutes of Health guidelines. Fresh-frozen postmortem human brain tissue from non-diseased control individuals, Down syndrome individuals, and individuals with Alzheimer's disease were obtained from the NICHD Brain and Tissue Bank for Developmental Disorders at the University of Maryland, the Institute for Brain Aging and Dementia Tissue Repository at the University of California, Irvine, and Dr. Edward Koo at the University of California, San Diego. Alzheimer's disease was histologically confirmed and samples were scored for amyloid beta plaques (Braak score). Human peripheral blood was obtained from healthy donors at The Scripps Research Institute Normal Blood Donor Services (**Table 1.1**).

Table 1.1. Human tissue samples used in the study.

FCTX	Sex	Age	Sample	PMI	Braak score
AD	F	81	1521	23	VI
N = 32	F	83	1562		
	F	74	**1866**	U	U
	F	79	**1868** *	U	U
	F	82	**1875** *	U	U
	F	83	1893		
	F	87	1899	5	VI
	F	62	**1912** *	U	U
	F	80	**1913**	U	U
	F	54	**1916**	U	U
	F	72	**1921** †	U	U
	F	77	2400	3.7	V
	F	80	2500	2.3	VI
	F	101	50341	19	V
	F	91	61788	11	V
	F	98	62405	11	V
	F	89	62439	11	V
	F	77	62509	18	VI
	M	88	**102** *†	3	IV
	M	90	268	91	V
	M	83	736	U	U
	M	82	1211	U	U
	M	79	**1252**	9	U
	M	92	1748	5.5	V
	M	85	**1861**	U	U
	M	85	**1870**	U	U
	M	82	**2401** *†	3	VI
	M	84	**2499** *†	3.4	VI
	M	63	**4199** *	3	VI
	M	80	13173	22	IV
	M	94	30022	20	V
	M	91	60987	22.5	V
Average =		**82.1**			
NON-AD	F	74	**1901** †	2.3	II
N = 7	F	74	**299**	2.8	II
	F	84	**703** *	5.8	III
	F	80	60728	13	II
	F	53	**1379**	15	III
	M	95	**1301**	3.5	I
	M	79	**827**	U	U
Average =		**77**			

CBL	Sex	Age	Sample	PMI	Braak score
AD	F	74	**1866**	U	U
N = 15	F	79	**1868** *	U	U
	F	82	**1875** *	U	U
	F	80	**1913**	U	U
	F	62	**1912** *	U	U
	F	54	**1916**	U	U
	F	72	**1921** †	U	U
	M	88	**102** *†	3	IV
	M	79	**1252**	9	U
	M	70	1625	1	U
	M	85	**1861**	U	U
	M	85	**1870**	U	U
	M	82	**2401** *†	3	VI
	M	84	**2499** *†	3.4	VI
	M	63	**4199** *	3	VI
Average =		**75.9**			
NON-AD	F	74	**1901** †	2.3	II
N = 10	F	74	**299**	2.8	II
	F	84	**703** *	5.8	III
	F	77	1569	8	III
	F	83	719	U	U
	F	53	**1379**	15	III
	F	71	1571	U	U
	M	95	**1301**	3.5	I
	M	53	1344	U	U
	M	79	**827**	U	U
Average =		**74.3**			

DS/AD	Sex	Age	Sample	PMI	Braak score
N = 5	F	51	M1864 †	19	U
	F	44	1258 *	13	U
	F	47	M3233 *	24	U
	M	56	1623	7	U

LYM	Sex	Age	Sample	PMI
N=7	F	40	5162	N/A
	F	40	3963	N/A
	F	63	4984	N/A
	F	60	4519	N/A
	M		Lym 1	N/A
	M	35	4651	N/A
Average =		**50.75**		

Abbreviations: AD - Alzheimer's disease; NON-AD – non-diseased; DS - Down syndrome; FCTX - frontal cortex; CBL – cerebellum; LYM - peripheral blood lymphocytes; PMI - post-mortem interval. Bold lettering denotes samples with paired CBL and CTX. * denotes samples analyzed by SybrGreen quantitative PCR; † denotes samples analyzed by TaqMan quantitative PCR.

Flow cytometry (FCM) and fluorescence-activated cell sorting (FACS)

FCM and FACS were performed at TSRI Flow Cytometry Core, using a Becton Dickinson (BD Biosciences,San Jose, CA) LSRII and FACS-Aria II, respectively. FCM results were replicated on three different LSRII machines, verified and reproduced by independent researchers, and analyzed by FlowJo cytometry analysis program (TreeStar, Inc., Ashland, OR).

Human brain nuclei were isolated following standard laboratory protocols, as previously described [27]. Briefly, 0.3-0.5 g of tissue was incubated on ice in PBS containing 2 mM EGTA (PBSE), then triturated using P1000 tips with decreasing bore diameter. Cells were filtered through a 40 µm nylon filter, and lysed for nuclei extraction using 1% NP-40 in PBS buffer. Nuclei were fixed with ice-cold 70% EtOH; prior to FCM, nuclei were washed with PBSE and resuspended in staining solution composed of 50 µg/ml propidium iodide (PI)(Sigma, St. Louis, MO), 50 µg/ml RNaseA (Sigma), and chicken erythrocyte nuclei (CEN)(Biosure, Grass Valley, CA). Samples were incubated at room temperature for 90 minutes, and then refiltered through a 40 µm filter prior to analysis. Using electronic gating settings on the flow cytometer, all nuclei were gated on forward scatter (FSC) (nuclear size) and side scatter (SSC) (nuclear granularity) to remove doublet nuclei. Assessment of PI-stained nuclei for DNA content versus nuclear size generated histograms; the main peak is the G_0/G_1 population, containing cells in the G_0/G_1 stage of the cell cycle (the predominant cell cycle stage in the brain, as the majority of the cells are non-cycling neurons and non-neuronal cells). For DNA content FACS, nuclei were also labeled with NeuN antibody (1:100 dilution)(Chemicon, Temecula, CA) and an Alexa Fluor 488 goat anti-mouse IgG secondary (1:250 dilution) (Life Technologies, San Diego, CA). Cells were counterstained with the above PI solution and gated in a similar fashion. Electronic gating of the G_0/G_1 peak and subsequent gating for NeuN immunoactivity allowed for sorting into NeuN+ and NeuN- fractions; these fractions were collected either in bulk in Eppendorf tubes containing 200 µl PBS, or in 96-well plates containing 4 µl of QuickExtract DNA Extraction Solution (Epicentre, Madison, WI); DNA was kept at -20°C before use. Genomic DNA from single cells in 96 well plates containing QuickExtract buffer was extracted according to the manufacturer's protocol;

briefly, the solution was heated to 65°C for six minutes followed by 98°C for two minutes. Genomic DNA from bulk samples was isolated using the DNeasy Blood and Tissue kit (Qiagen, Valencia, CA). As controls for flow cytometry, positive and negative selection gates were determined using samples stained with DNA dye alone or secondary antibody alone.

Quantitative PCR

Real-time quantitative (q)PCR was used to quantify gene copy number from human brain nuclei and lymphocyte genomic DNA by either SYBR Green or Taqman qPCR. SYBR Green qPCR was performed on 0.5 ng (~75 genomes) of sample DNA from nuclei isolated by FACS and quantified by Quant-iT PicoGreen dsDNA reagent (Life Technologies). Assays were designed against one exon of the *APP* gene (exon 16, which along with exon 17 encodes the Aβ peptide found in amyloid plaques (Yoshikai 1990 Gene)) compared to reference assays (*SEMA4A*, *CCL18*, *PCDH11X*; targeted genetic loci (1) are not associated with AD and (2) are not on chromosome 21). Primer sets were synthesized by Valuegene (San Diego, CA); all sets were optimized to an annealing temperature of 59°C. The specificity of qPCR assays was determined by gel electrophoresis, confirming a single PCR product of the expected length (**Table 1.2**).

Table 1.2. Genomic targets for quantitative PCR analysis.

Gene	Protein	Locus	Assay Type	Primer Sequence	Probe	Product Length	Efficiency
APP, Exon 16	Amyloid precursor protein	21q21.3	SybrGreen	F-TGCACGTGAAAGCAGTTGAAG R-AAAGATGGCATGAGAGCATCG	N/A	214	0.973
SEMA4A	Semaphorin 4A	1q22	SybrGreen	F- ATGCCCAGGGTCAGATACTAT R-TTCTCCGAGATCCTCTGTTTC	N/A	177	0.997
CCL18	Chemokine (C-C motif) ligand 18	17q11.2	SybrGreen	F-TTCCTGACTCTCAAGGAAAGG R-CTGGCACTTACATGACACCTG	N/A	209	1.006
PCDH11X	Protocadherin 11 X-linked	Xq21.3	SybrGreen	F-TCTTTTGGTCAGTGTTGTGCG R-CAACAAGTCGCCTATCAGGAC	N/A	188	0.993
APP, Exon 16	Amyloid precursor protein	21q21.3	TaqMan	CGGTCAAAGATGGCATGAGAGCATC * Assay Hs01255859_cn	FAM-MGB	91	1.040
APP, Exon 5	Amyloid precursor protein	21q21.3	TaqMan	F-GCACTTCTGGTCCCAAGCAT R-CCAGTTCTGGATGGTCACTG	ROX-IB	140	0.992
SEMA4A	Semaphorin 4A	1q22	TaqMan	GTTCAAGGGTATGTGAGGTGAGATG * Assay Hs00329046_cn_VIC	VIC-MGB	90	1.016
CDK1	Cyclin-dependent Kinase 1	10q21.2	TaqMan	GTAGACACAAAACTACAGGTCAAGT * Assay HS00428497_cn	FAM-MGB	101	1.170

* Denotes reference sequence provided by manufacturer

Samples were run in triplicate on a Rotor-Gene RG-3000 72-well thermocycler (Qiagen). A master mix of the following reaction components was prepared to the following end-concentration: 5 µl of mixed forward and reverse primer of a specific primer set (100 ng primer mix, 20 ng/µl final); 12.5 µl of 2x GoTaq qPCR master mix (Promega); and 2.5 µl of nucleotide-free H_2O to a final volume of 25 µl. The following run was performed on the thermocycler: denaturation at 95°C for 5 min; amplification (95°C for 25 sec, 59°C for 30 sec and 72°C for 30 sec) and quantification (single fluorescent end measurement) through 40 cycles; and a melting curve determination (55-99°C, 30 sec on the 1st step, 5 sec for each subsequent step). The crossing threshold (Ct) was determined for each primer set, defined as the point at which fluorescence emission rises above the background fluorescence (within the linear region of the amplification curve).

A microfluidic qPCR system (the Fluidigm Biomark 48.48 Dynamic Array integrated fluidic circuit (IFC); Fluidigm, San Francisco, CA) was adapted for detection of genomic deletions and duplications of defined loci in single cells by TaqMan qPCR. Taqman assays (**Table 1.2**) were synthesized by Applied Biosystems (a Life Technologies company) or Integrated DNA Technologies (Coralville, IA); all sets were optimized to an annealing temperature of 60°C. Fluorescent probes used for these assays were 5'-FAM or 5'-VIC with a 3'-minor groove binding (MGB) non-fluorescent quencher, or 5'-ROX with a 3' Iowa Black quencher. Assays were again designed against *APP* exon 16, as above, as well as against a proximal exon from the *APP* locus, exon 5 (separated by ~176 kb). *SEMA4A* was again used as the reference gene, as was *CDK1*. A single PCR product was confirmed for each primer set by gel electrophoresis. Primers were also assessed *in silico* to determine whether SNPs were present in the targeted genomic region that would decrease primer binding and amplification efficiency. Genomic DNA from single nuclei, isolated by FACS and extracted as described above, was preamplified with a target-specific primer set as per Fluidigm protocols [35-40], the same primer set that would be used to assess copy number on the Biomark. This amplification is distinct from whole genome amplification, as only certain loci are amplified for interrogation. This preamplification step used a low number of

cycles to minimize primer bias and to generate sufficient copy numbers to ensure that each IFC chamber has DNA but is not overloaded, which would in turn decrease reaction efficiency.

Initial 20x primer concentrations were 18 µM, and 5 µM for probes; primer and probes sets combined and diluted to a 0.2x solution of each set for preamplification. A preamplification mix was prepared with the following end concentrations: 1x PCR reaction buffer (Roche Applied Science, Indianapolis, IN), 1.7mM $MgCl_2$ (Roche); 280nM dNTPs (Denville, South Plainfield, NJ); 0.5 Units Taq Polymerase (Denville); 0.02x primer mix; and nuclease-free H_2O. 5 µl of mix was added to each well of the 96 well plate containing extracted gDNA for a total volume of 10 µl. The following preamplification run was performed on a Verite thermocycler (Applied Biosystems), following the Fluidigm recommended protocol: 95°C denaturation for 5 min; 18 amplification cycles of a 95°C denaturation for 15 sec, followed by a 60°C annealing and extension step for 4 minutes; and a final extension step at 72°C for 7 minutes. Presence of preamplified DNA was confirmed on a Roche LightCycler in a reaction combining 1.5 µl of preamplified DNA from individual wells with 2.5 µl of TaqMan Gene Expression Master Mix (Applied Biosystems), 0.2 µl of one 20x TaqMan assay, and 0.8 µl nuclease-free H_2O, to a final volumes of 5 µl.

Successfully preamplified gDNA was diluted 1:5 for use in the 48.48 Dynamic Array IFC (Fluidigm). Array setup was performed according to the manufacturer's protocol. The chip was first primed with 300 µl of priming solution using the Priming function of the IFC Controller MX. A master mix for the samples was prepared, combining 3 µl of 2x TaqMan Universal PCR Master Mix (1x final concentration; Applied Biosystems) and 0.3 µl 20x Gene Expression Loading Reagent (Fluidigm) with 2.7 µl of diluted preamplified gDNA. Independently, 3 µl of individual TaqMan assays were combined with 3 µl of 2x Assay Loading Reagent (Fluidigm) for loading. Samples were run in triplicate while assays were run in sextuplicate, yielding 18 replicates per single cell analyzed. Following the loading and partitioning of samples and assays into the array chip by the Loading function of the IFC Controller MX, the array was run on the Biomark HD (Fluidigm). The following thermocycling program was performed on the Biomark: 95°C for 10 min, then 55 cycles of 95°C denaturation and 60°C annealing and extention. Detectors were set to

collect the fluorescent signal from FAM-MGB, VIC-MGB and ROX-Iowa Black probes. Ct values were calculated using the Fluidigm Real-Time PCR Analysis Software, with the fluorescent threshold set as described above. Reproducibility for sample comparison across chips was also assessed (**Table 1.3**).

Table 1.3. Replication of Ct values across 48.48 Dynamic Arrays.

		Cell 1		Cell 2		Cell 3		Cell 4	
Assay		Ct	SEM	Ct	SEM	Ct	SEM	Ct	SEM
APP Exon 16	Run 1	18.73	0.02	19.55	0.04	19.07	0.02	18.80	0.03
	Run 2	18.93	0.02	19.41	0.06	19.09	0.03	18.81	0.01
APP Exon 5	Run 1			20.65	0.09	19.43	0.02	18.65	0.05
	Run 2			20.78	0.11	19.93	0.10	18.85	0.03
SEMA4A	Run 1	22.83	0.16	22.98	0.17	22.60	0.14	20.13	0.38
	Run 2	22.71	0.14	23.20	0.15	23.05	0.12	22.38	0.08
CDK1	Run 1	17.37	0.02	17.54	0.05	17.19	0.02	16.59	0.06
	Run 2	17.68	0.04	17.63	0.06	17.41	0.04	16.99	0.02

Standard curves for quantifying gene copy number in both qPCR systems were created by serially diluting purified pGEM-T Easy plasmid DNA (Promega, Madison, WI) containing a single copy of the gene of interest. DNA concentrations of plasmid DNA were converted to gene copy number by calculating the weight (in g/mol) of the plasmid and insert used for generating the standard curve, and converting this into copy number (g/molecule) by using Avogadro's number (mol/molecule). Only standard curves with R^2 values of greater than 0.99 were used; primer efficiency was determined with the equation $E = 10^{-1/slope}$ (**Table 1.2**).

Relative quantification, or the $2^{-\Delta\Delta Ct}$ method was used to determine CNVs [41-44]. The target assays (T) for copy number variation were *APP*$_{\text{Exon 16}}$ and *APP*$_{\text{Exon 5}}$, and the reference assays (R), which serve as internal controls, were *SEMA4A* and *CDK1*. For each cell, the mean Ct, standard deviation (s) and standard error of the mean (**S**$\bar{x}$) were determined for all assays

from the 18 replicates (n). The equation for the Ct is as follows, using the target assay T as an example:

$$Ct_T \pm \frac{s_T}{\sqrt{n_T}} = Ct_T \pm \mathbf{S}\bar{x}$$

To determine the copy number of the target compared to the reference gene within the sample, which normalizes differences in input concentrations, the ΔCt and the error ($\mathbf{S}\bar{x}_{\Delta\mathrm{Ct}}$) are calculated:

$$\Delta Ct_T = Ct_T - Ct_R$$

$$\mathbf{S}\bar{x}_{\Delta\mathrm{Ct}} = \sqrt{\mathbf{S}\bar{x}^2{}_T + \mathbf{S}\bar{x}^2{}_R} = \sqrt{\frac{s^2{}_T}{n_T} + \frac{s^2{}_R}{n_R}}$$

The sample ΔCt values are then normalized to a calibrator sample (C) containing a single-copy gene (two copies per diploid genome), giving the ΔΔCt value. Because of the potential genetic variability across reference genes (*SEMA4A* and *CDK1*) and samples, multiple calibrator samples were compared. The calibration is calculated as follows:

$$\Delta\Delta Ct = (\Delta Ct - \Delta Ct_C) \pm \sqrt{\mathbf{S}\bar{x}^2{}_{\Delta Ct} + \mathbf{S}\bar{x}^2{}_{\Delta Ct_C}}$$

$$\mathbf{S}\bar{x}_{\Delta\Delta\mathrm{Ct}} = \sqrt{\mathbf{S}\bar{x}^2{}_{\Delta Ct} + \mathbf{S}\bar{x}^2{}_{\Delta Ct_C}} = \sqrt{\frac{s^2{}_T}{n_T} + \frac{s^2{}_R}{n_R} + \frac{s^2{}_{T,C}}{n_{T,C}} + \frac{s^2{}_{R,C}}{n_{R,C}}}$$

Using the E values determined by standard curve analysis (above), relative copy number (RCN) in a diploid sample is calculated with this equation:

$$RCN = 2 * (1 + E)^{-\Delta\Delta Ct}$$

The 95% confidence interval upper and lower bounds for RCN are determined from the $\mathbf{S}\bar{x}_{\Delta\Delta\mathrm{Ct}}$ multiplied by the critical t value for a two-tailed t-distribution with p = 0.05.

$$RCN = 2 * (1 + E)^{-\Delta\Delta Ct \pm t * \mathbf{S}\bar{x}_{\Delta\Delta\mathrm{Ct}}}$$

A system standard deviation of 0.25 was assumed to calculate 95% confidence intervals (CIs) for 1-8 copies of DNA; modeled CIs were used to call copy numbers for each gene assay in each cell. For example, if the RCN calculated for a *APP*$_{(\text{exon 16})}$ fell inside the predicted CI for 4 copies, the sample was recorded as having 4 copies; if the RCN fell outside the predicted CI for 4 copies, but

the error bars of that assay (representing 95% CI of the sample itself, RCN_{max} and RCN_{min}) fell inside the predicted CI, the sample was recorded as having 4 copies. Relative quantification was chosen, versus absolute quantification, because of the variation between primer efficiencies, and the mosiac nature of both the sample and control gDNA.

Results

Alzheimer's diseases shows increased DNA content variation (DCV)

To interrogate the DNA content of brain cells from both normal individuals and those with sporadic Alzheimer's disease, a flow cytometry-based strategy relying on the isolation of intact cellular nuclei was utilized [27], thus bypassing difficulties in single cell separation stemming from the intrinsic interconnectivity of the brain. Non-diseased human lymphocyte nuclei (LYM, N= 7) served as euploid reference samples, while chick erythrocyte nuclei provide an internal reference standard for ease of comparison across multiple samples and FCM runs. The DCV of propidium iodide (PI)-stained reference samples was compared to the DCV of brain cell nuclei populations (>10,000 nuclei per sample) from both the frontal cortex and the cerebellum of non-diseased brains (ND CTX, N=7; CBL, N=10) and pathologically confirmed Alzheimer's brains (AD CTX, N=32; AD CBL, N=15), controlling for age and sex (**Table 1.1**). Previously published increases in DCV in the non-diseased frontal cortex compared to both the cerebellum and lymphocyte controls [27] were recapitulated prior to this analysis. A representative electronic gating profile of cells (**Fig. 1.1**) illustrates how nuclei were analyzed based on nuclear size (FSC) and granularity (SSC), and histogram construction.

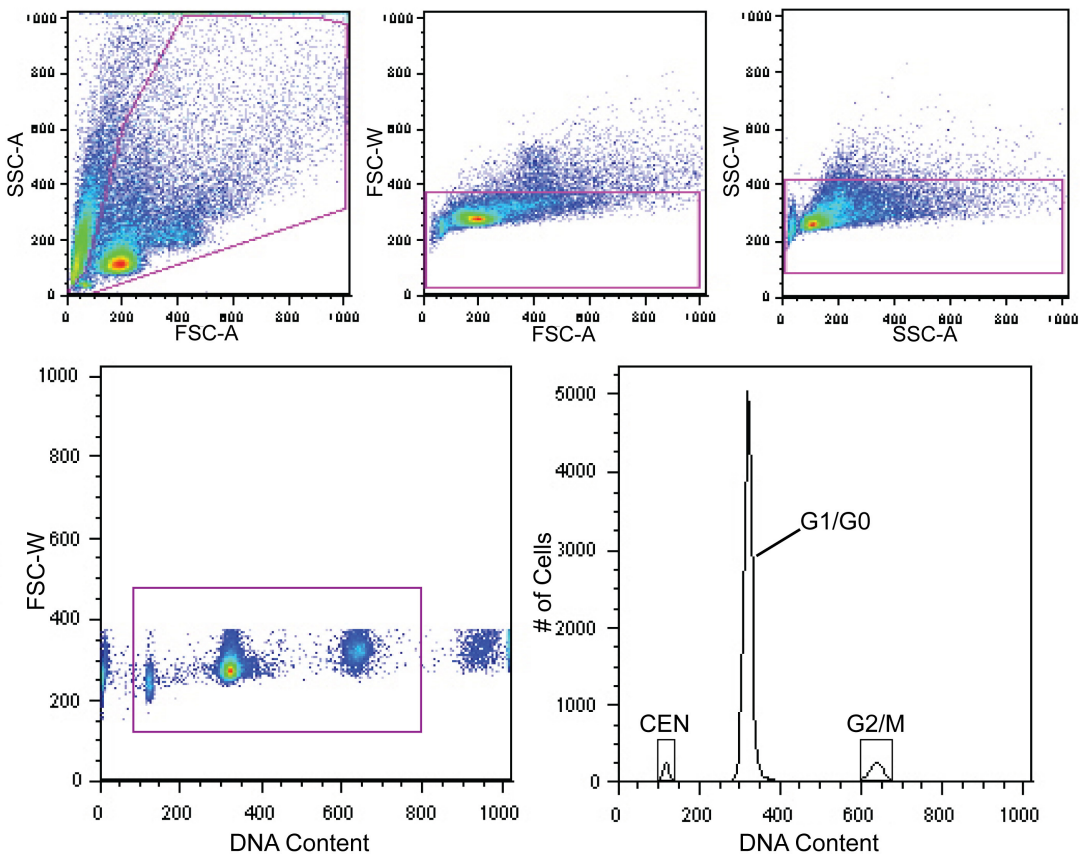

Figure 1.1. Electronic gating for human nuclear samples stained with propidium iodide and analyzed by flow cytometry. Representative human cerebellar nuclear shown here were isolated from postmortem samples, treated with RNase A and stained with propidium iodide for 90 minutes prior to analysis by FCM. Chicken erythrocyte nuclei (CEN) were included as internal controls for cross-sample calibration. Magenta boxes on each dot plot show selection of nuclei populations based on forwards scatter (FSC), a measure of nuclear size, and side scatter (SSC), a measure of nuclear granularity; the upper row of dot plots show doublet elimination. Propidium iodide staining was used to measure DNA content and generate histograms. The G_0/G_1 peak represents the “diploid” (2N) DNA content from which mean DNA content values were obtained.

DNA content analysis of CEN, lymphocytes and nuclei from both non-diseased and AD cerebellum show low DCV, characterized by DNA content histograms with sharp peaks, and narrow bases, superimposable amongst all experiments (**Fig. 1.2 A**). Additionally, non-diseased brain showed increased DCV in cortical nuclei as previously reported [27], with DNA histograms characterized by a broader base (increased range of DNA content) and irregular shapes, including right-hand shoulders or subpeaks (increased net DNA content, leading to a rightward shift of the peak). By comparison, AD cortical samples display markedly more prominent right-hand shifts and increased DCV compared to that found in non-diseased frontal cortical nuclei (**Fig. 1.2 B**). This increased DCV of the AD frontal cortex is particularly striking in histogram overlays of cerebellar and cortical nuclei from the AD brain (**Fig. 1.2 C & D**). These results identify neuroanatomically distinct, somatic changes in AD DCV.

Figure 1.2. DNA content analysis of AD human nuclei by flow cytometry. **A & B**: Representative DNA content histograms for lymphocytes, non-diseased (ND) and Alzheimer's disease (AD) cerebellar (CBL) (**A**) and cortical (CTX) (**B**) nuclei stained with propidium iodide (PI) and analyzed by FCM. Red, blue, black and green histograms are separate individuals in each set; all CTX and CBL samples are from separate brains. Chicken erythrocyte nuclei (CEN) were included as internal calibration controls. Lymphocytes and cerebellar samples from both non-diseased and AD brains demonstrated indistinguishable histograms when overlaid (**A**, left), that appeared qualitatively homogenous when compared side by side (**A**, right). AD cortical histograms showed heterogeneous histograms with broad bases (red) and right-hand shoulders (blue) when overlaid (**B**, left); cortical histogram shapes were distinct for each sample, including non-diseased cortex (**B**, right). **C & D**: Overlays of two sets of AD cerebellar (red) and cortical histograms (blue) identify a prominent area of increased DNA content and more complex histogram shape in each cortex, characterized in **C** by a rightward shift such that the cerebellar and cortical histograms have very little overlap, and in **D** by a broad right-hand shoulder.

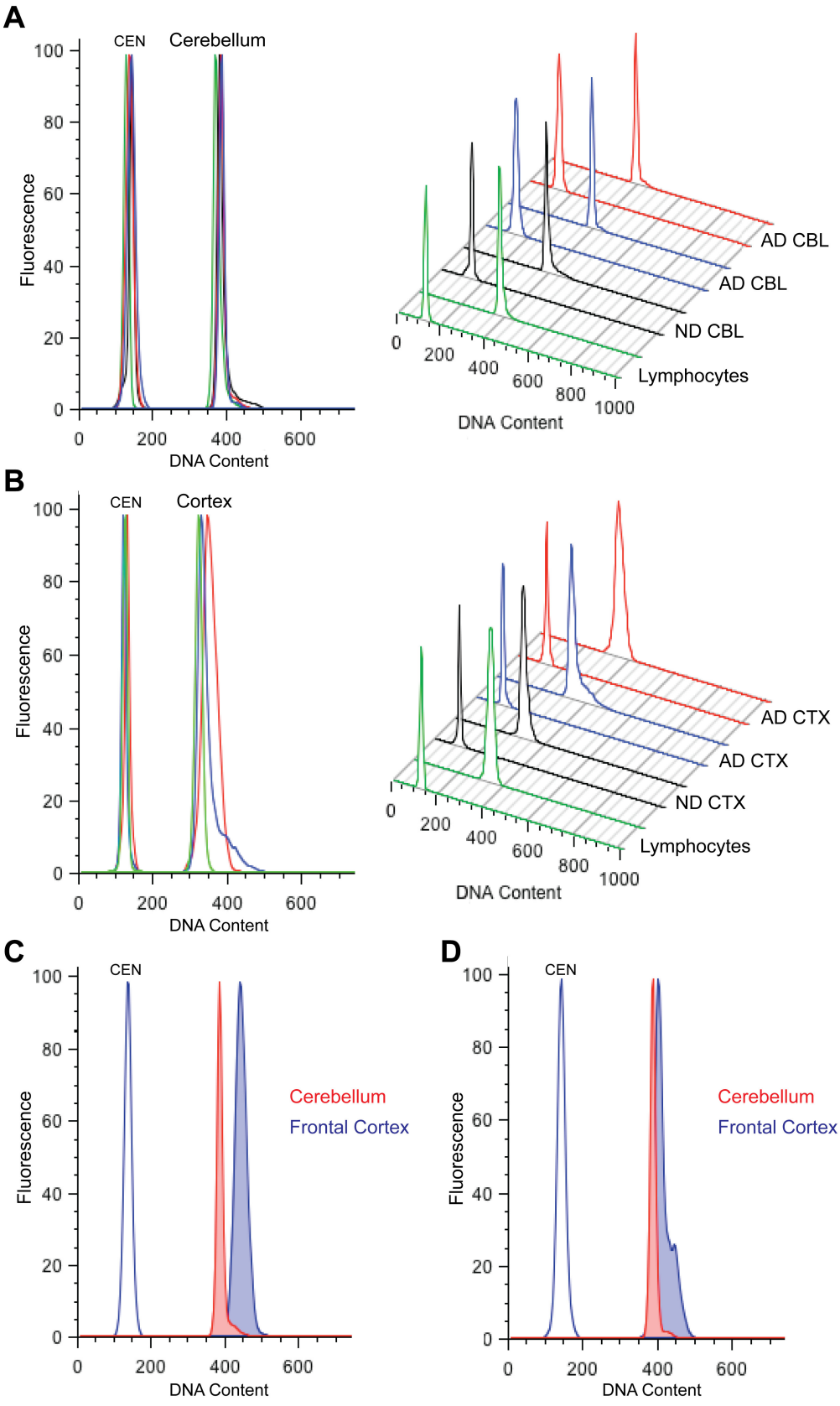
A
CEN
Cerebellum
Fluorescence
DNA Content
AD CBL
AD CBL
ND CBL
Lymphocytes
B
CEN
Cortex
Fluorescence
DNA Content
AD CTX
AD CTX
ND CTX
Lymphocytes
C
CEN
Cerebellum
Frontal Cortex
Fluorescence
DNA Content
D
CEN
Cerebellum
Frontal Cortex
Fluorescence
DNA Content

To quantitate and normalize DNA content comparisons between samples, the DNA Index (DI) [27, 45, 46] was calculated, taking the ratio of the mean of the G_0/G_1 peak to the mean of the lymphocyte control peak, normalized to the mean of the CEN standard (**Fig. 1.3 A**). In AD samples, the mean DI for cortex was 1.06, significantly higher than the cerebellum (0.95) ($P < 0.0001$, one-way ANOVA and Tukey's multiple comparison test) (**Fig. 1.3 B**). AD samples also showed an increased range of DI values (from 0.94 to 1.28) compared to lymphocytes (0.98 to 1.05) -- corresponding to a -6 to 28% percent change in the amount of DNA, and an average increase of ~5%. In a 2N, diploid genome (~6,600Mb), this corresponds to ~330Mb gain, with a range extending up to 1,800Mb. In addition to having a higher average DI and an increased range of DI values, 11 of the 32 AD individuals (>30%) showed a DI of 1.10 or greater, values never observed in non-diseased frontal cortex [27]. AD cortical samples also displayed significantly higher coefficients of variation (CVs) than both AD and non-diseased cerebellum and lymphocytes (**Fig. 1.3 C**), which corresponds to the broad base of the peaks, and the increased range of DI values. To determine whether age correlated with DCV, a linear regression analysis was performed on DI values versus age of the individual for both the AD frontal cortex and cerebellum. No significant correlation was seen between age and DI in brain regions individually (slope of 0.00022, $P = 0.9001$ for a non zero slope for CBL; and slope of -0.00155, $P = 0.1508$ for a non zero slope for CTX) (**Fig. 1.3 D**), nor between age and pooled DI values from all AD brain regions (slope of -0.000014; $P = 0.883$ for a non zero slope) (**Fig. 1.3 E**).

DCV was also analyzed in 14 AD individuals by comparing paired cerebellum and cortical regions from the same individual. Unique histogram shapes displaying broad bases and irregularly shaped peaks were observed for each sample (**Fig. 1.4 A**). All 14 sets of paired samples showed increased cortical DNA compared to cerebellum (**Fig. 1.4 B-D**), which highlights the neuroanatomical differences in DCV found in regions that developed at distinct times and serve distinct functions within a single AD brain. The data support diverse and individually unique DNA changes arising somatically in cells of the AD brain.

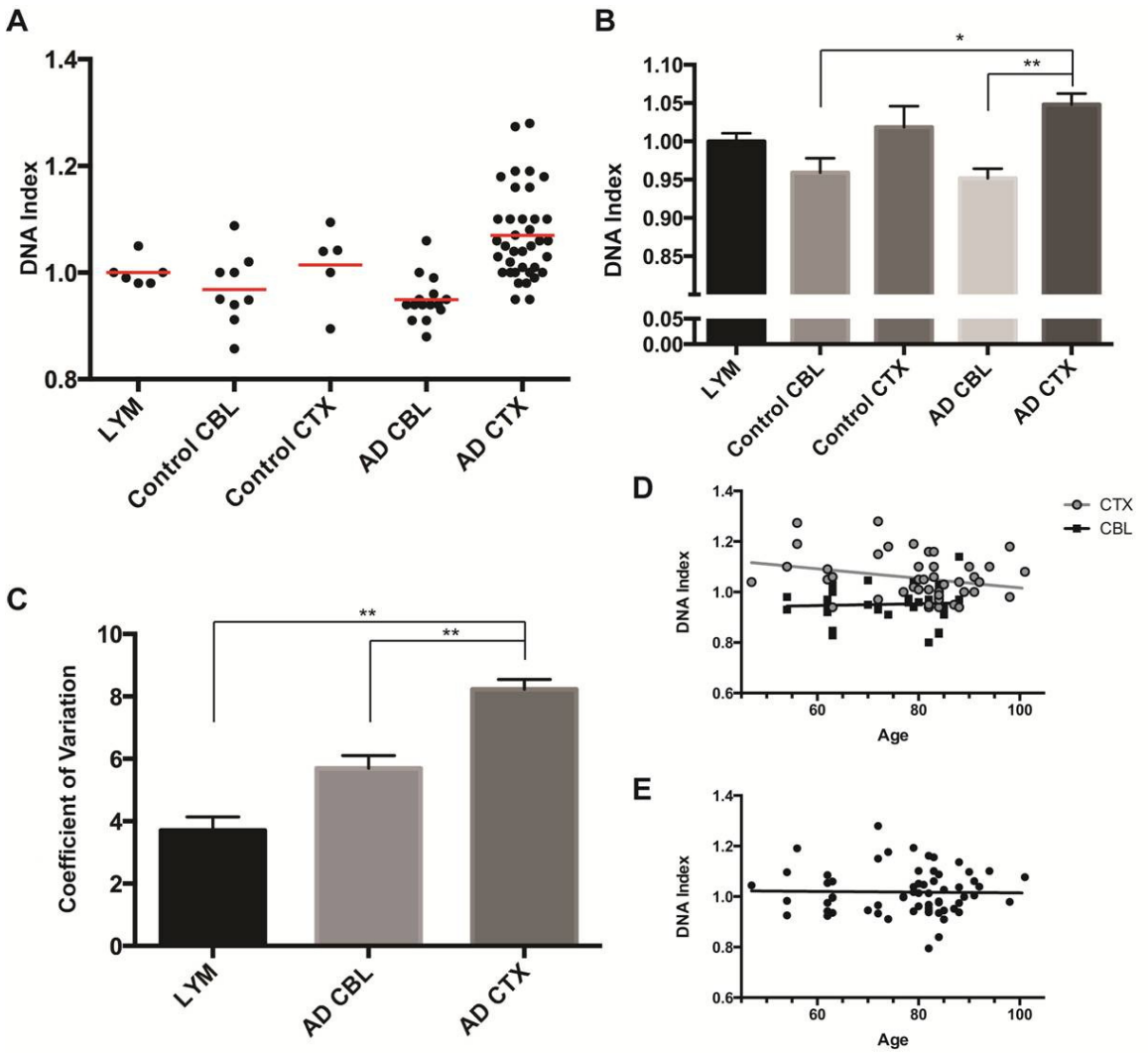

Figure 1.3. Quantitative analysis of DNA content in AD nuclei. **A**: Individual DNA indices (DI) for human lymphocytes (LYM), non-diseased cerebellar (CBL) and cortical (CTX), and AD CBL and CTX samples. The DNA index was calculated as the ratio of the mean DNA content value of brain nuclei to the average of the sex-matched lymphocyte control. Red bars mark the mean DI for each set of samples group. **B**: Mean DI for each sample group (1.0 for lymphocytes, 0.96 for control CBL, 1.04 for control CTX, 0.95 for AD CBL and 1.06 for AD CTX). The AD cortical group had a significantly higher mean DI than either AD CBL or control CBL ($p<0.0001$ and $p<0.001$, respectively; ANOVA and Tukey's multiple comparison test). **C**: Significantly higher coefficient of variation values were seen in AD cortical samples (8.23 mean, 3.06-13.3 range) compared to AD cerebellum (5.69 mean, 2.38-9.75 range) or lymphocyte (3.70 mean, 1.75-5.69 range) samples ($P < 0.0001$). **D**. DNA indices of AD CTX (grey) or CBL (black) samples plotted against age. Linear regression analysis (black lines) showed no correlation between age and DNA index in the AD CTX ($P = 0.1508$ for a non-zero slope) or CBL ($P = 0.9001$ for a non-zero slope). **E**. DNA indices of combined AD CTX and CBL samples plotted against age (samples shown in E are the same samples as in D, but analyzed as a single group). Linear regression analysis (black line) revealed no correlation between age and DNA index when CTX and CBL samples were analyzed as a group ($P = 0.883$ for a non-zero slope).

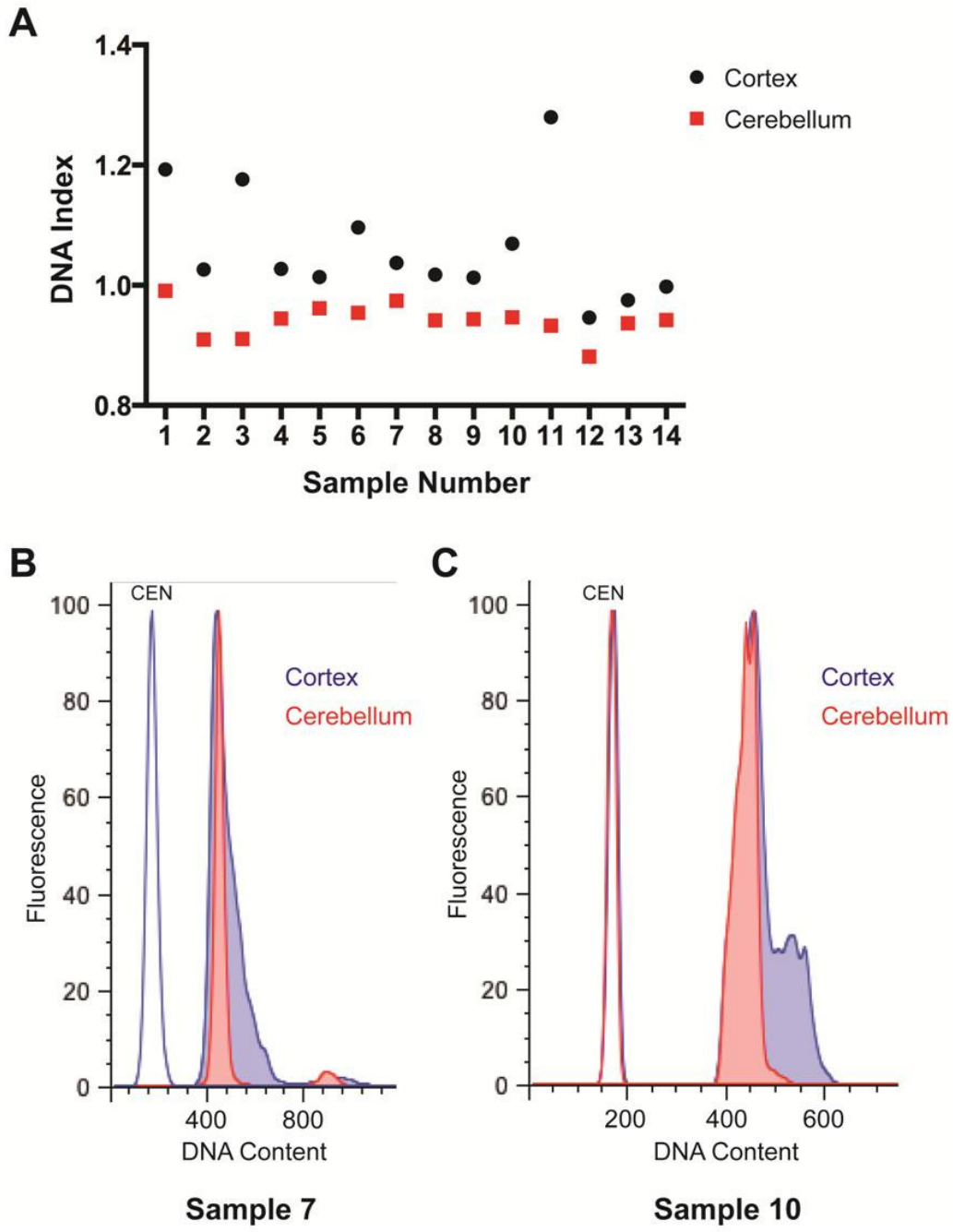

Figure 1.4. DNA content analysis of AD cerebellar and cortical nuclei from the same individuals. **A**. Pairwise analysis of DNA indices in the same AD individual (samples #1-14; each sample represents a unique AD individual) from the cerebellum (red) vs. frontal cortex (black). In all samples, the cortical DI was higher than in the cerebellar DI. **B & C**: Examples of nonidentity between DNA content histograms from cerebellar (red) and cortical (blue) nuclei for individuals #7 (**B**) and #10 (**C**). The cortical sample from individual #7 had a broad peak with nuclei showing increased DNA content (blue shading in **B**). The cortical sample from individual #10 had a prominent right-hand shoulder of nuclei with increased DNA content (blue shading in **C**).

DCV increases occur in neurons of the AD brain

Neurons within the frontal cortex of the non-diseased brain display a significant increase in DNA compared to non-neuronal cell types [27]. To determine whether neurons were also responsible for increased DCV in the AD brain, they were immunolabeled for NeuN (a neuronal nuclear antigen) analysis in conjunction with DNA content FCM (**Fig. 1.5 A**). NeuN+ nuclei showed a right-shifted histogram and increased DCV compared to NeuN- nuclei (**Fig. 1.5 B**). Quantitatively, NeuN+ nuclei from each cortical sample (n = 4) showed a significant increase in average DI, ~8-10% greater than observed in NeuN- cells from the same region (**Fig. 1.5 C**). A comparison of the cortex and the cerebellum of the same individual also showed significantly increased DNA content in cortical versus cerebellar NeuN+ nuclei, quantified using the DI, with increases up to 23% (**Fig. 1.5 D**). These distinctions do not rule out AD-specific affects on the DCV of non-neuronal cells, but implicate neurons as the major cellular locus for increased DNA content.

Figure 1.5. DNA content analysis of NeuN immunolabeled nuclei from the AD frontal cortex and cerebellum. **A**: AD brain nuclei were isolated, immunolabeled for NeuN, and stained with the spectrally distinct DNA dye DRAQ5. All DRAQ5-positive nuclei (upper left panel) were gated on NeuN immunoreactivity (upper right panel); positive and negative NeuN were determined using nuclei stained with secondary antibody only (upper middle panel). Numbers above the gates represent the percentage of nuclei that fall within the gates. **B**: NeuN positive nuclei (red histograms) had higher DNA content than NeuN-negative (black); both populations fell within the ungated DNA content histogram (green shaded histogram). For the two representative AD individuals are shown, each ungated cortical histogram displays characteristic distinct shape: the sample on the left has a prominent right-hand shoulder; the sample on the right has a right-hand subpeak. **C**: Quantitative analysis of the DNA indices of NeuN positive nuclei vs NeuN negative nuclei for the four samples analyzed (NeuN- set to 1.0 as a reference). Every sample (n = 4) shows an increased DNA content in NeuN+ nuclei (grey) with respect to NeuN- nuclei (black), with an average increase of 8% (DNA index of 1.08). **D**: Quantitative analysis of the DNA indices of NeuN+ nuclei from AD cortex vs cerebellum from the same individual (AD cerebellum set to 1.0 as a reference). Within each individual (n = 4), the NeuN+ cortical nuclei (grey) show an increased DNA content relative to NeuN+ cerebellar nuclei (black), with an average increase of 16% (DNA index of 1.16).

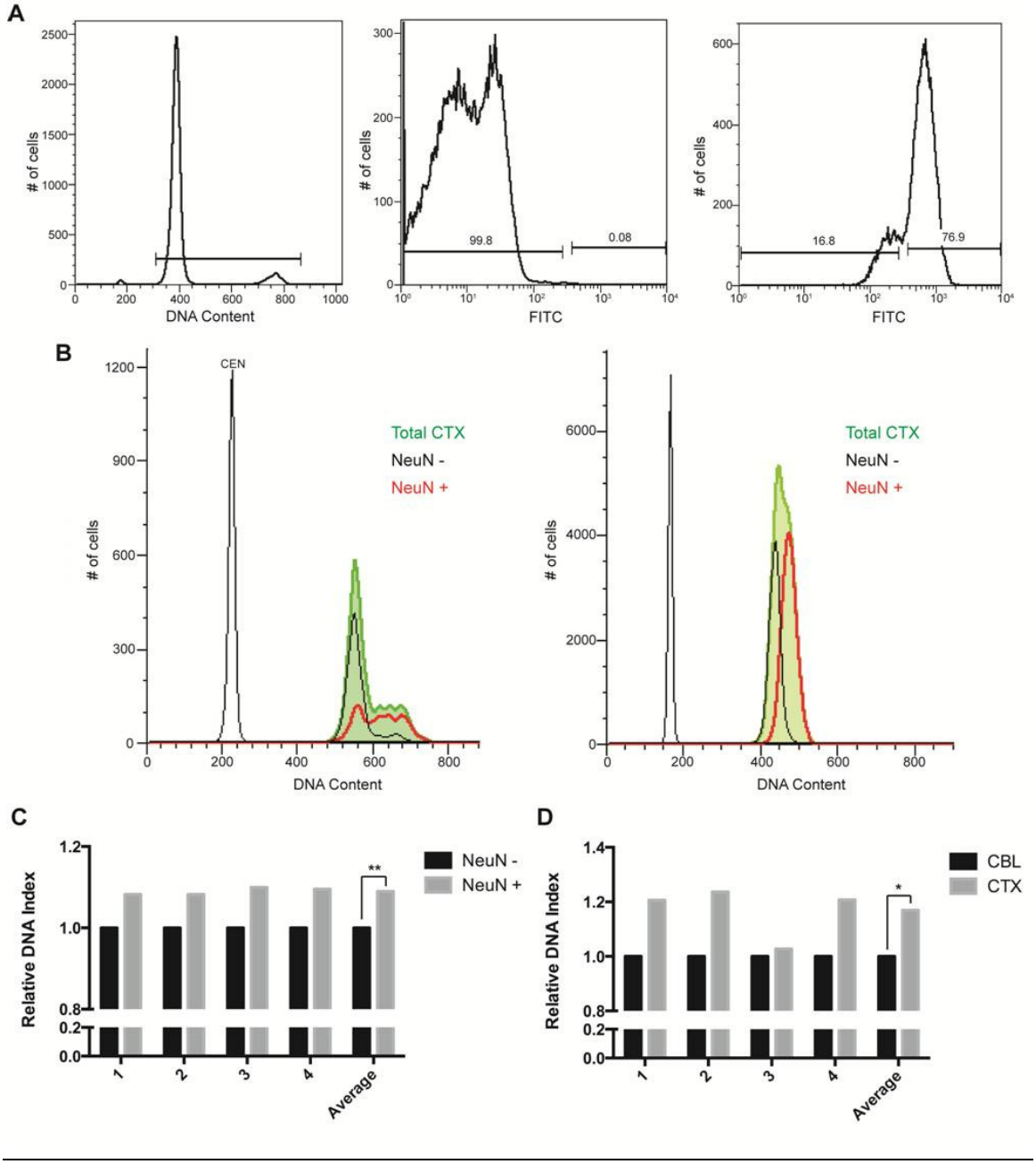
A
# of cells
DNA Content
99.8
0.08
FITC
16.8
76.9
FITC
B
CEN
Total CTX
NeuN -
NeuN +
# of cells
DNA Content
Total CTX
NeuN -
NeuN +
# of cells
DNA Content
C
Relative DNA Index
NeuN -
NeuN +
**
1
2
3
4
Average
D
Relative DNA Index
CBL
CTX
*
1
2
3
4
Average

DCV increases in AD are not clearly associated with trisomy 21

Prior studies have hypothesized that trisomy of chromosome 21, resulting in a triplication of the *APP* gene, contributes to sporadic AD, in view of the neuropathological changes observed in Down syndrome patients [3, 10-12]. To determine whether the increased DCV observed in AD cortices was in part due to trisomy 21, dual FISH point probes (red and green) targeting the *APP* locus on chromosome 21 were used in FISH analyses. Low levels of aneuploidy were detected for each brain sample (n = 8, 4 each AD and non-diseased) (**Fig. 1.6 A**), but no significant difference in aneuploidy was observed in cells from AD brains (1.38% total aneuploidy) versus controls (1.30%) (**Fig. 1.6 B**). Within the low level aneuploidy that was observed in AD samples, monosomy was more common than trisomy (0.83% and 0.55%, respectively). Isolation of cells from the upper 20% of the DNA content histogram also showed no significant difference in chromosome 21 aneuploidy levels (0.70% aneuploidy in upper 20% fraction, 1.09% in total cell fraction) (**Fig. 1.6 C**). The absence of a significant increase in chromosome 21 trisomy, consistent with previous reports of the AD brain [19, 20], suggests that DCV increases in AD involve other chromosomal loci or sub-chromosomal amplification distinct from chromosome 21 trisomy.

AD neurons show mosaic gene amplification of *APP*

Small subpopulations of AD neurons were interrogated for hypothesized sub-chromosomal genomic amplifications; the *APP* locus was targeted in view of its pathogenic validation [3, 10, 11, 47] for assessment by qPCR. Samples of ~75 genomes (0.5 ng of gDNA) were obtained by FACS of isolated nuclei, with gating based on DNA content histograms to collect either the entire G_0/G_1 peak, or subsets of the G_0/G_1 peak such as the right hand shoulder (**Fig. 1.7 A**, denoted CTX HI). Relative copy number was determined using the $2^{-\Delta\Delta Ct}$ method (Methods and Materials), normalizing Ct values to *SEMA4A* and using cerebellum neurons or lymphocytes as the calibrator sample within the run.

Paired cerebellum and cortex samples from non-diseased individuals (n=2) were compared to analogous regions from AD brains (n =7). Nuclei isolated from the frontal cortex of two Down syndrome (trisomy 21) samples were used as a copy number control for duplication of the *APP* locus (**Fig. 1.7 B**). Four of the seven tested AD samples displayed no increases in *APP* copy number compared to controls (data not shown). Three brain samples showed significantly increased *APP* compared to controls, with copy numbers ranging from 2.78 to 11.62 (p values < 0.001, Student's t-test comparing *APP* to *SEMA4A* RCN values for each sample) (**Fig. 1.7 C**). Interestingly, an increase in *APP* signal did not correspond to higher DI values. Repeated qPCR of the same paired AD samples also revealed differences in locus amplification (**Fig. 1.7 D & E**): while some AD samples showed no varied amplification across runs, other samples showed different degrees of amplification (**Fig. 1.7 D**), or amplification in a different nuclear fraction (**Fig. 1.7 E**). Nuclei used for these repeat experiments were isolated from the same tissue sample block (~1cm^3) and processed in an identical manner (standard nuclear isolation and staining with same reagents, flow cytometric sorting with the same machine and settings) by a single individual on two separate days, but contained non-overlapping populations of cells from within the tissue block. The differences observed in the amplification of the *APP* locus are consistent with DCV and genomic mosaicism within these samples.

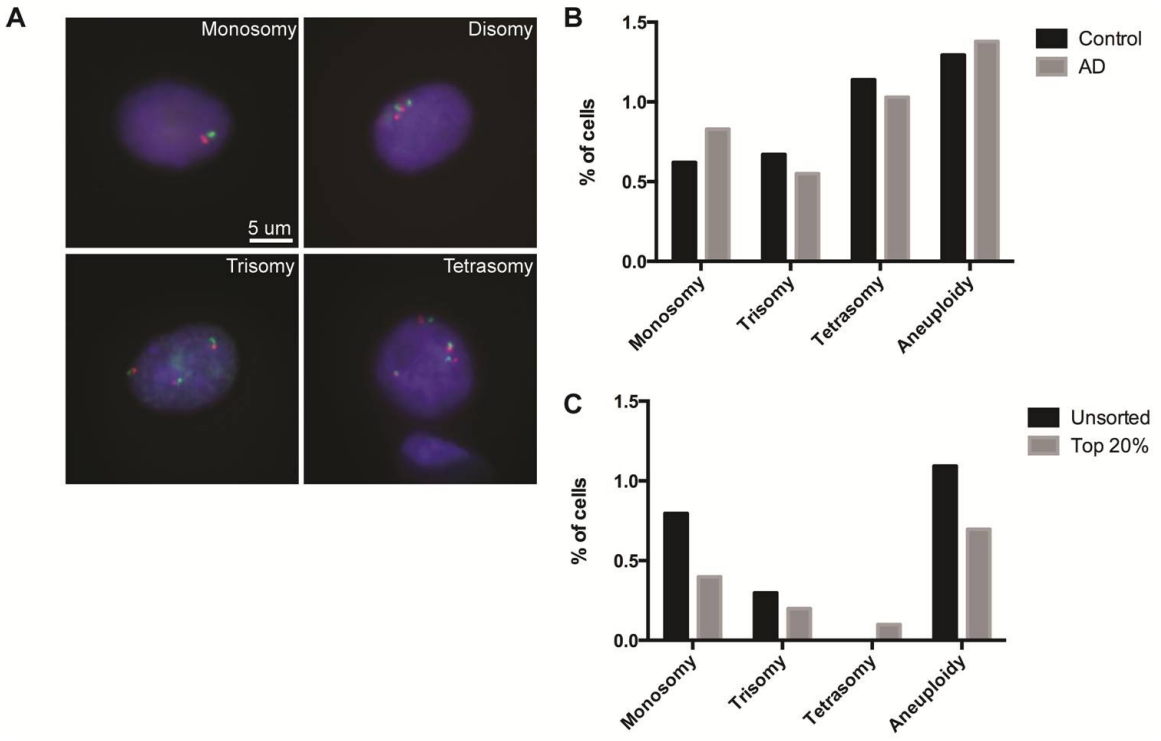

Figure 1.6. Chromosome 21 aneuploidy in the AD frontal cortex. **A**: Representative images of AD cortical nuclei hybridized with chromosome 21 FISH dual point probes (red and green). In each sample analyzes, aneusomic nuclei (nuclei with chr 21 monosomy, trisomy and tetrasomy) were observed, as well as disomic nuclei. Only cells with both colors both probes present were counted to exclude possible hybridization artifacts and pseudo-aneusomic cells. **B**: Comparison of chromosome 21 aneusomy rates in control (non-diseased) and AD cortices (n = 4 samples from each group). No significant differences were observed between total aneuploidy for the control vs. AD nuclei (1.30% vs 1.38%; likewise, no significant differences were seen between types of aneusomy in control vs. AD nuclei (monosomy: 0.62% vs 0.83%; trisomy: 0.67% vs 0.55%; tetrasomy: 1.14% vs 1.03%). **C**. Comparison of chromosome 21 aneusomy in total nuclei vs. the upper 20% of nuclei, gated from a DNA content histogram, for an AD cortical sample. No significant differences were seen between the two nuclei fractions (total aneuploidy rates of 1.09% for unsorted nuclei, 0.70% for upper 20% fraction).

Figure 1.7. Mosaic amplification of the *APP* locus in small neuronal populations from the AD frontal cortex. **A**: Representative gating for cortex (CTX) HI and LO cell populations. The LO fraction is based on the DNA content histogram of the cerebellar nuclei – all cortical nuclei with DNA content overlapping the CBL G_0/G_1 peak fall into this gate. The HI fraction includes nuclei in the cortical DNA content histogram with DNA content greater than that of the cerebellar nuclei. **B**. Comparison of relative copy number of APP in Down syndrome cortical nuclei versus lymphocyte nuclei (used as a calibrator) shows locus-specific amplification of APP (lymphocytes normalized to 2.0 as reference for a diploid cell). Down syndrome nuclei, trisomic for chromosome 21, from two female individuals show 3 copies of APP relative to SEMA4A reference gene and PCDH11X, a gene on the X chromosome, present in 2 copies the diploid genome. **C**: Comparison of relative copy number of APP in cerebellum (CBL) and cortical fractions (CTX LO and CTX HI) from three AD individuals (samples 1-3). APP locus-specific amplification, relative to SEMA4A reference gene (not shown), is shown in each sample; relative copy number values are given below the graph. Amplification was present each cortical fraction. DNA index for each individual cortical sample is listed next to the sample, showing no correlation between DI value and degree of amplification. Cerebellar nuclei were used as a calibrator, normalized to 2.0 for a diploid cell; within samples, APP amplification is relative to the SEMA4A reference gene (not shown). **D & E**: Comparison of relative copy number of APP from two sets of nuclei isolated from the same individual (sample 1 & 3 from **C**). Samples show variation across runs, with different degrees of amplification detected between nuclei sets (sample 3, **D**) and amplification in a different DNA content-based fraction (sample 1, **E**). Relative copy number values are given below each graph. As above, cerebellar nuclei were used as a calibrator; APP amplification in each fraction is relative to SEMA4A reference gene (not shown). Error bars for all graphs represent the 95% confidence intervals for each sample and assay, determined by multiplying the standard error of the mean for each sample by the critical t value for a two tailed t-distribution with p=0.05.

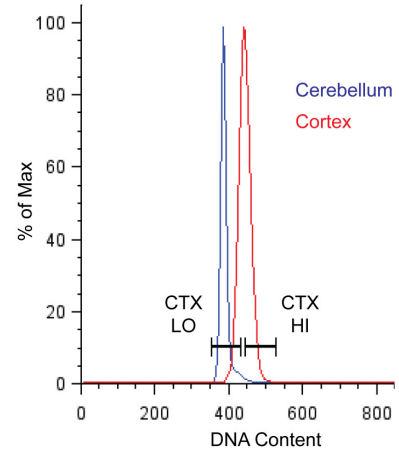

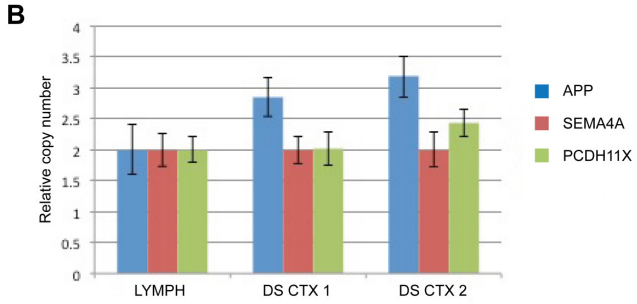

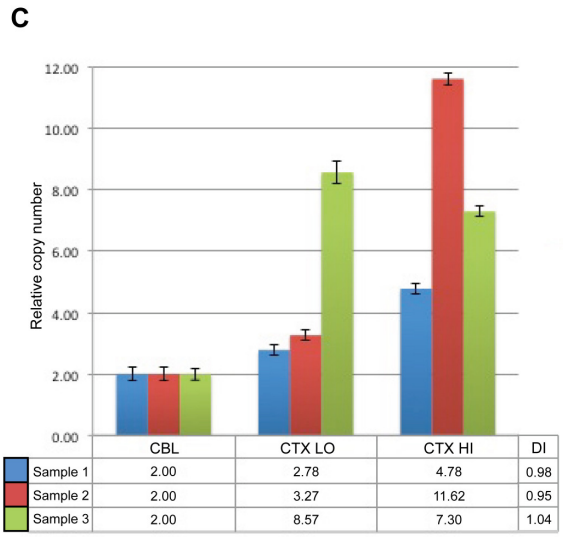

	CBL	CTX LO	CTX HI	DI
Sample 1	2.00	2.78	4.78	0.98
Sample 2	2.00	3.27	11.62	0.95
Sample 3	2.00	8.57	7.30	1.04

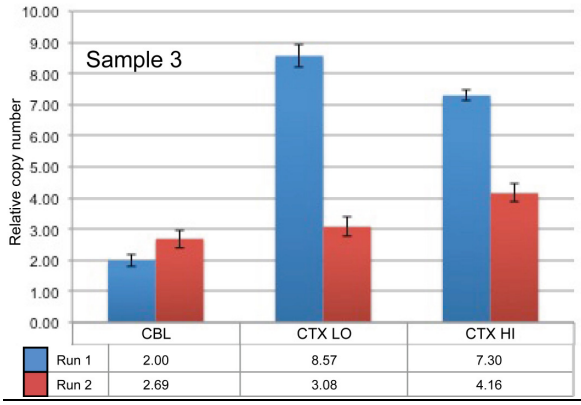

	CBL	CTX LO	CTX HI
Run 1	2.00	8.57	7.30
Run 2	2.69	3.08	4.16

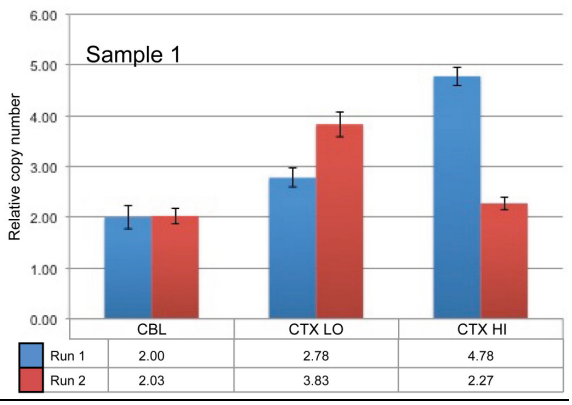

	CBL	CTX LO	CTX HI
Run 1	2.00	2.78	4.78
Run 2	2.03	3.83	2.27

APP locus amplification in single AD neurons

To evaluate population mosaicism formally, single cell analyses were pursued, interrogating the *APP* locus in 118 single neuronal nuclei. Samples from paired AD (n = 3 individuals, total of 49 CTX and 38 CBL nuclei) or non-diseased (n = 1, 7 CTX and 10 CBL nuclei analyzed) cortex and cerebellum were analyzed for relative copy number compared to Down syndrome cortex (14 nuclei total) that was used as a copy number control. For each sample, the difference in signal between a target gene, either $APP_{(exon\ 16)}$ or $APP_{(exon\ 5)}$, and the reference gene (*SEMA4A*) was analyzed by unpaired, two-tailed t-test; nuclei with <1 copy were excluded. Representative nuclei with significant differences in *APP* exon copy number (both losses and gains) are shown (**Fig. 1.8 A**). AD cortical nuclei showed a mean of 3.36 copies (**Fig. 1.8 B**), compared to the mean for the AD cerebellar nuclei of 2.25 copies. Greater than 50% of AD cortical nuclei displayed copy number gains, with 35% of these nuclei having a copy number of 4 or more, while over 50% of AD cerebellar nuclei have the normal 2 copies (**Table 1.4**).

Table 1.4. Frequency of APP locus loss and gain in Alzheimer's and Down syndrome neurons.

Sample	Assay	Cells with Losses	%	Cells with no change	%	Cells with Gains	%	Total Cell Number
AD CTX								
	APP16	5	12.5	10	25.0	25	62.5	40
	APP5	7	16.3	14	32.6	22	55.0	43
AD CBL								
	APP16	7	21.9	17	53.1	8	25.0	32
	APP5	7	25.0	15	53.6	6	21.4	28
DS CTX								
	APP16	1	7.7	2	15.4	10	76.9	13
	APP5	0	0.0	2	20.0	8	80.0	10

Nuclei from the AD cortex show an increased range of RCN values (0.75 to 12.4) compared to other groups (high RCN of 6.10 in AD CBL, 4.26 in non-diseased CTX, 5.84 in non-diseased CBL) (**Fig. 1.8 B**), which corresponds to the increased range of DI values from DNA content flow cytometry. Nuclei from a Down syndrome cortex have a mean of 3.07 copies, consistent with a

trisomy of chromosome 21, but several cells do display duplications or losses (RCN values range from 1 to 5), further evidence of the genomic variability within the brain. Interestingly, the non-diseased cerebellum and cortex have group means of 3.16 and 2.65, respectively; these higher-than-expected RCN values, particularly in the cerebellum, may simply be reflective of the small number of cells represented. Difference observed between the two *APP* assays may indicate that there exists an unidentified systematic error that impaired the accuracy of one or both assays for the particular sample; errors in small volume pipetting and DNA concentration are controlled for with the use of reference gene normalization. Alternatively, these differences may reflect partial-locus duplication or deletion; deep sequencing technologies would be necessary to assess this possibility.

Figure 1.8. *APP* locus amplification in single neurons from the AD cortex. **A**: Relative copy numbers of APP exons 5 and 16 from representative single nuclei isolated from the cerebellum (CBL) and cortex (CTX) of Down syndrome (DS) and AD brains show both losses and gains of the APP locus. For each nuclei shown, the relative copy number for both exon 16 and exon 5 of APP is significantly different than the SEMA4A 2-copy reference gene (not shown) ($p<0.05$ for all comparisons of APP exon 16 vs SEMA 4A and APP exon 5 vs SEMA4A, Student's t-test). Down syndrome nuclei were included as a copy number control, with 3 copies of the APP locus expected due to trisomy of chromosome 21. Error bars represent the 95% confidence intervals for each sample and assay, determined by multiplying the standard error of the mean for each sample by the critical t value for a two tailed t-distribution with $p=0.05$. Horizontal orange bars represent the 95% confidence intervals for each copy number (1-6), determined from an assumed system standard deviation of 0.25; these modeled CIs were used to determine the copy numbers for each gene assay in each nucleus. **B**: Relative copy number (RCN) of the APP exon 16 assay for each individual nucleus examined, grouped by the type of sample (AD cortex and cerebellum, non-diseased (ND) cortex and cerebellum, Down syndrome cortex). Red bars represent the mean relative copy number for each group: AD CTX mean RCN of 3.36 (range of 0.75 to 12.4); AD CBL mean of 2.25 (range of 0.99 to 6.10); ND CTX mean of 2.65 (range of 1.44 to 4.26); ND CBL mean of 3.16 (range of 1.20 to 5.84); and DS mean of 3.07 (range of 1.21 to 5.34).

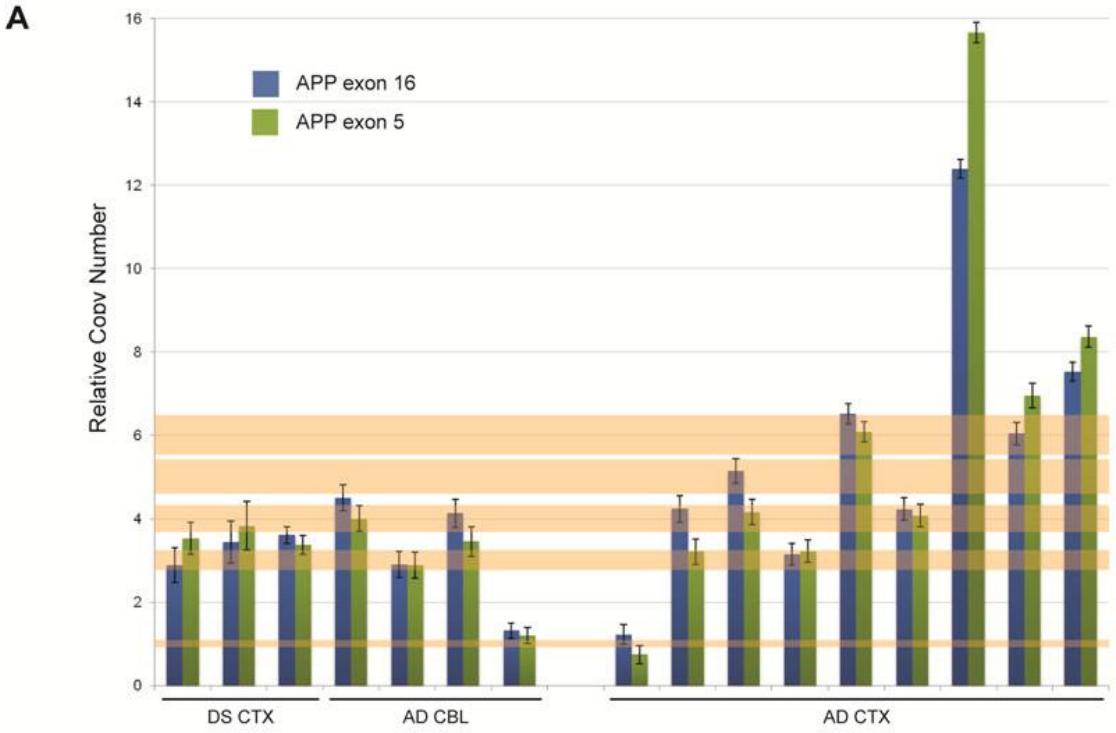
A
APP exon 16
APP exon 5
Relative Copy Number
0
2
4
6
8
10
12
14
16
DS CTX
AD CBL
AD CTX

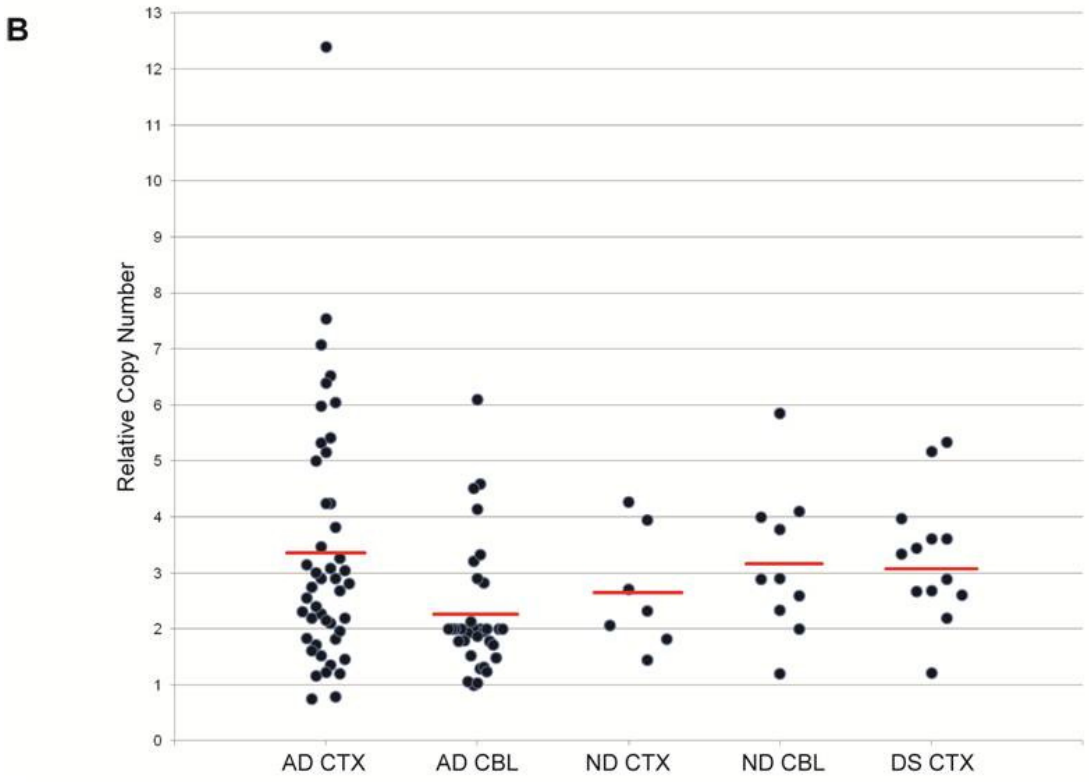
B
Relative Copy Number
0
1
2
3
4
5
6
7
8
9
10
11
12
13
AD CTX
AD CBL
ND CTX
ND CBL
DS CTX

Discussion

DNA content variation is an unusual and unexpected characteristic of the human frontal cortex, yet is consistent with reports of genomic heterogeneity in the central nervous system. Here we present evidence of increased DCV in a disease setting: the frontal cortices of sporadic AD cases have a dramatic increase in DCV compared not only to lymphocytes and non-diseased controls, but also between neuroanatomical regions of the same individual's brain. This increase in DCV, characterized by DNA content histograms with prominent right-hand shifts and broad bases, corresponds to genomic gains averaging ~330 MB and ranging up to 1800 MB. It is important to note that this gain of DNA, representing over a quarter of the genome, is unambiguously less than a 4N tetraploid genome (~13,200Mb); 4N populations were easily distinguishable by FCM. Exploration of the source of the sub-genomic increase using the advanced sensitivity and accuracy of the Fluidigm Biomark microfluidic qPCR system identified mosaic copy number variation in the disease-related *APP* locus, suggesting a role for DCV in AD pathology.

The significant increase in DCV in the AD brain was only observed in the frontal cortex, one of the first regions affected by Aβ plaque formation and neuronal cell death in AD [33, 34, 48], suggesting a connection between changes in DNA content in the frontal cortex and other neuropathological traits of AD. Amyloid plaque development in the cerebellum, which shows low DCV, only occurs late in disease progression [33, 49]. Intriguingly, neuronal populations of AD cortices exhibit the most striking DCV. This population is particularly susceptible to cell death in AD due to the neurotoxic effects of Aβ [2, 50], but the death of cortical neurons in AD seems to unmask a set of neurons with previously unrecognized genomic variability. Whether an increase in DCV could bestow some protective effect, giving high DCV cells a survival advantage in the disease landscape, is unclear. Determining the positioning of these surviving neurons within the neocortical layers, as well as evaluating the proximity and connectivity of these cells to Aβ plaques is critical in assessing whether DCV may promote survival or contribute to AD pathology. A related line of inquiry into the observed increase in DCV in non-diseased cortices could

distinguish if DCV serves as a harbinger of neurodegenerative processes that have not yet manifested as clinical signs.

The role of *APP* in AD neurodegeneration has been extensively examined. Early seminal studies failed to detect evidence of *APP* trisomy or duplication in AD using classical Southern blot techniques [19, 20]. Our FISH data are consistent with these observations, suggesting that significant changes in whole chromosome 21 aneuploidy rates do not occur in AD brains. However, these results do not exclude the potential for sub-chromosomal genomic changes, as these approaches would not be able to detect somatic mosaic changes in genomic loci, particularly at the single cell level. The existence of genomic mosaicism, manifested here as increased DCV in AD, suggests that should it occur, genomic amplification of the *APP* locus might be detectable in small populations of neurons by more sensitive techniques, including qPCR.

Dual qPCR approaches revealed prominent copy number variations of the *APP* locus in AD frontal cortex. Quantitative PCR on small populations of cells, combining 75 genomes-worth of DNA, allowed for the detection of an averaged increase in the gene locus, but did not address the degree to which the locus may be amplified in an individual cell. Two major possibilities could account for an increased *APP* copy number within a population. First, the majority of the cells in the population may have small sub-genomic increases in DNA, such as a germline gene amplification, leading to an increased average copy number. The second possibility is that the majority of cells have the expected copy number of 2, with a few cells having an extreme somatic increase in gene dosage, creating a mosaic effect and leading to the average increase observed. While either possibility would create the right-shifted DNA content histograms observed, our qPCR data support the latter. Observed differences in the level of amplification, along with cell populations showing amplification from the same individual, suggest that there may exist “hot spots” within regions of the same brain that have a higher proportion of cells with increased DCV. If the majority of cells had small subgenomic changes or germline genomic amplification, these differences between cells from different regions would not be detected.

Single cell qPCR analysis allowed us to delve deeper into the degree of *APP* amplification in individual nuclei from each brain region, as the generation of high numbers of replicate data points on the IFC system allowed for improved quantitative resolution between copy numbers to an extent not possible by conventional qPCR thermocyclers [38, 41]. This approach revealed a wide range of *APP* copy numbers – both losses and gains – in nuclei from the AD cortex, and a gain of at least one copy in the majority of nuclei interrogated. Of the nuclei with gains, 35% showed more than 4 copies of *APP*. While the number of nuclei sampled represents a tiny fraction compared to the number of cells in the human brain, the random selection of so many nuclei with altered *APP* copy number evinces the genomic variability of the AD cortex and can help to explain the increased DCV observed in these samples. It is important to note that while the AD cerebellum did show *APP* CNVs, this is not inconsistent with the low level of DCV observed for this region by DNA content FCM. The cerebellum displayed a decreased copy number range compared to the cortex, with only 13% having 4 or more copies, and no cells with more than 6 copies of *APP* were detected. As the majority of cells assessed showed 2 copies, cells with aberrant copy number would be averaged out in the histogram. A larger cohort of single cells from the non-diseased cortex is needed to establish the extent of copy number variation in this region relative to the documented DCV [27].

An increase in *APP* in the AD cortex ties into the amyloid cascade hypothesis of Alzheimer's, which hypothesizes that the aggregation of the Aβ cleavage peptide $A\beta_{1-42}$ into senile plaques also triggers an inflammatory response mediated by microglia and astrocytes, prompts Tau neurofibrillary tangle formation, and leads to neuronal cell death [2, 51]. The mosaic nature of the CNV observed in this study may provide an important link between the amyloid hypothesis and the later onset of sporadic AD. Cells with varying copy numbers of *APP* could produce similarly varying amounts of protein aggregate. In the healthy brain, those cells with increased gene dosage could be compensated for, but once a certain amount of amyloid aggregation occurs – leading to local cell death – the effects of gene dosage might tip the system over the disease threshold.

These findings do not discount other hypotheses of AD, and could prove a connection between the amyloid cascade hypothesis and others, such as the pathogenic cell cycle hypothesis, in which mature, fully differentiated neurons are thought to reenter the cell cycle [52-58]. Prior literature on aberrant cell-cycle changes and a range of DNA-altering enzymes support postnatal DNA synthesis mechanisms relevant to increasing DCV. Cell cycle re-entry in the brain is not thought to reach completion of metaphase and cell division, instead terminating after S phase [59-61]. Increased copy number of *APP* and other loci could be a result of DNA replication before cell termination. While cell cycle re-entry and DNA synthesis would explain the rightward shift in cortical DNA content histograms, with a large set of neurons entering S phase shifting the mean DNA content peak, the increased DCV of non-diseased cortices (without a resulting disease state) is not well-suited to this theory. New studies suggest a mechanism by which AB and Tau instigate cell cycle re-entry, independent of their incorporation into plaques and tangles [58]; in this sequence of events the *APP* locus amplification observed here that contributes to DCV in AD brains could play critical pathogenic role in AD onset.

Alternatively, and non-mutually exclusively, copy number variation could arise during neurogenesis. Mosaic genomic changes including aneuploidy are recognized occurrences in cells found in both the human cortex and cerebellum, as well as in neural progenitor cells in mice and in human neuronal stem cells in culture. Emerging stem cell technologies, including the reprogramming of patient fibroblasts into pluripotent stem cells and neurons, could allow researchers to determine when DCV arises, elucidate differences in DCV-generating mechanisms between disease and non-diseased states, and determine the sequence of pathological triggers in diseases like AD (as discussed above). Continuing exploration of single cell genomic mosaicism from different brain areas may lead to the identification of other amplified regions which could have positive or negative effects in disease [62] (through both loss and gain of genetic loci) and may potentially help to establish therapies preventing pathogenic DCV.

We would like to thank the Flow Cytometry Core operator at The Scripps Research Institute, particularly Cody Fine and Betsy Razner, for their assistance with flow cytometric analysis and fluorescent cell sorting. We would like to thank Uma Dandekar and Hemani Wijesuriya at the University of California, Los Angeles Genotyping and Sequencing core for their aid with Fluidigm Biomark experimental design. We would like to thank Caroline Dando and Susan Robelli of Fluidigm for their technical assistance. We would like to thank Geoff Weiner for his assistance developing qPCR assays, Kristen Carney and Hope Mirendil for statistical advice, and Hope Mirendil and Danielle Jones for editing assistance.

Chapter 1, in part, is currently being prepared for submission for publication of this material. The dissertation author was the primary investigator and author of this material. Willem Westra and Yun C. Yung assisted with the design of the project, performed flow cytometric data collection and analysis, and FISH analyses. Jerold Chun supervised the project and provided advice.

References

[1] World Alzheimer Report. In: Prince M, Jackson J, editors. London: Alzheimer's Disease International; 2009.

[2] Hardy J, Selkoe DJ. The amyloid hypothesis of Alzheimer's disease: progress and problems on the road to therapeutics. Science 2002;297:353-6.

[3] Glenner GG, Wong CW. Alzheimer's disease and Down's syndrome: sharing of a unique cerebrovascular amyloid fibril protein. Biochem Biophys Res Commun 1984;122:1131-5.

[4] Gatz M, Reynolds CA, Fratiglioni L, Johansson B, Mortimer JA, Berg S, et al. Role of genes and environments for explaining Alzheimer disease. Arch Gen Psychiatry 2006;63:168-74.

[5] Bertram L, Lill CM, Tanzi RE. The genetics of Alzheimer disease: back to the future. Neuron 2010;68:270-81.

[6] Kingsbury MA, Yung YC, Peterson SE, Westra JW, Chun J. Aneuploidy in the normal and diseased brain. Cell Mol Life Sci 2006;63:2626-41.

[7] Goldgaber D, Lerman MI, McBride OW, Saffiotti U, Gajdusek DC. Characterization and chromosomal localization of a cDNA encoding brain amyloid of Alzheimer's disease. Science 1987;235:877-80.

[8] St George-Hyslop PH, Tanzi RE, Polinsky RJ, Haines JL, Nee L, Watkins PC, et al. The genetic defect causing familial Alzheimer's disease maps on chromosome 21. Science 1987;235:885-90.

[9] Tanzi RE, Gusella JF, Watkins PC, Bruns GA, St George-Hyslop P, Van Keuren ML, et al. Amyloid beta protein gene: cDNA, mRNA distribution, and genetic linkage near the Alzheimer locus. Science 1987;235:880-4.

[10] Masters CL, Multhaup G, Simms G, Pottgiesser J, Martins RN, Beyreuther K. Neuronal origin of a cerebral amyloid: neurofibrillary tangles of Alzheimer's disease contain the same protein as the amyloid of plaque cores and blood vessels. EMBO J 1985;4:2757-63.

[11] Potter H. Review and hypothesis: Alzheimer disease and Down syndrome--chromosome 21 nondisjunction may underlie both disorders. Am J Hum Genet 1991;48:1192-200.

[12] Wisniewski HM, Wrzolek M. Pathogenesis of amyloid formation in Alzheimer's disease, Down's syndrome and scrapie. Ciba Found Symp 1988;135:224-38.

[13] Rovelet-Lecrux A, Hannequin D, Raux G, Le Meur N, Laquerriere A, Vital A, et al. APP locus duplication causes autosomal dominant early-onset Alzheimer disease with cerebral amyloid angiopathy. Nat Genet 2006;38:24-6.

[14] Blom ES, Viswanathan J, Kilander L, Helisalmi S, Soininen H, Lannfelt L, et al. Low prevalence of APP duplications in Swedish and Finnish patients with early-onset Alzheimer's disease. Europ J Hum Genet 2008;16:171-5.

[15] McNaughton D, Knight W, Guerreiro R, Ryan N, Lowe J, Poulter M, et al. Duplication of amyloid precursor protein (APP), but not prion protein (PRNP) gene is a significant cause of early onset dementia in a large UK series. Neurobiol Aging 2012;33:426 e13-21.

[16] Hooli BV, Mohapatra G, Mattheisen M, Parrado AR, Roehr JT, Shen Y, et al. Role of common and rare APP DNA sequence variants in Alzheimer disease. Neurology 2012;78:1250-7.

[17] Prasher VP, Farrer MJ, Kessling AM, Fisher EM, West RJ, Barber PC, et al. Molecular mapping of Alzheimer-type dementia in Down's syndrome. Ann Neurol 1998;43:380-3.

[18] Jonsson T, Atwal JK, Steinberg S, Snaedal J, Jonsson PV, Bjornsson S, et al. A mutation in APP protects against Alzheimer's disease and age-related cognitive decline. Nature 2012;488:96-9.

[19] St George-Hyslop PH, Tanzi RE, Polinsky RJ, Neve RL, Pollen D, Drachman D, et al. Absence of duplication of chromosome 21 genes in familial and sporadic Alzheimer's disease. Science 1987;238:664-6.

[20] Tanzi RE, Bird ED, Latt SA, Neve RL. The amyloid beta protein gene is not duplicated in brains from patients with Alzheimer's disease. Science 1987;238:666-9.

[21] Podlisny MB, Lee G, Selkoe DJ. Gene dosage of the amyloid beta precursor protein in Alzheimer's disease. Science 1987;238:669-71.

[22] Rehen SK, Yung YC, McCreight MP, Kaushal D, Yang AH, Almeida BS, et al. Constitutional aneuploidy in the normal human brain. J Neurosci 2005;25:2176-80.

[23] Yurov YB, Iourov IY, Monakhov VV, Soloviev IV, Vostrikov VM, Vorsanova SG. The variation of aneuploidy frequency in the developing and adult human brain revealed by an interphase FISH study. J Histochem Cytochem 2005;53:385-90.

[24] Yurov YB, Iourov IY, Vorsanova SG, Liehr T, Kolotii AD, Kutsev SI, et al. Aneuploidy and confined chromosomal mosaicism in the developing human brain. PLoS ONE 2007;2:e558.

[25] Pack SD, Weil RJ, Vortmeyer AO, Zeng W, Li J, Okamoto H, et al. Individual adult human neurons display aneuploidy: detection by fluorescence in situ hybridization and single neuron PCR. Cell Cycle 2005;4:1758-60.

[26] Iourov IY, Vorsanova SG, Liehr T, Yurov YB. Aneuploidy in the normal, Alzheimer's disease and ataxia-telangiectasia brain: differential expression and pathological meaning. Neurobiol Dis 2009;34:212-20.

[27] Westra JW, Rivera RR, Bushman DM, Yung YC, Peterson SE, Barral S, et al. Neuronal DNA content variation (DCV) with regional and individual differences in the human brain. J Comp Neurol 2010;518:3981-4000.

[28] Fischer HG, Morawski M, Bruckner MK, Mittag A, Tarnok A, Arendt T. Changes in neuronal DNA content variation in the human brain during aging. Aging Cell 2012.

[29] Evrony GD, Cai X, Lee E, Hills LB, Elhosary PC, Lehmann HS, et al. Single-neuron sequencing analysis of l1 retrotransposition and somatic mutation in the human brain. Cell 2012;151:483-96.

[30] Baillie JK, Barnett MW, Upton KR, Gerhardt DJ, Richmond TA, De Sapio F, et al. Somatic retrotransposition alters the genetic landscape of the human brain. Nature 2011;479:534-7.

[31] Muotri AR, Chu VT, Marchetto MC, Deng W, Moran JV, Gage FH. Somatic mosaicism in neuronal precursor cells mediated by L1 retrotransposition. Nature 2005;435:903-10.

[32] Peterson SE, Westra JW, Paczkowski CM, Chun J. Chromosomal mosaicism in neural stem cells. Methods Mol Biol 2008;438:197-204.

[33] Braak H, Braak E. Neuropathological stageing of Alzheimer-related changes. Acta Neuropathol (Berl) 1991;82:239-59.

[34] Braak H, Braak E, Bohl J. Staging of Alzheimer-related cortical destruction. Eur Neurol 1993;33:403-8.

[35] Fan HC, Quake SR. Detection of aneuploidy with digital polymerase chain reaction. Anal Chem 2007;79:7576-9.

[36] Jones MA, Bhide S, Chin E, Ng BG, Rhodenizer D, Zhang VW, et al. Targeted polymerase chain reaction-based enrichment and next generation sequencing for diagnostic testing of congenital disorders of glycosylation. Genet Med 2011;13:921-32.

[37] Qin J, Jones RC, Ramakrishnan R. Studying copy number variations using a nanofluidic platform. Nucleic Acids Res 2008;36:e116.

[38] Whale AS, Huggett JF, Cowen S, Speirs V, Shaw J, Ellison S, et al. Comparison of microfluidic digital PCR and conventional quantitative PCR for measuring copy number variation. Nucleic Acids Res 2012;40:e82.

[39] White AK, VanInsberghe M, Petriv OI, Hamidi M, Sikorski D, Marra MA, et al. High-throughput microfluidic single-cell RT-qPCR. Proc Natl Acad Sci U S A 2011;108:13999-4004.

[40] Dube S, Mir A, Jones RC, Ramakrishnan R, Sun G. Computation of Maximal Resolution of Copy Number variation on a nanofluidic device using digital PCR. South San Francisco, CA: Fluidigm Corporation; 2008.

[41] Weaver S, Dube S, Mir A, Qin J, Sun G, Ramakrishnan R, et al. Taking qPCR to a higher level: Analysis of CNV reveals the power of high throughput qPCR to enhance quantitative resolution. Methods 2010;50:271-6.

[42] D'Haene B, Vandesompele J, Hellemans J. Accurate and objective copy number profiling using real-time quantitative PCR. Methods 2010;50:262-70.

[43] Livak KJ, Schmittgen TD. Analysis of relative gene expression data using real-time quantitative PCR and the 2(-Delta Delta C(T)) Method. Methods 2001;25:402-8.

[44] Pfaffl MW. A new mathematical model for relative quantification in real-time RT-PCR. Nucleic Acids Res 2001;29:e45.

[45] Darzynkiewicz Z, Huang X. Analysis of cellular DNA content by flow cytometry. Curr Protoc Immunol 2004;Chapter 5:Unit 5 7.

[46] Darzynkiewicz Z, Juan G, Srour EF. Differential staining of DNA and RNA. Curr Protoc Cytom 2004;Chapter 7:Unit 7 3.

[47] Sawa A. Alteration of gene expression in Down's syndrome (DS) brains: its significance in neurodegeneration. J Neural Transm Suppl 2001:361-71.

[48] Braak H, Braak E, Bohl J, Bratzke H. Evolution of Alzheimer's disease related cortical lesions. J Neural Transm Suppl 1998;54:97-106.

[49] Thal DR, Capetillo-Zarate E, Del Tredici K, Braak H. The development of amyloid beta protein deposits in the aged brain. Sci Aging Knowledge Environ 2006;2006:re1.

[50] Schubert D, Cole G, Saitoh T, Oltersdorf T. Amyloid beta protein precursor is a mitogen. Biochem Biophys Res Commun 1989;162:83-8.

[51] Herrup K. Reimagining Alzheimer's disease--an age-based hypothesis. J Neurosci 2010;30:16755-62.

[52] Bonda DJ, Bajic VP, Spremo-Potparevic B, Casadesus G, Zhu X, Smith MA, et al. Review: cell cycle aberrations and neurodegeneration. Neuropathol Appl Neurobiol 2010;36:157-63.

[53] Hernandez-Ortega K, Ferrera P, Arias C. Sequential expression of cell-cycle regulators and Alzheimer's disease-related proteins in entorhinal cortex after hippocampal excitotoxic damage. J Neurosci Res 2007;85:1744-51.

[54] Herrup K, Arendt T. Re-expression of cell cycle proteins induces neuronal cell death during Alzheimer's disease. J Alzheimers Dis 2002;4:243-7.

[55] Lopes JP, Oliveira CR, Agostinho P. Cdk5 acts as a mediator of neuronal cell cycle re-entry triggered by amyloid-beta and prion peptides. Cell Cycle 2009;8:97-104.

[56] Nagy Z, Esiri MM, Smith AD. Expression of cell division markers in the hippocampus in Alzheimer's disease and other neurodegenerative conditions. Acta Neuropathol (Berl) 1997;93:294-300.

[57] Raina AK, Zhu X, Rottkamp CA, Monteiro M, Takeda A, Smith MA. Cyclin' toward dementia: cell cycle abnormalities and abortive oncogenesis in Alzheimer disease. J Neurosci Res 2000;61:128-33.

[58] Seward ME, Swanson E, Norambuena A, Reimann A, Cochran JN, Li R, et al. Amyloid-beta Signals Through Tau to Drive Ectopic Neuronal Cell Cycle Re-entry in Alzheimer's Disease. J Cell Sci 2013.

[59] Zekanowski C, Wojda U. Aneuploidy, chromosomal missegregation, and cell cycle reentry in Alzheimer's disease. Acta Neurobiol Exp (Wars) 2009;69:232-53.

[60] Zhu X, Lee HG, Perry G, Smith MA. Alzheimer disease, the two-hit hypothesis: an update. Biochim Biophys Acta 2007;1772:494-502.

[61] Zhu X, Raina AK, Perry G, Smith MA. Alzheimer's disease: the two-hit hypothesis. Lancet Neurol 2004;3:219-26.

[62] Bradley WE, Raelson JV, Dubois DY, Godin E, Fournier H, Prive C, et al. Hotspots of large rare deletions in the human genome. PLoS ONE 2010;5:e9401.

CHAPTER 2

Aneuploid cells are differentially susceptible to caspase-mediated death during embryonic cerebral cortical development

Abstract

Neural progenitor cells, neurons, and glia of the normal vertebrate brain are diversely aneuploid, forming mosaics of intermixed aneuploid and euploid cells. The functional significance of neural mosaic aneuploidy is not known; however, the generation of aneuploidy during embryonic neurogenesis, coincident with caspase-dependent programmed cell death (PCD), suggests that a cell's karyotype could influence its survival within the central nervous system (CNS). To address this hypothesis, PCD in the mouse embryonic cerebral cortex was attenuated by global pharmacological inhibition of caspases or genetic removal of caspase-3 or caspase-9. The chromosomal repertoire of individual brain cells was then assessed by chromosome counting, spectral karyotyping (SKY), fluorescence *in situ* hybridization (FISH) and DNA content flow cytometry. Reducing PCD resulted in markedly enhanced mosaicism that was comprised of increased numbers of cells with: 1) numerical aneuploidy (chromosome losses or gains); 2) extreme forms of numerical aneuploidy (>5 chromosomes lost or gained); and 3) rare karyotypes, including those with coincident chromosome loss and gain, or absence of both members of a chromosome pair (nullisomy). Interestingly, mildly aneuploid (<5 chromosomes lost or gained) populations remained comparatively unchanged. These data demonstrate functional non-equivalence of distinguishable aneuploidies on neural cell survival, providing evidence that somatically generated, cell-autonomous genomic alterations have consequences for neural development and possibly other brain functions.

Introduction

A surprising feature of the vertebrate CNS is mosaic aneuploidy, wherein numerous forms of aneuploidy are intermixed amongst euploid cells [1-3]. Aneuploidy is the gain and/or loss of chromosomes, deviating from haploid multiples; in mosaic aneuploidy, no single chromosome is uniformly affected. CNS aneuploidy arises during embryonic neurogenesis through mechanisms involving chromosome segregation defects in neural progenitor cells (NPCs) [3]. Aneuploid NPCs account for approximately 33% of the total NPC pool at embryonic day (E) 13 [2], and the gene expression profiles of mosaically aneuploid NPCs can vary compared to euploid counterparts [4]. As the brain matures, aneuploid karyotypes are maintained in postmitotic neurons and non-cycling glia, into adult life, as revealed by fluorescence *in situ* hybridization (FISH) [2, 5-8]. Aneuploidies have clear consequences for cellular fitness, including decreasing the cell proliferation rate and causing protein level imbalances [9-13]; thus, integration of active aneuploid neurons into adult brain circuitry [14] underscores their potential to affect brain function. Well-known constitutive aneuploidies (*i.e.*, uniform organismal chromosomal gain) such as Trisomy 21, Down syndrome, have profound effects on CNS development and function [15, 16].

Despite these observations, proven functions of mosaic aneuploidy in the CNS are lacking. NPC aneuploidy correlates with neurogenesis (E12-18 in the mouse) and programmed cell death (PCD) within the ventricular zone (VZ) and subventricular zone (SVZ) of the embryonic cerebral cortex [17-23]. PCD regulates cell number, cortical size and shape [24-27]; an aneuploid karyotype could provide a cell-specific selective mechanism to drive the survival or death of an NPC. Developmental PCD, operating through apoptotic mechanisms, can be reduced *in vivo* by genetic deletion of either effector caspase-3, or the upstream initiator caspase-9, producing a severe neurodevelopmental phenotype characterized by exencephaly, expansion of the ventricular zone, neuronal hyperplasia and early postnatal death [21, 28-33].

Here we report the effects on aneuploidy in mitotic cortical cells, including NPCs, following inhibition of caspase-mediated PCD: suppressing PCD leads to markedly increased levels of overall aneuploidy in mitotic and post-mitotic cerebral cortical populations, including a preferential increase in extreme forms of aneuploidy that are rarely observed in wild type cells while mild forms are relatively unaffected. These data indicate that caspase-mediated PCD differentially affects aneuploid neural populations, supporting a mechanism of neural cell selection based upon somatically generated mosaic aneuploidy.

Materials and Methods

Animals and tissue collection

Caspase-$3^{+/-}$ and caspase-$9^{+/-}$ mice (*Mus musculus*) in a C57BL/6J background (Jackson Laboratories, Bar Harbor, ME) were a generous gift from R.A. Flavell (Yale School of Medicine, New Haven, Connecticut), and were expanded in-house. Mutants were also backcrossed onto a 129S1/SvlmJ background (Jackson Laboratories, Bar Harbor, ME) for 6 or more generations. Timed-pregnant mice were killed by deep anesthesia followed by cervical dislocation and embryos rapidly removed at E14 for analysis of mitotic cells or E19 for post-mitotic cells. Both background strains were examined and demonstrated consistent shifts in aneuploid populations; presented data are from mice of the 129S1/SvlmJ background. These caspase-null embryos displayed the most extreme forms of neuronal hyperplasia characterized by exencephaly produced by reduced cell death, as originally reported [29, 32]. All animal protocols were approved by the Institutional Animal Care and Use Committee at The Scripps Research Institute (La Jolla, CA), and conform to the National Institutes of Health guidelines and public law.

Genotyping and sex determination

Caspase-3 embryos were genotyped using the following primers:

5’-GCGAGTGAGAATGTGCATAAATTC-3’

5’-GGGAAACCAACAGTAGTCAGTCCT-3’

5’-TGCTAAAGCGCATGCTCCAGACTG-3’

Caspase-9 embryos were genotyped using these primers:

5’-AGGCCAGCCACCTCCAGTTCC-3’

5’-CAGAGATGTGTAGAGAAGCCCACT-3’

5’-TCTCCTCTTCCTCATCTCCGGGCC-3’

5’-GAACAGTTCGGCTGGCGCGAGCCC-3’

PCR conditions for both genotyping reactions were 94°C for 5 minutes; 6 cycles of 94°C for 30 seconds, 65°C for 30 seconds, 72°C for 1 minute; 30 cycles of 94°C for 30 seconds, 58°C for 30 seconds, 72°C for 1 minute. Embryo sex was determined by Sry PCR, as previously described [34]. Female embryos were used exclusively for DNA content flow cytometry to control for genomic size differences between chromosomes X and Y; embryos of both sexes were used for all other experiments, and were sex-matched to employed wild type controls.

zVAD-fmk treatment of *ex vivo* cortical hemispheres

Following isolation of E14 embryonic cerebral cortices, intact hemispheres were separated and incubated individually in OptiMem media (Life Technologies, Carlsbad, CA) containing 50 ng/ml basic fibroblast growth factor (bFGF; Life Technologies) and either vehicle control (DMSO) or 100 nM zVAD-fmk (Enzyme Systems Products, Livermore, CA) at 37°C, 5% CO_2 with gentle agitation (70-90 rpm) for up to 2 days as previously described [27]. Cortices were then prepared for sectioning and immunolabeling as described [35] or for karyotype analysis as detailed below.

Metaphase spread preparation and spectral karyotyping

Preparation of E14 cortical cells for karyotyping was carried out as previously described [2]. Briefly, freshly isolated cortices from wild type and caspase null mutant embryos were incubated with 100 ng/ml Karyomax Colcemid (Life Technologies) in OptiMem media for 3 hours at 37°C with gentle agitation (70-90 rpm). Cortices were then triturated and centrifuged at 1000

rpm for 5 minutes at 4°C. Following media aspiration, cells were gently resuspended in 0.075 M KCl and incubated at 37°C for 7-10 minutes. Cells were then fixed in 3:1 methanol:glacial acetic acid, added dropwise while slowly vortexing. Metaphase spreads were prepared on Superfrost Plus slides (Fisher Scientific, Pittsburgh, PA) following standard protocols [36]. Spectral karyotyping (SKY) and 4',6-diamidino-2-phenylindole (DAPI, Life Technologies) staining were performed according to manufacturer's instructions (Applied Spectral Imaging, Carlsbad, CA). Images of chromosome spreads were acquired using a Zeiss 63x or 100x objective with an interferometer and charge-coupled device camera (Applied Spectral Imaging). For DAPI counts, 100 metaphase spreads were analyzed per embryo, from three E14 litters of paired wild type and caspase-3 or caspase-9 null embryos. For SKY analysis, approximately 150 spreads were analyzed from E14 wild type, caspase-3, and caspase-9 embryos in the 129S1/SvlmJ background, and approximately 250 spreads were analyzed from embryos in the C57BL/6J background.

Fluorescence *in situ* hybridization

Interphase or non-mitotic nuclei from E19 wild type, caspase-3, and caspase-9 null mutant embryos were harvested for FISH. Embryos were dissected and cortices sequentially triturated in cold PBS containing 2 mM EGTA, using p1000 tips with decreasing bore diameter, then filtered through a 40 µm nylon filter. This filtered single cell suspension was centrifuged at 1000 rpm for 5 minutes at 4°C, then gently resuspended in cell lysis buffer (10 mM TrisCl, pH 7.4, 3 mM $CaCl_2$, 2 mM $MgCl_2$, 1% NP-40) while slowly vortexing. Cells were lysed on ice for 5 minutes, centrifuged again and resuspended in 3:1 methanol:glacial acetic acid fixative, then affixed to glass slides for hybridization. Prepared slides were pretreated with 50 µg/ml pepsin (Sigma-Aldrich, St. Louis, MO) in 0.01 M HCl for 5 minutes at 37°C, then sequentially incubated at room temperature with 50 mM $MgCl_2$ in PBS for 5 minutes, and 50 mM $MgCl_2$ with 1% formaldehyde in PBS for 10 minutes. Slides were dehydrated and stored in a dessicator at -20°C until use. FISH probes were generated using FISHTag kits for AlexaFluor 488 and 555,

according to the manufacturer's instructions (Life Technologies). Template DNA used for nick translation was obtained from the following BAC inserts: mouse chromosome 16 (RP23-99P18 and RP23-83P8), and mouse chromosome 8 (RP23-188E13) (CHORI, Oakland, CA). For hybridization, FISH probes were denatured at 80℃ for 10 minutes then reannealed at 37℃ for 60 minutes. Slides were denatured at 75℃ for 1.5 minutes in 2x SSC and 50% formamide, and immediately dehydrated. Probes were then applied to the slide on a coverslip, sealed with rubber cement and hybridized overnight at 37℃. The following day, slides were washed at 45℃ for 5 minutes each in 2x SSC with 50% formamide, pH 7.0, 1x SSC, and 2x SSC with 0.1% Tween-20. Finally, slides were stained with DAPI (0.3 µg/ml), dehydrated and mounted with a coverslip and Vectashield (Vector Labs, Burlingame, CA). Three sets of E19 wild type and caspase null littermate cortices were analyzed for both caspase-3 and caspase-9; between 2500 and 3500 nuclei from both background strains were analyzed per cortex per chromosome. Error rates for FISH probes were determined to be less than 0.05% using metaphase spreads from lymphocyte controls.

DNA content analysis by flow cytometry

DNA content was determined as previously described [2, 37, 38]. Cells from isolated cortices were triturated to a single cell suspension as described above, then fixed in ice cold 70% ethanol and stored at -20℃ until use. On the day of analysis, cells were washed with PBS then treated with RNase A (40 µg/ml) for 20 minutes at 37℃. Cells were washed again with PBS and resuspended in a staining solution containing 50 µg/ml propidium iodide (Sigma-Aldrich) for 60-90 minutes. Each sample was spiked with chick erythrocyte nuclei (CEN) as an internal control (Biosure, Grass Valley, CA). Just prior to analysis, samples were filtered through a 40 µm nylon filter. DNA content was then assessed with a FACSort flow cytometer (Becton Dickinson, San Diego, CA); 25,000 to 50,000 events were analyzed per sample. Relative DNA content was expressed as a ratio of the mean fluorescent intensity of the G_0/G_1 peak divided by that of the CEN peak. Three sets of wild type and caspase null sex-matched littermates for both caspase-3

and caspase-9 were used for DNA content comparisons; samples were processed blind to identity.

Results

To analyze neural aneuploidy in the embryonic cortex, four independent procedures were used: 1) DAPI staining of chromosomes from mitotic cortical cells including NPCs; 2) spectral karyotyping (SKY) [39] of chromosomes from mitotic cortical cells including NPCs; 3) DNA content analyses of non-mitotic cells; and 4) fluorescence *in situ* hybridization (FISH) of interphase or non-mitotic nuclei to assess specific aneusomies (**Fig. 2.1**). A representative DAPI-stained mitotic cortical cell chromosome spread containing 38 chromosomes (**Fig. 2.1 A**, "DAPI") identifies an aneuploid cell (the euploid chromosome number for *Mus musculus* is 40). The complete karyotype of this spread was determined by SKY, where each chromosome is painted with a spectrally distinct combination of hybridized probes, identifying this cortical cell as 38, XY, -6, -13 (**Fig. 2.1 A**, "SKY"). Non-mitotic cells (post-mitotic neurons, non-cycling glia and interphase cells) do not produce condensed, metaphase chromosomes. These cells can be analyzed for chromosomal gains or losses by measuring DNA content (*e.g.*, **Fig. 2.1 B**), and by FISH, to identify aneusomic cells (cells that have gained or lost an assessed chromosome pair, albeit without knowledge of the remaining chromosomes) (**Fig. 2.1 C**). These techniques were applied to wild type versus experimental conditions in which PCD was attenuated through pharmacological inhibition or genetic deletion of caspases.

Figure 2.1. Schematic for analyzing aneuploidy in mitotic and non-mitotic cortical cells. **A**: Cortices were dissected from embryos at embryonic day (E) 14, triturated, and placed in culture in colcemid (100 ng/ml) to arrest cells in metaphase and obtain chromosome spreads. Each cell's chromosomal complement was analyzed in one of two ways. First, chromosomes were stained with DAPI and counted using fluorescence microscopy (bottom left). Second, metaphase chromosome spreads were processed for SKY to determine exact karyotypes (bottom right). **B**: E14 cortices were isolated, triturated, and fixed for staining with the DNA-intercalating dye Propidium Iodide. Dye-saturated cells were analyzed by flow cytometry, where the dominant peak on a DNA content histogram contains cells in the G_0/G_1 phase of the cell cycle. Relative DNA content was expressed as a ratio of the mean fluorescent intensity of the G_0/G_1 peak divided by the peak of an internal standard, chick erythrocyte nuclei (CEN). **C**: For analysis of interphase or non-mitotic cells, E19 cortices were triturated, cell nuclei were isolated, applied to a slide, and hybridized with chromosome-specific FISH probes. For these experiments, nuclei were hybridized with probes for chromosomes 16 (green) and 8 (red), and stained with DAPI (blue). Normal, euploid cells would be disomic for both chromosome 8 and 16 and thus would have 2 green dots and 2 red dots. The nucleus on the left is monosomic for chromosome 16 and the nucleus on the right is trisomic for chromosome 16, meaning both nuclei are aneuploid. Both nuclei are disomic for chromosome 8.

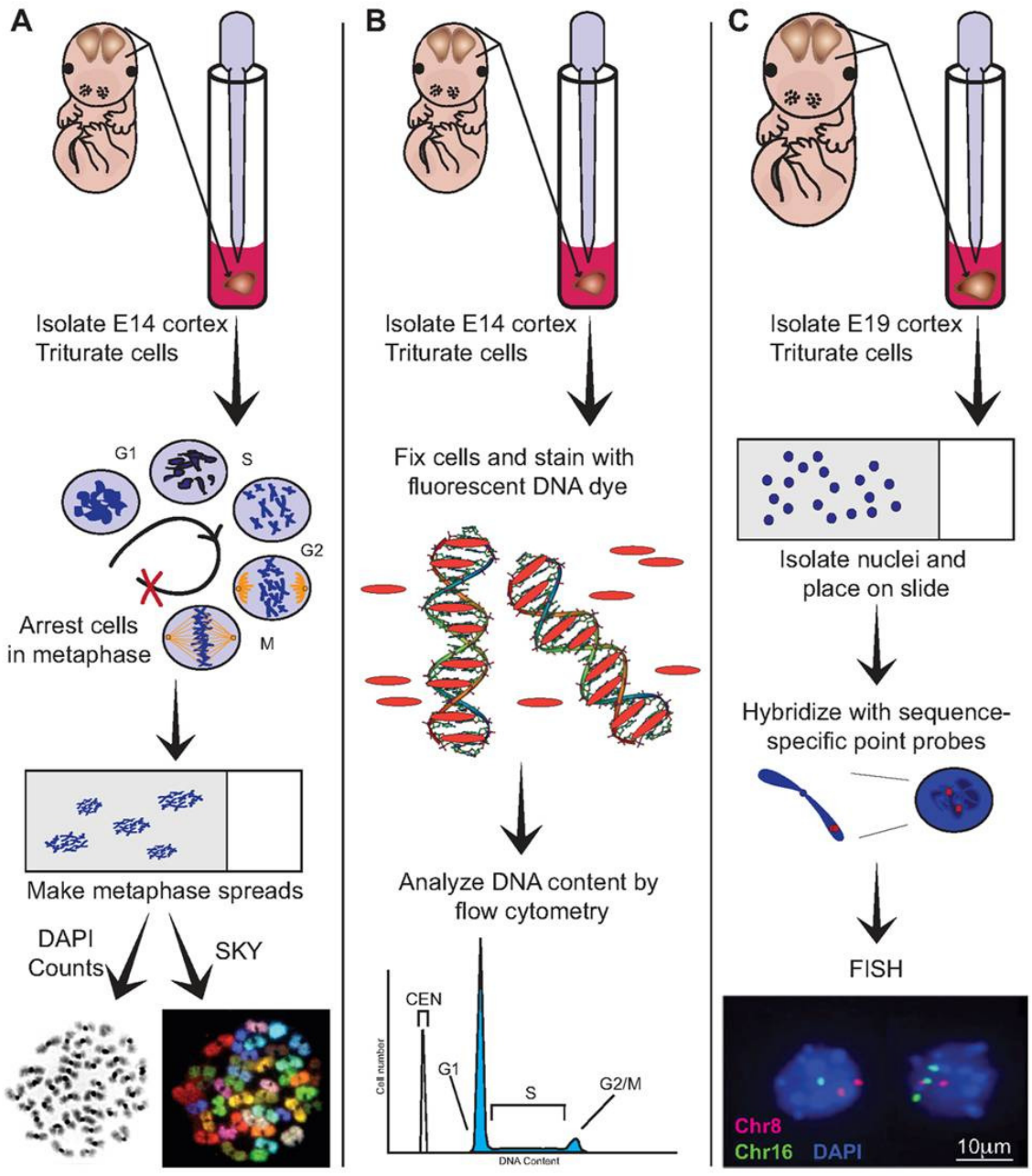
A
Isolate E14 cortex
Triturate cells
G1
S
G2
M
Arrest cells
in metaphase
Make metaphase spreads
DAPI
Counts
SKY
B
Isolate E14 cortex
Triturate cells
Fix cells and stain with
fluorescent DNA dye
Analyze DNA content by
flow cytometry
CEN
G1
S
G2/M
Cell number
DNA Content
C
Isolate E19 cortex
Triturate cells
Isolate nuclei and
place on slide
Hybridize with sequence-
specific point probes
FISH
Chr8
Chr16
DAPI
10µm

Pharmacological inhibition of caspases increases aneuploidy levels

The effects of pharmacological caspase inhibition on aneuploidy were assessed using *ex vivo* cortical cultures [27, 35] exposed to the synthetic peptide, pan-caspase inhibitor zVAD-fmk (benzyloxycarbonyl-Val-Ala-Asp-fluoromethylketone) [40-42]. This cell-permeable, irreversible caspase inhibitor inactivates both initiator caspases (*e.g.*, caspase-8 and -9) and effector caspases (*e.g.*, caspase-3) [43-45]. Pharmacological inhibition by zVAD-fmk is not optimal for *in vivo* studies because of its cytotoxicity. However, *ex vivo* cortical hemisphere cultures retain normal organization and molecular processes observed *in vivo*, including interkinetic nuclear migration, DNA synthesis, and cell cycle progression [27, 35], providing a model system to assess the effects of pharmacological caspase inhibition on mitotic cortical cell aneuploidy. In cortical hemispheres cultured in the presence of 100 nM zVAD-fmk, a significant reduction in activated caspase-3 immunoreactivity occurs in the ventricular zone compared to the vehicle-treated control cortical hemispheres from the same embryos (**Fig. 2.2 A**, from 15.3% in vehicle treated samples to 0.4% in zVAD-fmk treated cortices; P=0.01, Student's t-test). Mitotic cortical cell aneuploidy following zVAD-fmk exposure was therefore assessed by chromosome counts using the *ex vivo* system. A 58% increase in aneuploidy was observed (Control = 24% aneuploidy; zVAD-fmk = 38%; P=0.03, Student's t-test). The increase in aneuploid cells following caspase inhibition was accompanied by a wider range of numerical aneuploidy forms in brains exposed to the caspase inhibitor (**Fig. 2.2 B**). This was also reflected in a higher standard deviation from the mean chromosome number in zVAD-fmk-treated mitotic cortical cells. For all experimental and control conditions, both hypo- and hyperploid cells were observed; however, hypoploidy (*i.e.*, having fewer than the euploid number of chromosomes) was the predominant form of aneuploidy recorded (**Fig. 2.2 B**), which is consistent with *in vivo* observations of NPC aneuploidy [2].

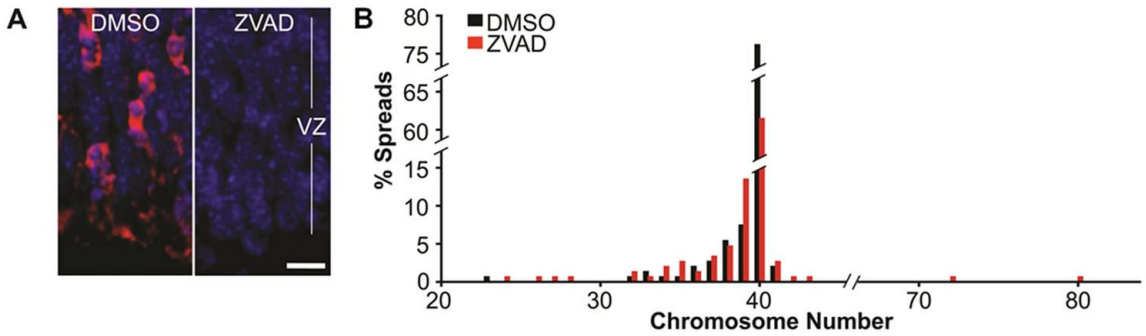

Figure 2.2. Pharmacological inhibition of caspases leads to increased aneuploidy in mitotic cells from the embryonic mouse cortex. **A**: Intact hemispheres of E14 cortex were treated *ex vivo* with vehicle control (DMSO) or the pan caspase inhibitor zVAD-fmk (100 nM). DMSO-treated sections show high levels of immunoreactivity for cleaved caspase-3 (red), while those treated with zVAD-fmk showed markedly reduced immunoreactivity (from 15.3% to 0.4%, respectively; P = 0.01, Student's t-test). Tissues were counterstained with DAPI (blue). Scale bar = 20 μm, VZ = ventricular zone. **B**: Histogram of the distribution of aneuploid cells identified following exposure of cortices to vehicle control (DMSO) (black) and zVAD-fmk (red).

Null mutants of caspase-3 or caspase-9 show increased aneuploidy in mitotic cortical cells

To determine whether aneuploidy levels increased *in vivo* in the absence of caspase activity required for apoptosis, we assessed caspase-3 and caspase-9 null mutants. The ablation of either of these two caspases, both integral to cell-intrinsic apoptotic mechanisms, attenuates cell death and can produce hyperplasic brain growth by reducing cortical PCD [28, 29, 32, 46]. Mitotic cortical cells from caspase-3 and caspase-9 null homozygotes that showed enlarged brains were harvested for metaphase chromosome spread analysis. Compared to wild type embryos which displayed 29% aneuploidy, a respective 79% and 60% increase in aneuploidy was observed in mitotic cortical cells from caspase-3 (50% total aneuploidy) and caspase-9 (46% aneuploidy) nulls (**Fig. 2.3 A**, P=0.02 and P=0.04, respectively, Student's t-test). This increase in total aneuploidy was accompanied by an expanded range of numerically distinct aneuploidies identified in both caspase-3 and caspase-9 null mutants (**Fig. 2.3 C**), similar to that seen with *ex vivo* zVAD-fmk treatment. As with the wild type mitotic cortical cells, aneuploidies in both of the caspase null mutants were predominantly hypoploid. This effect was observed in both genetic backgrounds (data from the C57Bl/6J background not shown).

Null mutants of caspase-3 or caspase-9 show decreased DNA content and increased aneusomy in non-mitotic cortical cells

Independent support for the increased aneuploidy identified in metaphase chromosome spreads was obtained through examination of non-mitotic cells that do not have condensed chromosomes, using two distinct methodologies. First, DNA content was assessed in non-mitotic cells, similar to approaches previously used to identify aneuploidy in cancer specimens [47] and to identify different sex chromosomes in spermatozoa [48]. Caspase-3 and caspase-9 null cortices from E14 embryos were processed for DNA content analysis, wherein single-cell suspensions were stained with propidium iodide to determine DNA content by flow cytometry (**Fig. 2.1 B**). As an internal standard, chick erythrocyte nuclei (CEN) were spiked into the preparation and processed simultaneously with all samples [49], followed by construction of DNA content

histograms. The dominant peak on a DNA content histogram contains cells in the G_0/G_1 phase of the cell cycle, consisting of cells with diploid DNA content. Deviations in the G_0/G_1 peak relative to the internal control CEN peak were used to determine differences in relative DNA content, as reported previously [38]. Cortical cells from both caspase-3 and caspase-9 null mutants showed a 3-4% decrease in total DNA content compared to age- and sex-matched wild type controls (**Fig. 2.3 B**, P=0.002 and P=0.03, respectively, Student's t-test), consistent with increased hypoploidy. This decrease in DNA content was replicated using a distinct DNA dye, DAPI (data not shown).

DNA content analysis does not have the capacity to identify changes in specific chromosome pairs. To determine whether the changes in aneuploidy levels persist at later ages in post-mitotic neurons and other non-mitotic cell populations that cannot be analyzed by metaphase spreads, individual chromosomes were interrogated using fluorescence *in situ* hybridization (FISH) (**Fig. 2.1 C**). Cortical cells from E19 caspase-null mutants were compared to wild type for the presence or absence of representative autosomes (chromosomes 8 and 16). A significant increase in overall aneusomy of chromosome 16 was observed in both caspase nulls compared to wild type: caspase-3 increased to 2.9% from 2.1% in wild type, and caspase-9 increased to 2.6% (n = 3; P=0.0002 and P=0.004 by χ^2, respectively). A significant increase was also seen for chromosome 8 in caspase-3 null mutants, from 1.6% in wild type to 2.1% in the mutant (n = 3; P=0.04 by χ^2). It is important to note that aneusomy rates of 1-3% reflect interrogation of only a single chromosome pair, 1/20th of the total chromosomal complement, contrasting with the full karyotypic assessments achievable by metaphase spread counts.

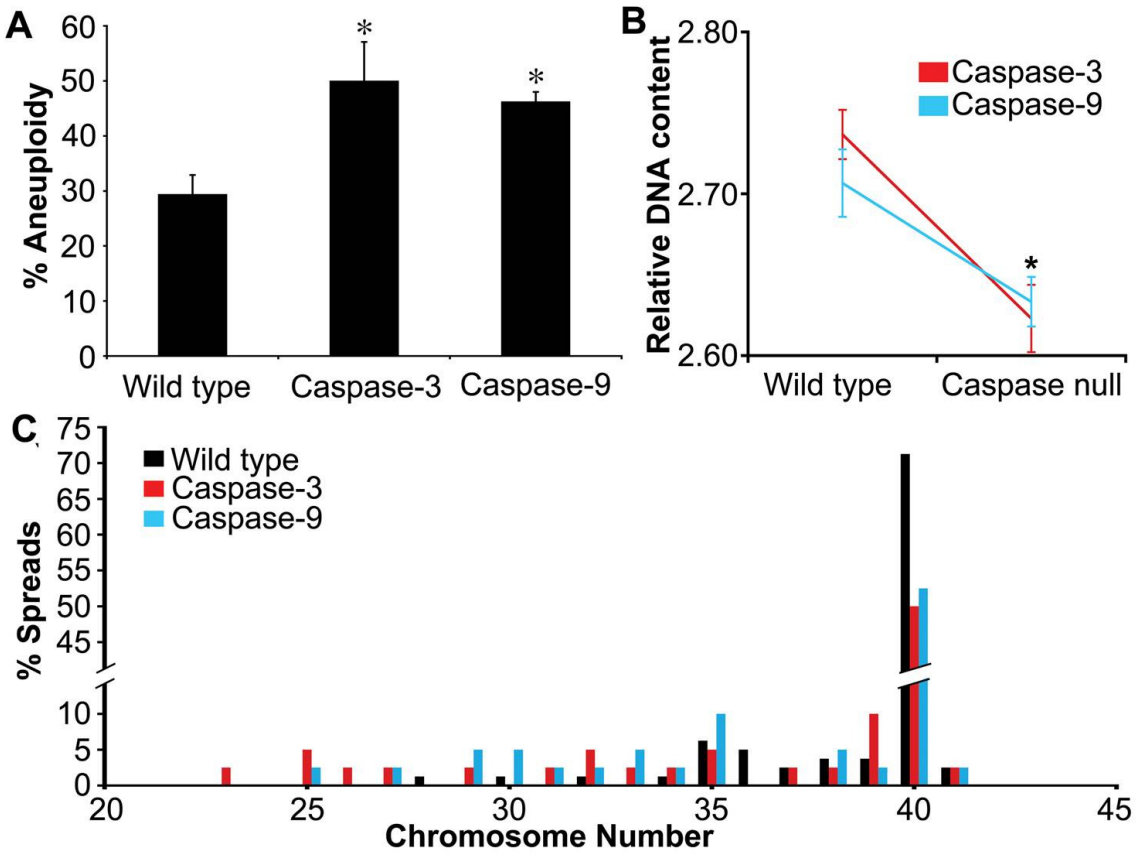

Figure 2.3. Genetic ablation of caspases leads to increased aneuploidy in mitotic cells from the embryonic mouse cortex. **A**: Analysis of metaphase chromosome counts showed increased aneuploidy in E14 caspase-3 and caspase-9 null cortices compared to wild type cortices from littermates (100 metaphase spreads were counted per embryo; for caspase-3, n = 3; * P = 0.02; for caspase-9, n = 3; * P = 0.04, Student's t-test). **B**: Quantitation of DNA content by flow cytometry showed a significant 3-4% decrease in overall DNA content from cortices of E14 caspase nulls compared to sex-matched, wild type littermates (caspase-3 wild type and nulls, n = 4, * indicates P = 0.002, Student's t-test; caspase-9 wild type and nulls, n = 3, * indicates P = 0.03, Student's t-test). **C**: Histogram of the distribution of aneuploidy in E14 wild type (black), caspase-3 null (red), and caspase-9 null (blue) NPCs. Caspase deficient cells showed expanded distribution of numerical aneuploidies.

Null mutants of caspase-3 or caspase-9 show increases in extreme aneuploidies

Caspase inhibition by pharmacological means as well as through genetic deletion of either caspase-3 or caspase-9 increases the distribution of numerical aneuploidies observed in mitotic cortical cells. To determine the effects of PCD attenuation on karyotypes, one hundred aneuploid metaphase chromosome spreads from each of three litters containing age-matched wild type and caspase-null embryos were plotted as a histogram then arbitrarily divided into distinct bins designed to capture major effects on chromosome number within analyzed cells (**Fig. 2.4 A & B**). Bin 1 represents "mild" aneuploidies where chromosome numbers flank the euploid chromosome number of 40 (light grey: 35-39 and 41-45 chromosomes). Bins 2 and 3 represent more "extreme" aneuploidies (bin 2, medium grey: 30-34 and 46-50 chromosomes; bin 3, black: 0-29 and 51 or more). Compared to wild type aneuploidy levels, caspase-3 nulls displayed a significant increase in the percent of cells with "extreme" aneuploidies: bin 2 increases from 2.5% in wild type embryos to 12.5% in mutants, and bin 3 increases from 2.5% to 15% (**Fig. 2.4 B**, $P<0.003$, Student's t-test). Caspase-9 nulls displayed a similar trend, with bin 2 increasing from 5% to 17.5% and bin 3 from 0% in wild type to 10% in nulls (**Fig. 2.4 B**, $P<0.003$, Student's t-test). No statistically significant change in the percentage of cells with mild aneuploidies (bin 1) was observed, indicating that the increase in total aneuploidy was due to these "extreme" aneuploidies. The expansion of the extremely aneuploid population of mitotic cortical cells (bins 2 and 3 together) constituted over half of the caspase-3 and -9 aneuploid populations. Note that the size of the entire pie represents the total amount of aneuploidy, resulting in larger pies produced following attenuated cell death compared to controls. Similar results were observed in caspase null mutants on a C57Bl/6J background (data not shown).

Null mutants of caspase-3 or caspase-9 show increases in the frequency of rare mitotic cell karyotypes

Numerical aneuploidies do not identify specific chromosomes that have been lost and/or gained. SKY was therefore used to assess karyotypic alterations. Coincident chromosomal gain

and loss (**Fig. 2.5 A**), as well as nullisomies, produced when both chromosomes of the same pair are lost (**Fig. 2.5 B**) showed increased prevalence following caspase inhibition (**Fig. 2.5 C-E**). In both caspase null mutants, there was a marked increase in rare karyotypes (**Fig 2.5 F**): incidence of nullisomy increased from 5% in wild type to 40% in caspase-3 and 35% in caspase-9 nulls ($p<0.05$, χ^2), while coincident gain and loss increased from 0% in wild type to 30% in caspase-3 and 35% in caspase-9 nulls ($p<0.03$, χ^2). Similar trends were observed in both genetic backgrounds (data from the C57Bl/6J background not shown).

Figure 2.4. Caspase attenuated mitotic cortical cells show an increase in extreme aneuploidy, while maintaining mild aneuploidy levels. **A**: One hundred aneuploid metaphase spreads were analyzed for each of 3 paired sets of wild type and caspase null littermates. Bin 1 represents "mild" aneuploidies where chromosome numbers flank the euploid chromosome number of 40 (light grey: 35-39 and 41-45 chromosomes). Bins 2 and 3 represent more "extreme" aneuploidies (bin 2, medium grey: 30-34 and 46-50 chromosomes; bin 3, black: 0-29 and 51 or more). Euploid spreads are not shown. Caspase attenuation resulted in a preferential expansion of extreme aneuploidies (bins 2 and 3, * $P < 0.003$, Student's t-test); no significant change was observed in cells showing mild aneuploidies (bin 1). **B**: Pie charts of mild and extreme aneuploidies from control versus caspase null cortices were constructed to reflect relative percentages of cells in each bin (pie slice, colors as in Fig. 4A), and percent of total aneuploidy (pie area). Pronounced expansion of bins 2 and 3 by percentage were coincident with PCD attenuation.

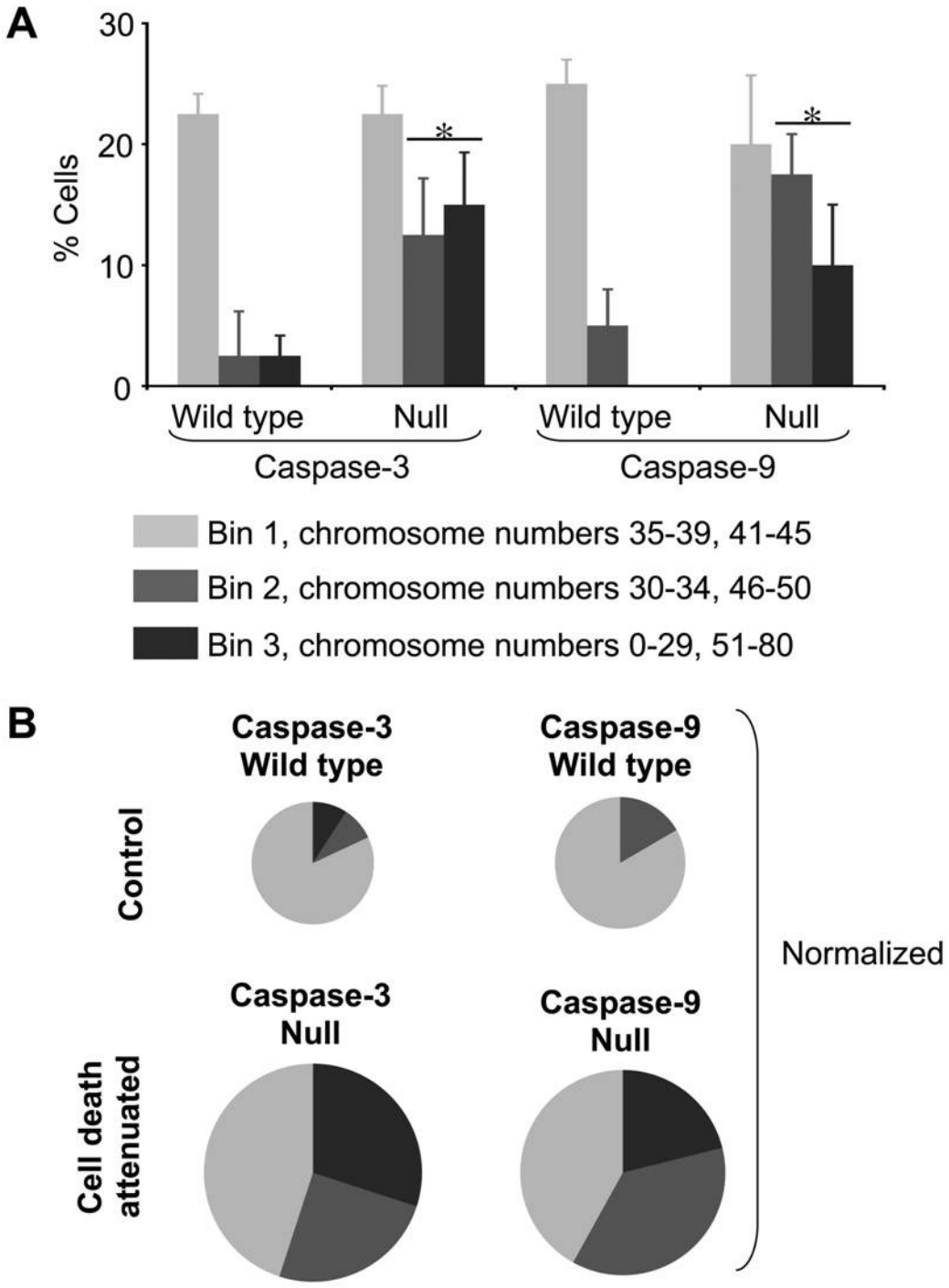
A
30
20
10
0
% Cells
*
*
Wild type
Null
Wild type
Null
Caspase-3
Caspase-9
Bin 1, chromosome numbers 35-39, 41-45
Bin 2, chromosome numbers 30-34, 46-50
Bin 3, chromosome numbers 0-29, 51-80
B
Caspase-3
Wild type
Caspase-9
Wild type
Control
Normalized
Caspase-3
Null
Caspase-9
Null
Cell death
attenuated

Figure 2.5. Caspase attenuation increases rare aneuploidies including nullisomy and coincident chromosomal gain and loss, identified by spectral karyotyping (SKY). **A-B**: Representative metaphase spreads from E14 caspase-3 null cortices analyzed by SKY showing coincident chromosome gain and loss (**A**) and nullisomy (**B**). SKY analyses of each cell included pseudocolor chromosome spread (left panel), DAPI counterstain (middle panel), and karyotype table (right panel). **C-E**: Tabular representation of 20 aneuploid karyotypes from E14 wild type (**C**), caspase-3 null (**D**) and caspase-9 null (**E**) mitotic cortical cells. Chromosome numbers are indicated across the top row. Each row below shows the karyotype of an individual aneuploid cortical cell. The rightmost column indicates the total number of chromosomes in each spread. The last row reports the number of times a chromosome is involved in a gain or loss event. Orange squares: gain of one chromosome. Red squares: gain of a chromosome pair. Light blue squares: loss of one chromosome. Deep blue squares: loss of a chromosome pair (*i.e.*, nullisomy). Spreads containing a nullisomy and/or coincident chromosomal gain and loss are indicated with stars and circles, respectively, along the left most column. **F**: Frequencies of nullisomy and coincident gain and loss of chromosomes among wild type, caspase-3 and caspase-9 null aneuploid cortical cells. * indicates $p<0.05$, χ^2 for nullisomy; $p<0.03$, χ^2 for coincident loss and gain.

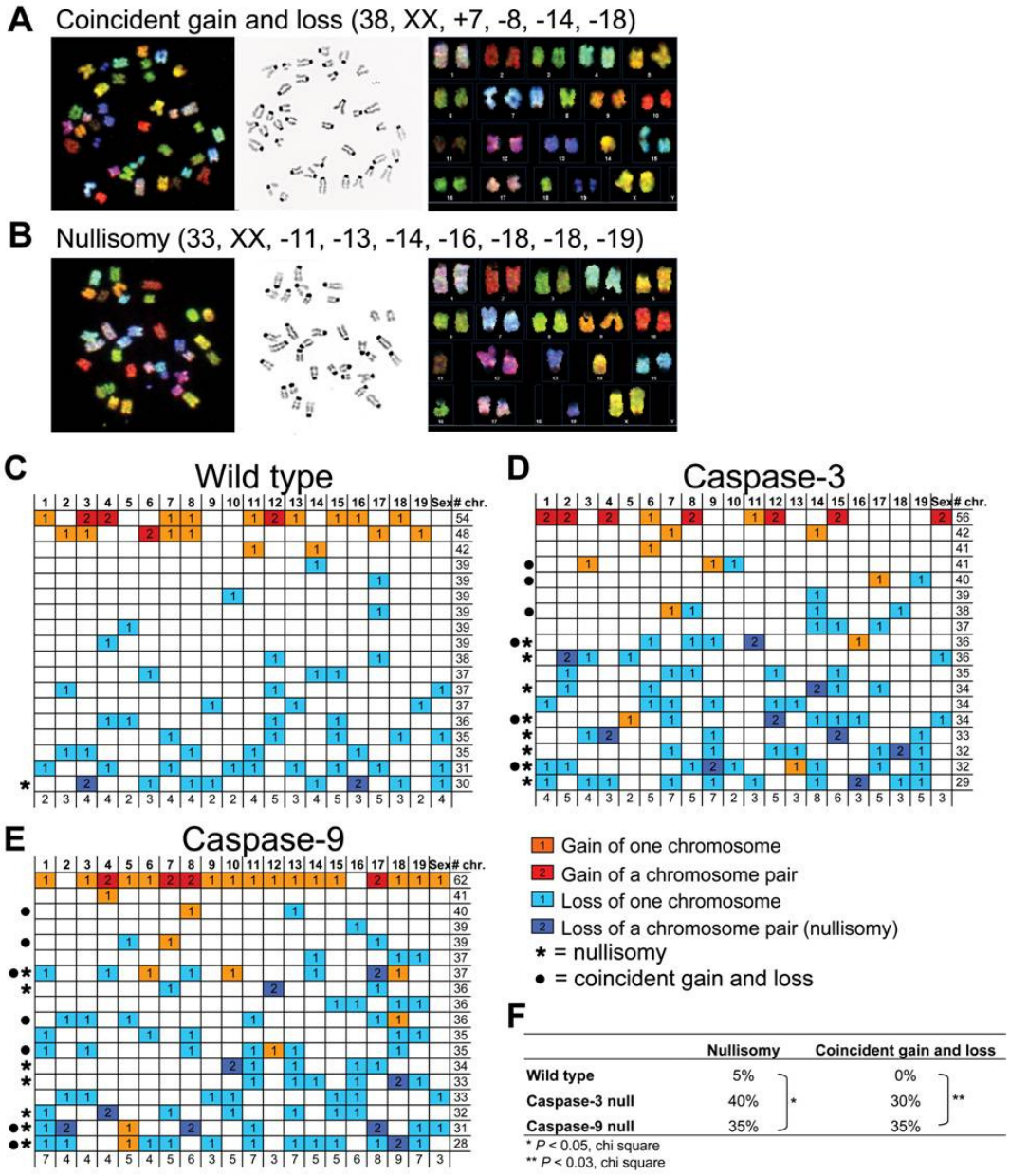

F

	Nullisomy		Coincident gain and loss	
Wild type	5%		0%	
Caspase-3 null	40%	*	30%	**
Caspase-9 null	35%		35%	

* $P < 0.05$, chi square
** $P < 0.03$, chi square

Discussion

Over the past decade, the initially surprising existence of mosaic aneuploidy within the CNS has now been verified in vertebrates from fish to humans [1, 2, 5, 7, 8, 50-54]. By contrast, the functions of these diverse, mosaic aneuploidies remain unknown. Here we report the essential regulation of mosaic neural aneuploidies by cell death pathways during the development of the embryonic brain, suggesting that without tight molecular constraints, somatically generated genomic alterations may have severe functional consequences for neural development. These conclusions are derived from attenuating cell death amongst mitotic cortical cells through both pharmacological and genetic perturbations of well-defined cell death mediators – caspases 3 and 9 – resulting in: 1) marked elevations of the total aneuploid cell population; 2) increases in the range of numerically diverse aneuploid cells; 3) differential increases in "extreme" aneuploidies over "mild" aneuploidies; and 4) increases in rare karyotypes defined by nullisomies as well as coincident gain and loss of chromosomes. These results indicate that inhibition of neural PCD not only increases cell number – as expected – but also increases the range and forms of genomically distinct cells that comprise the brain. These changes in mosaic aneuploidies may also contribute functionally to the phenotypic lethality observed in some caspase-null mutants [29, 32].

Our data are consistent with prevailing views on the functions of caspases, particularly caspases-3 and -9, in PCD. Caspase-dependent intrinsic apoptosis, which involves activation of caspase-9 and subsequently caspase-3 by the release of mitochondrial outer membrane proteins (MOMPs) including cytochrome c [55-58], underscores the sequential positioning of caspases along the same molecular death pathway. The similar results obtained using independent means of interrupting this pathway – pharmacological inhibition, caspase-3 or caspase-9 genetic deletion – strongly support the effects on aneuploid populations as being due to reductions in caspase-mediated PCD. Notably, the overall effect of caspase inhibition was to increase total cell number (**Fig. 2.4**), as would be expected after inhibiting PCD [29, 32]. Moreover, each of the three independent means of reducing caspase activity produced the same general result of expanding

the distributions and extreme forms of aneuploidy – including both hypo- and hyperploidies – yet left intact distributions of “mild” aneuploid populations.

Caspase-mediated PCD is not the only form of cell death operating in the developing cerebral cortex. Mitotic catastrophe, as noted by the 2012 Nomenclature Committee on Cell Death, may have prominent roles in PCD of mitotic cortical cells, serving as an oncosuppressive mechanism triggered during M phase by a heterogeneous group of stimuli [55]. It also shares many hallmarks of apoptosis, including the MOMP release, and mitotic errors resulting in premature or inappropriate entry into mitosis [55, 59-63]. Processes like necrosis may also contribute to cortical cell death [64], as could the actions of other caspases. Less than half of the observed cell death in the embryonic cortex is mediated by caspase-3 [21], indicating that other forms of PCD may contribute to the mosaically aneuploid landscape. These considerations suggest that the shifts in affected aneuploidies reported in this study would underestimate the genotypic diversity initially generated amongst mitotic cortical cells, including neural progenitor cells.

Aneuploidy produced by chromosome loss or gain is known to alter gene expression [4, 9, 65]. The dramatic increases in aneuploidy and the rare karyotypes – the coincident loss and gain of chromosomes, and nullisomies – that we observed in caspase-null mutants are virtually certain to vary the gene expression patterns within each affected cell. Variation of gene expression has consequences for both cell autonomous and non-cell autonomous activities, and implies phenotypic mosaicism that tracks with genotypic mosaicism throughout the brain. To this end, a most extreme, functional outcome of karyotypic diversity may be a “better dead than wrong” response [66]. This response has been related to possible oncosuppressive roles of karyotype regulation by caspases in progenitor cells, which has broader implications for other endogenous and cultured stem cell populations, including their therapeutic use. While cancers have long been reported to contain characteristic aneuploidies, particularly hyperploidies [67-69], more recent studies present evidence for both mosaic and constitutive aneuploidies in cultured stem cell populations as well [70-73]. Karyotypic mosaicism is prominent in commonly used human stem

cell lines [72], which may reflect the normal, biological mosaicism observed *in vivo* in mitotic cortical cells including NPCs. It is possible that the increased prevalence of rare karyotypes observed here could have an increased oncogenic potential that accompanies gene expression abnormalities. Thus, putative neuroprotective agents, such as caspase inhibitors and growth factors, for treating neurodegeneration and ischemic brain injury [74, 75] may inadvertently alter the genomic composition of endogenous or transplanted cell populations. Such hypothetical effects deserve further study.

The mechanisms underlying the generation and subsequent loss or maintenance of the different aneuploid populations observed here are not completely understood. The generation of neural aneuploidy involves known chromosome missegregation mechanisms [3] that occur concomitantly with PCD [17, 18, 21, 76]. Factors that might contribute to both the generation of aneuploidy and PCD may involve other forms of genomic variation within neural cells. Several proteins in the non-homologous end joining (NHEJ) pathway that includes the proteins XRCC4, DNA Ligase IV and Ku, can produce extensive NPC apoptosis in the CNS [77-79], as can other DNA modifying molecules [80]. In addition, LINE-1 retrotransposons may be active within neuronal populations, introducing further genomic heterogeneity [81, 82]. These genome-altering phenomena are members of a superset of genomic changes identified within brain cells, referred to as DNA content variation (DCV) [38]. In view of the data presented here, forms of DCV may serve as a basis for cell selection, reminiscent of the immune system that relies on genomic changes associated with antigen receptor DNA rearrangements (affecting T-cell receptors and immunoglobulins), which results in positive and negative selection, as well as death by neglect [83, 84].

These results add a new dimension to the consequences of PCD and its perturbation during the development of the embryonic cerebral cortex [17, 21, 28, 29, 32, 85, 86], wherein PCD shapes not only cell number, but also shapes the mosaic genomic landscape of the brain. In this view, cells with undesirable karyotypes are normally eliminated, contrasting with desirable karyotypes – including euploid cells – that are maintained (**Fig. 2.6**).

Figure 2.6. Model of aneuploidy-based selection in the developing cerebral cortex. The normal pathway (wild type) is compared to experimental manipulation using inhibition of caspase activity (cell death attenuated). Both mild and extremely aneuploid cells (cf. Fig. 4) are generated during neurogenesis ("Before PCD") to produce a mosaic of intermixed euploid and aneuploid cortical cells. During PCD, extremely aneuploid cells are normally eliminated (red "X"), but when caspase-mediated PCD is attenuated, these cells are preserved (red outline). In the wild type brain ("After PCD"), most cells are either euploid or mildly aneuploid. When PCD is attenuated, however, the brain becomes populated by more extremely aneuploid cells.

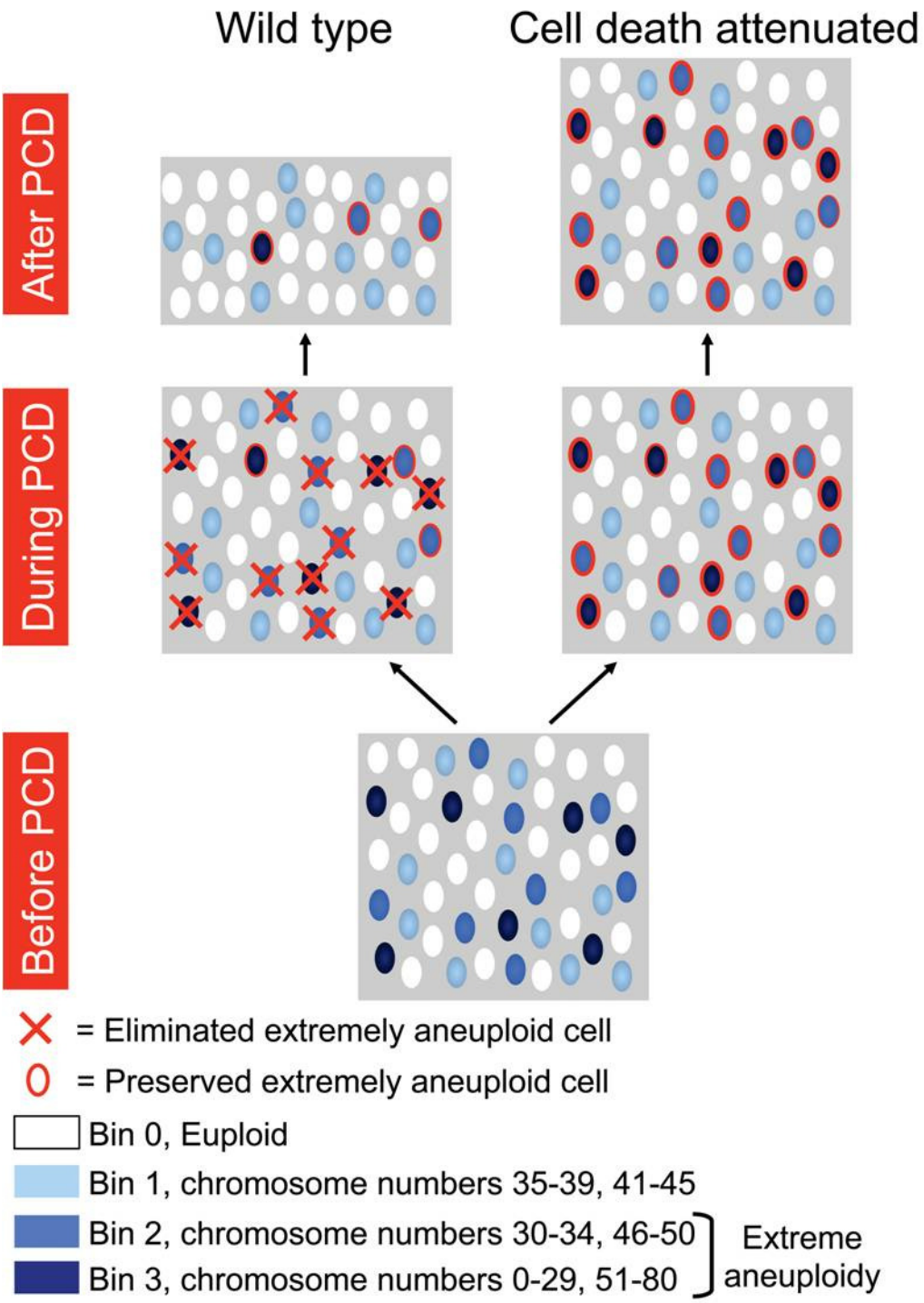
Wild type
Cell death attenuated
After PCD
During PCD
Before PCD
= Eliminated extremely aneuploid cell
= Preserved extremely aneuploid cell
Bin 0, Euploid
Bin 1, chromosome numbers 35-39, 41-45
Bin 2, chromosome numbers 30-34, 46-50
Bin 3, chromosome numbers 0-29, 51-80
Extreme aneuploidy

The need for cell selection to produce this complex mix of karyotypic diversity may in part explain neural proliferative cell death occurring during cortical neurogenesis as well as within other zones of neuroproliferation [17, 18, 23]. Our data highlight the functional non-equivalence of different karyotypes in PCD and cell survival, since mild aneuploidies are relatively preserved over extreme forms, and this non-equivalence may extend to other aspects of functionality. This mélange of mosaic aneuploidies intermixed with euploid cells may also be altered with respect to form, number, and neuroanatomical organization. We speculate that developmental perturbations to normal mosaicism – through genetic mechanisms as noted here, as well as myriad environmental insults – could contribute to variation in complex neural traits and to brain disorders [6, 87].

Chapter 2, in full, is a reprint of the material as it appearsin the Journal of Neuroscience. Peterson, S.E.*, Yang, A.H.*, **Bushman, D.M.** *, Westra, J.W., Yung, Y.C., Barral, S., Mutoh, T., Rehen, S.K. & J. Chun. *Aneuploid cells are differentially susceptible to caspase-mediated death during embryonic cerebral cortical development*. Journal of Neuroscience. 2012 Nov 14; 32 (46): 16213-22. The dissertation author was a co-primary author of this material.

References

[1] Rajendran RS, Zupanc MM, Losche A, Westra J, Chun J, Zupanc GK. Numerical chromosome variation and mitotic segregation defects in the adult brain of teleost fish. Dev Neurobiol 2007;67:1334-47.

[2] Rehen SK, McConnell MJ, Kaushal D, Kingsbury MA, Yang AH, Chun J. Chromosomal variation in neurons of the developing and adult mammalian nervous system. Proc Natl Acad Sci U S A 2001;98:13361-6.

[3] Yang AH, Kaushal D, Rehen SK, Kriedt K, Kingsbury MA, McConnell MJ, et al. Chromosome segregation defects contribute to aneuploidy in normal neural progenitor cells. J Neurosci 2003;23:10454-62.

[4] Kaushal D, Contos JJ, Treuner K, Yang AH, Kingsbury MA, Rehen SK, et al. Alteration of gene expression by chromosome loss in the postnatal mouse brain. J Neurosci 2003;23:5599-606.

[5] Pack SD, Weil RJ, Vortmeyer AO, Zeng W, Li J, Okamoto H, et al. Individual adult human neurons display aneuploidy: detection by fluorescence in situ hybridization and single neuron PCR. Cell Cycle 2005;4:1758-60.

[6] Kingsbury MA, Yung YC, Peterson SE, Westra JW, Chun J. Aneuploidy in the normal and diseased brain. Cell Mol Life Sci 2006;63:2626-41.

[7] Rehen SK, Yung YC, McCreight MP, Kaushal D, Yang AH, Almeida BS, et al. Constitutional aneuploidy in the normal human brain. J Neurosci 2005;25:2176-80.

[8] Yurov YB, Iourov IY, Monakhov VV, Soloviev IV, Vostrikov VM, Vorsanova SG. The variation of aneuploidy frequency in the developing and adult human brain revealed by an interphase FISH study. J Histochem Cytochem 2005;53:385-90.

[9] Torres EM, Sokolsky T, Tucker CM, Chan LY, Boselli M, Dunham MJ, et al. Effects of aneuploidy on cellular physiology and cell division in haploid yeast. Science 2007;317:916-24.

[10] Sheltzer JM, Amon A. The aneuploidy paradox: costs and benefits of an incorrect karyotype. Trends Genet 2011;27:446-53.

[11] Williams BR, Prabhu VR, Hunter KE, Glazier CM, Whittaker CA, Housman DE, et al. Aneuploidy affects proliferation and spontaneous immortalization in mammalian cells. Science 2008;322:703-9.

[12] Pavelka N, Rancati G, Zhu J, Bradford WD, Saraf A, Florens L, et al. Aneuploidy confers quantitative proteome changes and phenotypic variation in budding yeast. Nature 2010;468:321-5.

[13] Torres EM, Dephoure N, Panneerselvam A, Tucker CM, Whittaker CA, Gygi SP, et al. Identification of aneuploidy-tolerating mutations. Cell 2010;143:71-83.

[14] Kingsbury MA, Friedman B, McConnell MJ, Rehen SK, Yang AH, Kaushal D, et al. Aneuploid neurons are functionally active and integrated into brain circuitry. Proc Natl Acad Sci U S A 2005;102:6143-7.

[15] O'Doherty A, Ruf S, Mulligan C, Hildreth V, Errington ML, Cooke S, et al. An aneuploid mouse strain carrying human chromosome 21 with Down syndrome phenotypes. Science 2005;309:2033-7.

[16] Wiseman FK, Alford KA, Tybulewicz VL, Fisher EM. Down syndrome--recent progress and future prospects. Hum Mol Genet 2009;18:R75-83.

[17] Blaschke AJ, Staley K, Chun J. Widespread programmed cell death in proliferative and postmitotic regions of the fetal cerebral cortex. Development 1996;122:1165-74.

[18] Blaschke AJ, Weiner JA, Chun J. Programmed cell death is a universal feature of embryonic and postnatal neuroproliferative regions throughout the central nervous system. J Comp Neurol 1998;396:39-50.

[19] Weiner JA, Chun J. Png-1, a nervous system-specific zinc finger gene, identifies regions containing postmitotic neurons during mammalian embryonic development. J Comp Neurol 1997;381:130-42.

[20] Thomaidou D, Mione MC, Cavanagh JF, Parnavelas JG. Apoptosis and its relation to the cell cycle in the developing cerebral cortex. J Neurosci 1997;17:1075-85.

[21] Pompeiano M, Blaschke AJ, Flavell RA, Srinivasan A, Chun J. Decreased apoptosis in proliferative and postmitotic regions of the Caspase 3-deficient embryonic central nervous system. J Comp Neurol 2000;423:1-12.

[22] McConnell MJ, MacMillan HR, Chun J. Mathematical modeling supports substantial mouse neural progenitor cell death. Neural Dev 2009;4:28.

[23] Yung YC, Kennedy G, Chun J. Identification of neural programmed cell death through the detection of DNA fragmentation in situ and by PCR. Curr Protoc Neurosci 2009;Chapter 3:Unit 3 8.

[24] Haydar TF, Kuan CY, Flavell RA, Rakic P. The role of cell death in regulating the size and shape of the mammalian forebrain. Cereb Cortex 1999;9:621-6.

[25] Rakic P. Less is more: progenitor death and cortical size. Nat Neurosci 2005;8:981-2.

[26] Kuan CY, Roth KA, Flavell RA, Rakic P. Mechanisms of programmed cell death in the developing brain. Trends Neurosci 2000;23:291-7.

[27] Kingsbury MA, Rehen SK, Contos JJ, Higgins CM, Chun J. Non-proliferative effects of lysophosphatidic acid enhance cortical growth and folding. Nat Neurosci 2003;6:1292-9.

[28] Hakem R, Hakem A, Duncan GS, Henderson JT, Woo M, Soengas MS, et al. Differential requirement for caspase 9 in apoptotic pathways in vivo. Cell 1998;94:339-52.

[29] Kuida K, Haydar TF, Kuan CY, Gu Y, Taya C, Karasuyama H, et al. Reduced apoptosis and cytochrome c-mediated caspase activation in mice lacking caspase 9. Cell 1998;94:325-37.

[30] Leonard JR, Klocke BJ, D'Sa C, Flavell RA, Roth KA. Strain-dependent neurodevelopmental abnormalities in caspase-3-deficient mice. J Neuropathol Exp Neurol 2002;61:673-7.

[31] Oppenheim RW, Flavell RA, Vinsant S, Prevette D, Kuan CY, Rakic P. Programmed cell death of developing mammalian neurons after genetic deletion of caspases. J Neurosci 2001;21:4752-60.

[32] Kuida K, Zheng TS, Na S, Kuan C, Yang D, Karasuyama H, et al. Decreased apoptosis in the brain and premature lethality in CPP32-deficient mice. Nature 1996;384:368-72.

[33] Momoi T, Fujita E, Urase K. Strain-specific caspase-3-dependent programmed cell death in the early developing mouse forebrain. Neuroreport 2003;14:111-5.

[34] Lambert JF, Benoit BO, Colvin GA, Carlson J, Delville Y, Quesenberry PJ. Quick sex determination of mouse fetuses. J Neurosci Methods 2000;95:127-32.

[35] Rehen SK, Kingsbury MA, Almeida BS, Herr DR, Peterson S, Chun J. A new method of embryonic culture for assessing global changes in brain organization. J Neurosci Methods 2006;158:100-8.

[36] Barch MJ, Knutsen, T. & Spurbeck, J. L. The AGT Cytogenetics Laboratory Manual. Philadelphia: Lippincott; 1997.

[37] Capparelli R, Cottone C, D'Apice L, Viscardi M, Colantonio L, Lucretti S, et al. DNA content differences in laboratory mouse strains determined by flow cytometry. Cytometry 1997;29:261-6.

[38] Westra JW, Rivera RR, Bushman DM, Yung YC, Peterson SE, Barral S, et al. Neuronal DNA content variation (DCV) with regional and individual differences in the human brain. J Comp Neurol 2010;518:3981-4000.

[39] Schrock E, du Manoir S, Veldman T, Schoell B, Wienberg J, Ferguson-Smith MA, et al. Multicolor spectral karyotyping of human chromosomes. Science 1996;273:494-7.

[40] Slee EA, Zhu H, Chow SC, MacFarlane M, Nicholson DW, Cohen GM. Benzyloxycarbonyl-Val-Ala-Asp (OMe) fluoromethylketone (Z-VAD.FMK) inhibits apoptosis by blocking the processing of CPP32. Biochem J 1996;315 (Pt 1):21-4.

[41] Chow SC, Weis M, Kass GE, Holmstrom TH, Eriksson JE, Orrenius S. Involvement of multiple proteases during Fas-mediated apoptosis in T lymphocytes. FEBS Lett 1995;364:134-8.

[42] Zhu H, Fearnhead HO, Cohen GM. An ICE-like protease is a common mediator of apoptosis induced by diverse stimuli in human monocytic THP.1 cells. FEBS Lett 1995;374:303-8.

[43] Armstrong RC, Aja T, Xiang J, Gaur S, Krebs JF, Hoang K, et al. Fas-induced activation of the cell death-related protease CPP32 Is inhibited by Bcl-2 and by ICE family protease inhibitors. J Biol Chem 1996;271:16850-5.

[44] Sun XM, MacFarlane M, Zhuang J, Wolf BB, Green DR, Cohen GM. Distinct caspase cascades are initiated in receptor-mediated and chemical-induced apoptosis. J Biol Chem 1999;274:5053-60.

[45] Lopez-Hernandez FJ, Ortiz MA, Bayon Y, Piedrafita FJ. Z-FA-fmk inhibits effector caspases but not initiator caspases 8 and 10, and demonstrates that novel anticancer retinoid-related molecules induce apoptosis via the intrinsic pathway. Mol Cancer Ther 2003;2:255-63.

[46] Rubenstein JL, Rakic P. Genetic control of cortical development. Cereb Cortex 1999;9:521-3.

[47] Laerum OD, Farsund T. Clinical application of flow cytometry: a review. Cytometry 1981;2:1-13.

[48] Johnson LA. Sex preselection by flow cytometric separation of X and Y chromosome-bearing sperm based on DNA difference: a review. Reprod Fertil Dev 1995;7:893-903.

[49] Yu W, Centonze VE, Ahmad FJ, Baas PW. Microtubule nucleation and release from the neuronal centrosome. J Cell Biol 1993;122:349-59.

[50] Westra JW, Peterson SE, Yung YC, Mutoh T, Barral S, Chun J. Aneuploid mosaicism in the developing and adult cerebellar cortex. J Comp Neurol 2008;507:1944-51.

[51] Rajendran RS, Wellbrock UM, Zupanc GK. Apoptotic cell death, long-term persistence, and neuronal differentiation of aneuploid cells generated in the adult brain of teleost fish. Dev Neurobiol 2008;68:1257-68.

[52] Yurov YB, Iourov IY, Vorsanova SG, Liehr T, Kolotii AD, Kutsev SI, et al. Aneuploidy and confined chromosomal mosaicism in the developing human brain. PLoS ONE 2007;2:e558.

[53] Zupanc GK, Wellbrock UM, Sirbulescu RF, Rajendran RS. Generation, long-term persistence, and neuronal differentiation of cells with nuclear aberrations in the adult zebrafish brain. Neuroscience 2009;159:1338-48.

[54] Iourov IY, Vorsanova SG, Liehr T, Yurov YB. Aneuploidy in the normal, Alzheimer's disease and ataxia-telangiectasia brain: differential expression and pathological meaning. Neurobiol Dis 2009;34:212-20.

[55] Galluzzi L, Vitale I, Abrams JM, Alnemri ES, Baehrecke EH, Blagosklonny MV, et al. Molecular definitions of cell death subroutines: recommendations of the Nomenclature Committee on Cell Death 2012. Cell Death Differ 2011.

[56] Garrido C, Galluzzi L, Brunet M, Puig PE, Didelot C, Kroemer G. Mechanisms of cytochrome c release from mitochondria. Cell Death Differ 2006;13:1423-33.

[57] Gogvadze V, Orrenius S, Zhivotovsky B. Multiple pathways of cytochrome c release from mitochondria in apoptosis. Biochim Biophys Acta 2006;1757:639-47.

[58] Ow YP, Green DR, Hao Z, Mak TW. Cytochrome c: functions beyond respiration. Nat Rev Mol Cell Biol 2008;9:532-42.

[59] Broker LE, Kruyt FA, Giaccone G. Cell death independent of caspases: a review. Clin Cancer Res 2005;11:3155-62.

[60] Castedo M, Perfettini JL, Roumier T, Valent A, Raslova H, Yakushijin K, et al. Mitotic catastrophe constitutes a special case of apoptosis whose suppression entails aneuploidy. Oncogene 2004;23:4362-70.

[61] Vakifahmetoglu H, Olsson M, Zhivotovsky B. Death through a tragedy: mitotic catastrophe. Cell Death Differ 2008;15:1153-62.

[62] Vitale I, Galluzzi L, Castedo M, Kroemer G. Mitotic catastrophe: a mechanism for avoiding genomic instability. Nat Rev Mol Cell Biol 2011;12:385-92.

[63] King KL, Cidlowski JA. Cell cycle and apoptosis: common pathways to life and death. J Cell Biochem 1995;58:175-80.

[64] Vakifahmetoglu H, Olsson M, Tamm C, Heidari N, Orrenius S, Zhivotovsky B. DNA damage induces two distinct modes of cell death in ovarian carcinomas. Cell Death Differ 2008;15:555-66.

[65] Phillips JL, Hayward SW, Wang Y, Vasselli J, Pavlovich C, Padilla-Nash H, et al. The consequences of chromosomal aneuploidy on gene expression profiles in a cell line model for prostate carcinogenesis. Cancer Res 2001;61:8143-9.

[66] Zheng TS, Flavell RA. Apoptosis. All's well that ends dead. Nature 1999;400:410-1.

[67] Lengauer C, Kinzler KW, Vogelstein B. Genetic instability in colorectal cancers. Nature 1997;386:623-7.

[68] Lengauer C, Kinzler KW, Vogelstein B. Genetic instabilities in human cancers. Nature 1998;396:643-9.

[69] Rajagopalan H, Lengauer C. Aneuploidy and cancer. Nature 2004;432:338-41.

[70] Cervantes RB, Stringer JR, Shao C, Tischfield JA, Stambrook PJ. Embryonic stem cells and somatic cells differ in mutation frequency and type. Proc Natl Acad Sci U S A 2002;99:3586-90.

[71] Draper JS, Smith K, Gokhale P, Moore HD, Maltby E, Johnson J, et al. Recurrent gain of chromosomes 17q and 12 in cultured human embryonic stem cells. Nat Biotechnol 2004;22:53-4.

[72] Peterson SE, Westra JW, Rehen SK, Young H, Bushman DM, Paczkowski CM, et al. Normal human pluripotent stem cell lines exhibit pervasive mosaic aneuploidy. PLoS ONE 2011;6:e23018.

[73] Spits C, Mateizel I, Geens M, Mertzanidou A, Staessen C, Vandeskelde Y, et al. Recurrent chromosomal abnormalities in human embryonic stem cells. Nat Biotechnol 2008;26:1361-3.

[74] Deshmukh M. Caspases in ischaemic brain injury and neurodegenerative disease. Apoptosis 1998;3:387-94.

[75] Tai YT, Svendsen CN. Stem cells as a potential treatment of neurological disorders. Curr Opin Pharmacol 2004;4:98-104.

[76] Staley K, Blaschke AJ, Chun J. Apoptotic DNA fragmentation is detected by a semi-quantitative ligation-mediated PCR of blunt DNA ends. Cell Death Differ 1997;4:66-75.

[77] Barnes DE, Stamp G, Rosewell I, Denzel A, Lindahl T. Targeted disruption of the gene encoding DNA ligase IV leads to lethality in embryonic mice. Curr Biol 1998;8:1395-8.

[78] Gao Y, Sun Y, Frank KM, Dikkes P, Fujiwara Y, Seidl KJ, et al. A critical role for DNA end-joining proteins in both lymphogenesis and neurogenesis. Cell 1998;95:891-902.

[79] Gu Y, Sekiguchi J, Gao Y, Dikkes P, Frank K, Ferguson D, et al. Defective embryonic neurogenesis in Ku-deficient but not DNA-dependent protein kinase catalytic subunit-deficient mice. Proc Natl Acad Sci U S A 2000;97:2668-73.

[80] McConnell MJ, Kaushal D, Yang AH, Kingsbury MA, Rehen SK, Treuner K, et al. Failed clearance of aneuploid embryonic neural progenitor cells leads to excess aneuploidy in the Atm-deficient but not the Trp53-deficient adult cerebral cortex. J Neurosci 2004;24:8090-6.

[81] Muotri AR, Chu VT, Marchetto MC, Deng W, Moran JV, Gage FH. Somatic mosaicism in neuronal precursor cells mediated by L1 retrotransposition. Nature 2005;435:903-10.

[82] Muotri AR, Gage FH. Generation of neuronal variability and complexity. Nature 2006;441:1087-93.

[83] Chun J. Selected comparison of immune and nervous system development. Adv Immunol 2001;77:297-322.

[84] Malu S, Malshetty V, Francis D, Cortes P. Role of non-homologous end joining in V(D)J recombination. Immunol Res 2012.

[85] Wilkie AL, Jordan SA, Sharpe JA, Price DJ, Jackson IJ. Widespread tangential dispersion and extensive cell death during early neurogenesis in the mouse neocortex. Dev Biol 2004;267:109-18.

[86] Yoshida H, Kong YY, Yoshida R, Elia AJ, Hakem A, Hakem R, et al. Apaf1 is required for mitochondrial pathways of apoptosis and brain development. Cell 1998;94:739-50.

[87] Dykens EM, Sutcliffe JS, Levitt P. Autism and 15q11-q13 disorders: behavioral, genetic, and pathophysiological issues. Ment Retard Dev Disabil Res Rev 2004;10:284-91.

CHAPTER 3

Neural aneuploidy induced by substance abuse during fetal brain development

Abstract

Mosaic aneuploidy, defined as coincidental chromosome losses and/or gains to deviate from the haploid chromosome complement, has been identified in both the developing and the adult mammalian central nervous system, including neural progenitor cells and functionally integrated mature neurons. Aneuploidy arises through altered cellular mechanisms controlling growth, DNA synthesis and replication, and neurogenesis. Exposure to toxic insults such as alcohol and amphetamines can result in cell damage including oxidative stress and may contribute to DNA damage and misrepair through which aneuploidy can arise. When used during pregnancy, alcohol and amphetamines can cross the placental barrier from the mother into the fetal brain, and are linked to developmental defects including craniofacial abnormalities, central nervous system defects, behavioral and cognitive deficits, increased risk for preterm birth, pre- and postnatal growth retardation and Fetal Alcohol Spectrum Disorders (FASD). Here we show that *in utero* exposure to alcohol or amphetamines increases the incidence of mosaic aneuploidy in mitotic cortical progenitor cells in the developing fetal brain, and persists into postmitotic neurons.

Introduction

In utero exposure to substances of abuse such as alcohol and amphetamines has serious consequences to the health and development of a fetus, as these substances can easily pass through the placental barrier and into the fetal brain [1], causing neuroanatomical abnormalities and developmental defects. Fetal Alcohol Spectrum Disorder (FASD) is a descriptive clinical term that encompasses the effects of drinking alcohol during pregnancy, which

include pre- and postnatal growth retardation, developmental delays or dysfunction of the central nervous system (CNS), and craniofacial anomalies (http://www.ncbi.nlm.nih.gov/pubmedhealth/PMH0001909/). No comparable clinical term is used to describe the effects of prenatal exposure to amphetamines, although equally serious consequences of these drugs, which include methamphetamine and 3,4-methylenedioxymethamphetamine (MDMA, or ecstasy), are recognized: intrauterine growth restriction, preterm birth, learning and motor disabilities and behavioral problems [2]. Compounding the prenatal effects of exposure, women who used amphetamines like methamphetamine were also more likely to smoke cigarettes, use other illicit drugs, such as cocaine or marijuana, or binge drink alcohol while pregnant [3], increasing the risk of severe problems for the fetus.

For both alcohol and amphetamines, the severity and heterogeneity of birth defects from substance exposure *in utero* are believed to be a result of variable consumption by the mother during pregnancy [4-6], with neurotoxic affects dependent on the dosage and stage of fetal development. Pinpointing the temporal effects of substance abuse in the developing human CNS is particularly difficult, as numerous, overlapping stages of neurogenesis span the duration of the pregnancy and extend into post-natal life. In contrast, murine CNS development is much more temporally discrete and has been extensively studied [7], making mice an ideal model organism to study the effects of drugs of abuse on neurogenesis. Murine cortical neurogenesis occurs between embryonic days (E) 11 and 17 with E12-14 as the peak of neurogenesis in cortical layers V and VI (roughly correlating to the second trimester in human) [8]. E13 in mice is also the peak of neurogenesis for the subiculum (the main hippocampal output), while E14 is the peak of neurogenesis for the caudate nucleus and the putamen [7] – regions particularly important in the dopaminergic pathways impacted by amphetamines. Studies have shown that during this time, ethanol affects migration and proliferation [9] and leads to DNA damage through oxidative stress [10]; methamphetamine exposure during this period also induces DNA damage, leading to long term neurodevelopmental deficits in motor coordination [11].

While emphasis has been placed on the neuroanatomical and behavioral effects of substance abuse in the developing fetus, the consequences of alcohol and amphetamine neurotoxicity on genomic stability are not well known. Both teratogens are thought to compromise DNA integrity [12-14], though the mechanism of altered DNA integrity by alcohol and amphetamine has never been linked to a functional outcome. It is also known that E13 and 14 are the peak periods for normal cortical aneuploidy, a phenomenon that produces up to 33% non-euploid cells during neuroprogenitor cell (NPC) division [15]. The combination of genomic mutability via normal NPC aneuploidy and the fact that both alcohol and amphetamine compromise DNA integrity during embryonic neurogenesis in mice led to the hypothesis that prenatal exposure to alcohol or amphetamines would perturb the natural levels of mosaic aneuploidy observed in NPCs of the developing murine cortex. Furthermore, altered mosaic aneuploidy levels could persist into the mature brain and contribute to the wide heterogeneity of symptoms observed in children exposed *in utero* to substances of abuse. Altered aneuploidy levels during neurogenesis that persist in the mature brain would link the functional mechanism of compromised DNA integrity to the heterogeneous structural and behavioral deficits in individuals prenatally exposed to drugs of abuse.

Materials and Methods

Animals and treatments

All animal protocols were approved by the Institutional Animal Care and Use Committee at The Scripps Research Institute, and conform to the National Institutes of Health guidelines and public law. Timed-pregnant C57Bl/6J females were treated by a single interperitoneal injection at embryonic day 13.5 (E0.5 is defined as the day on which a copulation plug was observed) with d-amphetamine (10 mg/kg)(Sigma), 17.6% (v/v) alcohol (to a final dosage of 3 g/kg) or 26.4% (v/v) alcohol (to a final dosage of 4.5 g/kg). Control animals were exposed to equivalent volumes of saline vehicle. Treated dams were anesthetized using isoflurane (Isothesia, Butler Animal Health Supply, Dublin, OH), killed by cervical dislocation, and the embryos were collected. Embryonic

cortices from E14.5 were used for analysis of mitotic cells and lagging chromosomes; cortices from E19.5 were used for post-mitotic cell analysis by FISH.

Metaphase spread preparation

Freshly isolated E14.5 cortices from drug or vehicle treated embryos were incubated 100 ng/ml Karyomax Colcemid (Life Technologies, San Diego, CA) in OptiMem media (Life Technologies) supplemented with 10 ng/ml basic fibroblast growth factor (bFGF; Peprotech, Rocky Hill, NJ) for 3 hours at 37°C. Cortices were dissociated by trituration to a single cell suspension and centrifuged at 1000 rpm for 5 min at 4°C. Cells were gently resuspended in 0.075 M KCl and incubated at 37°C for 7-10 minutes to induce hypotonic swelling, before fixation in 3:1 methanol:glacial acetic acid, added dropwise while slowly vortexing. Metaphase spreads were prepared on Superfrost Plus slides (Fisher Scientific) following standard cytogenetic protocols [16], and stained with 4',6-diamidino-2-phenylindole (DAPI, Life Technologies). Images of chromosome spreads were acquired using a 100x oil-immersion objective on a Zeiss Imager D1 microscope (Carl Zeiss, Gottingen, Germany) with an AxioCamHR digital camera and Zeiss AxioVision software (Carl Zeiss), and analyzed using karyotyping software (Applied Spectral Imaging, Carlsbad, CA). For each treatment paradigm, 150-200 metaphase spreads were analyzed from 2 embryos from each of three litters.

Immunohistochemistry for lagging chromosome analysis

Intact cortical hemispheres from drug- or vehicle-treated embryos were embedded in Tissue-Tek OCT (Optimal Cutting Temperature, Miles Inc., Elkhart, NJ) and frozen on dry ice immediately following isolation. Coronal sections of 10 µm were mounted on slides, and preserved at -80°C until use, when sections were fixed in 4% paraformaldehyde. Antigen retrieval was performed by boiling slides for 20 minutes in 1x Sodium Citrate buffer, followed by an immediate wash in room temperature PBS. Sections were blocked in 5% normal goat serum (Vector Laboratories) and 0.2% Triton X-100 in PBS for 30 minutes. Primary antibodies for this study were rabbit polyclonal anti-phosphorylated (phospho) histone H3 (diluted 1:1000) and mouse anti-nestin (diluted 1:400); slides were incubated with primary overnight at 4°C. Slides

were then rinsed in PBS three times for five minutes each, and incubated in secondary antibodies (AlexaFluor 488-conjugated donkey anti-mouse IgG (1:1000) and AlexaFluor 568-conjugated goat anti-rabbit IgG (1:1000)). Images were obtained using a 63x objective on a DeltaVision deconvolution microscope (Applied Precision, Seattle, WA). For each three-dimensional image, the total number of cells that stained positive for both nestin and phospho-H3 was recorded, and nuclear length (longest point A-B within a nucleus) and the standard deviation from average nuclear length was determined. To discriminate lagging chromosomes from artifacts of tissue sectioning, a chromosome was considered a lagging chromosome for a particular cell if it was (1) within the area surrounding the cell determined by one standard deviation, and (2) immunoreactive for phospho-H3. Images were prepared using Photoshop (Adobe Systems, Mountain View, CA).

Fluorescent in situ hybridization (FISH)

FISH was performed against chromosomes 11 and 2, using TK (11qE1)(red) and AurKa (2qH3)(green) RF Poseidon mouse probes (supplied in a mix from Kreatech, Amsterdam, The Netherlands), and hybridized according to the manufacturer's instructions. Interphase nuclei from E19.5 cortices were isolated for FISH by detergent-lysis and mounted on slides, then left to air dry for 24 hours. Slides were rinsed in 2x saline-sodium citrate buffer (SSC), then treated with 100 mg/ml pepsin (Sigma) in 0.01 M HCl for seven minutes at 37°C. After a two minute phosphate-buffered saline (PBS) wash, slides were incubated in 1% formaldehyde in 1x PBS/50 mM $MgCl_2$ for 10 minutes at room temperature. Slides were washed in PBS three times, then dehydrated in 70%, 80% and 100% ethanol before air drying. Slides were then denatured in 70% formamide/2x SSC at 72°C for 2 minutes, followed immediately by dehydrating in ice-cold 70%, 80% and 100% ethanol. Chromosome probe mix was aliquoted at 10 µl per slide, and denatured for 10 minutes at 90°C. Probe was applied to the denatured slides and covered with glass cover slips; the edges of the cover slip were sealed with rubber cement and the slides were incubated overnight in a dark, humidified chamber at 37°C. The following day, the rubber cement and cover slip were removed, and the slides were washed in a series of varying stringency washes for 5

minutes each: 2x SSC at room temperature, 2x SCC/50% formamide at 45℃, 2x SSC with 0.1% Tween-20 at 45℃, 2x SSC at 45℃, before counter staining with DAPI for 10 minutes at room temperature. Slides were then mounted and imaged using the 100x oil-immersion objective on a Zeiss Imager D1 microscope (Carl Zeiss).

Results

In utero exposure to substances of abuse increases mosaic aneuploidy

To determine the changes in mosaic aneuploidy driven by *in utero* exposure to substances of abuse (ethanol and amphetamines), a "binge" treatment paradigm was used, exposing the dam to a single, moderate-to-high dose of drug. Aneuploidy levels in the fetal brain were assessed by analyzing metaphase spreads from E14.5 embryonic cortical neural progenitor cells, 24 hours after exposure to 3 g/kg ethanol, 4.5 g/kg ethanol, 10 mg/kg d-amphetamine or saline vehicle. The euploid mouse cell contains 40 chromosomes; aneuploid NPCs were observed in each treatment group (**Fig. 3.1**). The total amounts of aneuploidy in each treatment were significantly increased compared to vehicle controls: 25% in vehicle versus 64% in 3 g/kg ethanol; 54% in 4.5 g/kg ethanol, and 58% in the 10 mg/kg d-amphetamine group ($p < 0.0001$ for each comparison, Student's t-test) (**Fig. 3.2 A**). Loss of one chromosome was consistently the most frequent aneuploid karyotype observed (**Fig. 3.2 B & C**). Hypoploidy was significantly more common than hyperploidy in each group ($p < 0.05$ for each comparison, Student's t-test) (**Fig. 3.2 D**).

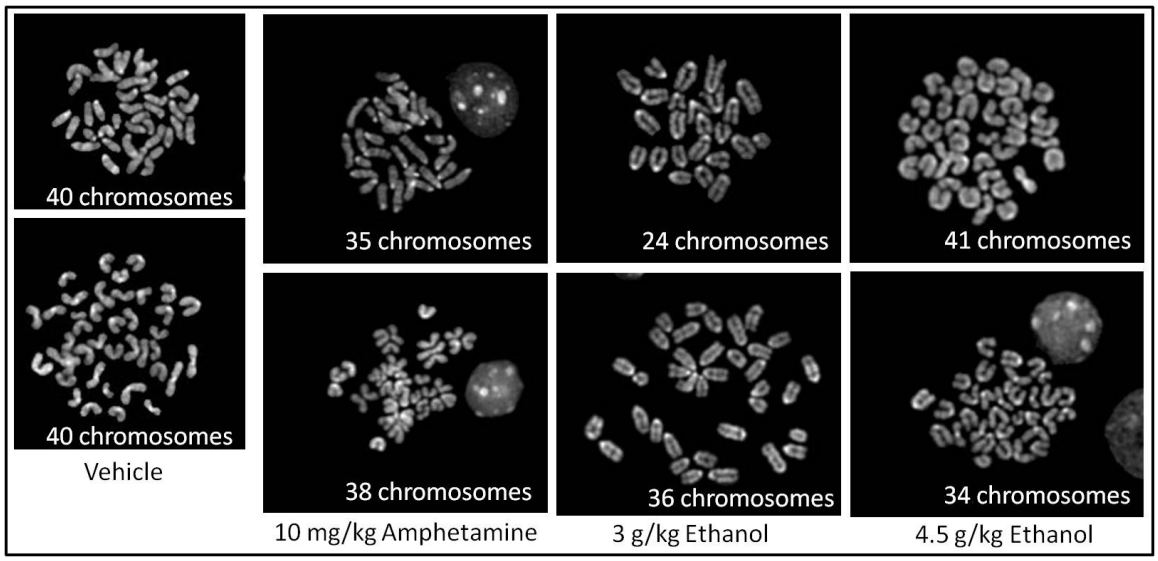

Figure 3.1. Aneuploidy in mitotic cortical cells following *in utero* drug exposure. Representative metaphase chromosome spreads from cortices of embryos exposed to 3 g/kg ethanol, 4.5 g/kg ethanol, or 10 mg/kg d-amphetamine or to saline vehicle at embryonic day (E) 13.5. The number of chromosomes is given for each spread; the euploid chromosome number for mice is 40.

Figure 3.2. Ethanol and amphetamine exposure *in utero* increases total incidence of aneuploidy in mitotic cells from the mouse embryonic cortex. **A**: Total aneuploidy measured at embryonic day (E) 14.5 in embryos exposed at E13.5 to 3 g/kg ethanol, 4.5 g/kg ethanol or 10 mg/kg d-amphetamine. Significant increases in aneuploidy were observed for each treatment group compared to vehicle control: 64% aneuploidy in 3 g/kg ethanol group; 54% aneuploidy in 4.5 g/kg ethanol group; and 58% aneuploidy in 10 mg/kg d-amphetamine group versus 25% aneuploidy in vehicle control ($p<0.0001$ for each comparison to vehicle control, Student's t-test). **B & C**: Histograms of the distribution of aneuploid cells identified following exposure to ethanol (B; 3 g/kg distribution shown in red, 4.5 g/kg distribution in blue) or d-amphetamine (**C**; distribution in red) compared to vehicle control (distribution shown in black in both **B** & **C**). **D**. Hypoploidy (chromosome loss) was significantly more frequent than hyperploidy (chromosome gain) in each treatment group ($p < 0.001$ for vehicle, 3 g/kg ethanol and 10 mg/kg d-amphetamine, $p = 0.013$ for 4.5 g/kg ethanol; Student's t test). Observed percentages of hypoploidy and hyperploidy are given below the graph.

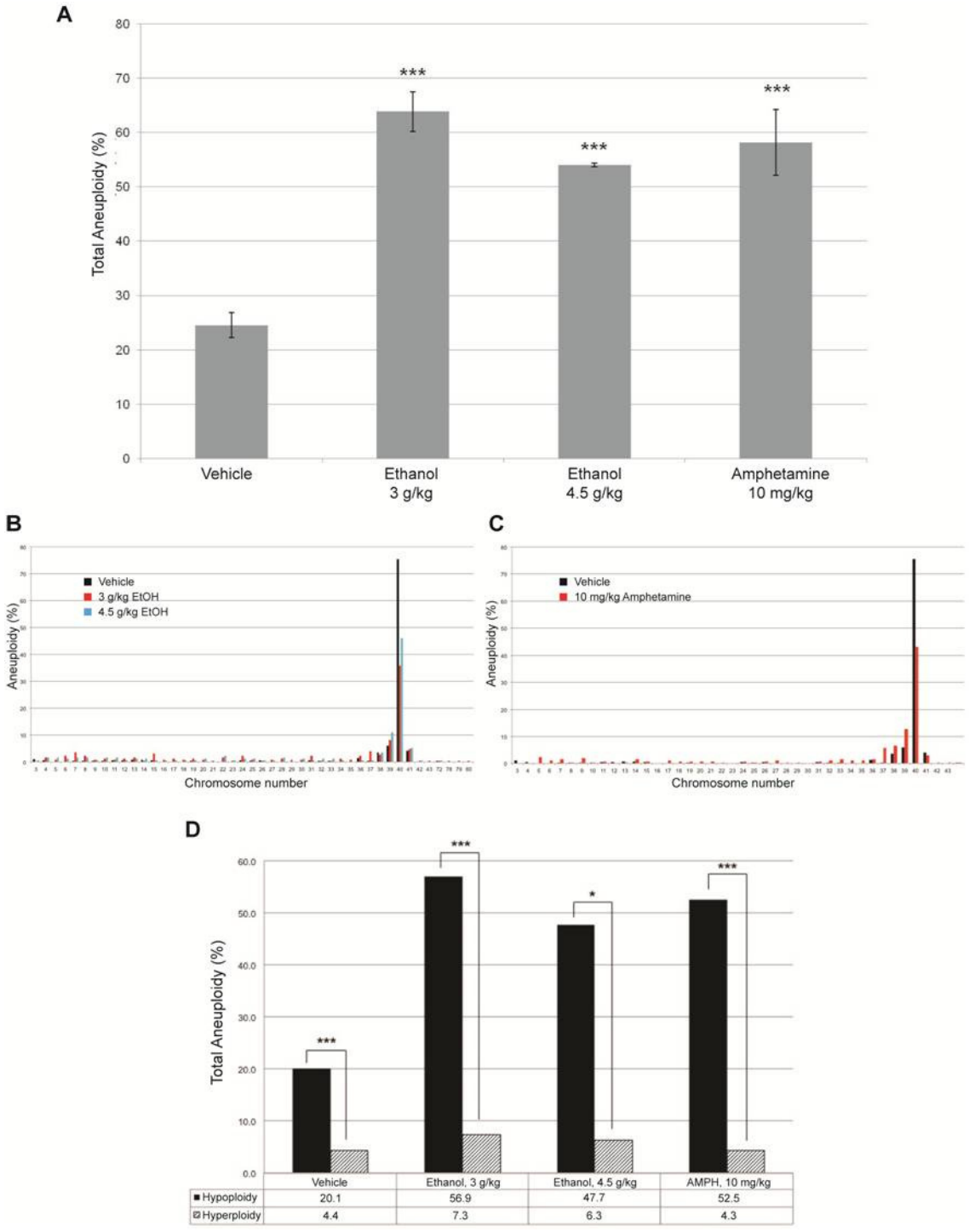
A
Total Aneuploidy (%)
80
70
60
50
40
30
20
10
0
***
***
***
Vehicle
Ethanol 3 g/kg
Ethanol 4.5 g/kg
Amphetamine 10 mg/kg
B
Vehicle
3 g/kg EtOH
4.5 g/kg EtOH
Aneuploidy (%)
Chromosome number
C
Vehicle
10 mg/kg Amphetamine
Aneuploidy (%)
Chromosome number
D
Total Aneuploidy (%)
60.0
50.0
40.0
30.0
20.0
10.0
0.0
***
***
*
***
Vehicle
Ethanol, 3 g/kg
Ethanol, 4.5 g/kg
AMPH, 10 mg/kg
Hypoploidy
20.1
56.9
47.7
52.5
Hyperploidy
4.4
7.3
6.3
4.3

Chromosome spreads were grouped into subcategories depending on severity: cells that had lost or gained fewer than 5 chromosomes were classified as mildly aneuploid; a loss or gain of more than 5 chromosomes was considered severe aneuploidy (**Fig. 3.3 A**). For the vehicle-injected control, mild aneuploidy occurred in 15% of metaphase spreads, and severe aneuploidy in 9%. In stark contrast, embryos exposed to 3 g/kg ethanol had four times the amount of severe aneuploidy (41.8%, $p<0.001$, Student's t-test) and only slightly more mild aneuploidy (22.0%, no significance) than controls (**Fig. 3.3 B**). Embryos from the 4.5 g/kg treatment group, which showed less total aneuploidy than the other treatment groups, had approximately the same amount of mild aneuploidy (21.9%) as observed in the 3 g/kg ethanol group. The 4.5 g/kg ethanol group also showed less severe aneuploidy than the 3 g/kg ethanol group (32.1% versus 41.8%, respectively) – a 256% increase compared to the 364% increase seen with 3g/kg – but still significantly more than vehicle controls ($p=0.02$, Student's t-test). Because of the marked increase in aneuploidy rates in the 3 g/kg ethanol treatment group and lesser degree of aneuploidy in the 4.5 g/kg ethanol treatment group, only animals exposed to 3 g/kg ethanol used for analyses of aneuploidy at other time points. Embryos exposed to 10 mg/kg amphetamine had approximately equal amounts of both mild aneuploidy (29.0%) and severe aneuploidy (29.2%, no significance).

Figure 3.3. Ethanol and amphetamine exposure *in utero* increases extreme aneuploidy. **A**: Mild aneuploidy (loss or gain of <5 chromosomes) and severe aneuploidy (loss or gain of >5 chromosomes) rates for each treatment group show significant increases in severe aneuploidy in embryos treated with 3 g/kg ethanol (41.8% total aneuploidy; $p<0.001$, Student's t-test) and 4.5 g/kg ethanol (32.1%; $p = 0.02$, Student's t-test) compared to vehicle controls (15.4%). Severe aneuploidy in d-amphetamine treated embryos was just short of significance compared to vehicle control (29.2% total aneuploidy; $p = 0.06$, Student's t-test). Increases in mild aneuploidy for each group were not significant (22.0% for 3 g/kg ethanol, 21.9% for 4.5 g/kg ethanol, and 28.9% for 10 mg/kg d-amphetamine). **B**: Pie charts showing the total percentages of euploidy and mild and severe aneuploidy for each treatment group illustrate the changes in types of aneuploidy detected; corresponding percentages are shown on each graph.

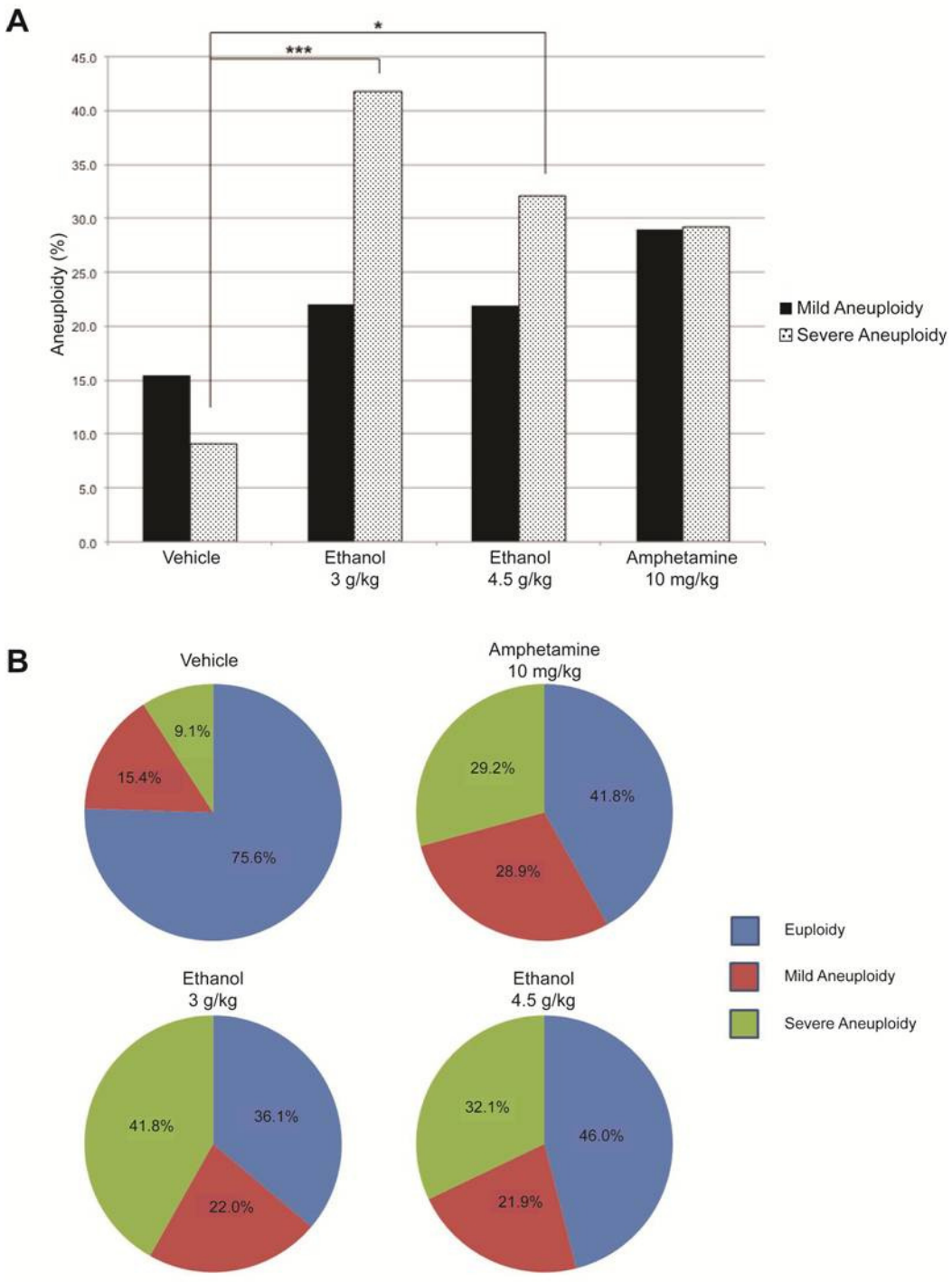
A
*
***
45.0
40.0
35.0
30.0
25.0
20.0
15.0
10.0
5.0
0.0
Aneuploidy (%)
Vehicle
Ethanol 3 g/kg
Ethanol 4.5 g/kg
Amphetamine 10 mg/kg
Mild Aneuploidy
Severe Aneuploidy
B
Vehicle
9.1%
15.4%
75.6%
Amphetamine 10 mg/kg
29.2%
41.8%
28.9%
Ethanol 3 g/kg
41.8%
36.1%
22.0%
Ethanol 4.5 g/kg
32.1%
46.0%
21.9%
Euploidy
Mild Aneuploidy
Severe Aneuploidy

Increased incidence of lagging chromosomes in ethanol exposed mitotic cortical neuroblasts

Cortical progenitor cells are found lining the lateral ventricle of the cerebral hemisphere, identifiable for their immunoreactivity for the intermediate filament protein, nestin (not shown); progenitors undergoing mitosis are also immunoreactive for phosphorylated histone H3. These neuronal and cell cycle markers allowed for the identification of dividing cells in this region as neuroblasts. Deconvolution microscopy produced three-dimensional images of mitotic cortical neuroblasts (representative Z-stack images are shown, **Fig. 3.4**), in which lagging chromosomes are physically separated from other condensed phospho-H3 labeled chromosomes. Cortices from ethanol-exposed embryos showed 16.4% of mitoses with lagging chromosomes, versus 9.8% in vehicle controls. These data confirm the presence of increased chromosomal instability in brains exposed *in utero* to substances of abuse.

Aneuploid cells survive through embryonic neurogenesis

The period of murine cortical neurogenesis (E11-17) coincides with a major period of caspase-mediated programmed cell death (PCD) [17, 18]. During this period, cells with extremely aneuploid karyotypes are targeted, while cells with mildly aneuploid karyotypes may survive [19]. To determine whether increased levels of aneuploidy, induced by either ethanol or amphetamines, persist past neurogenesis and survive PCD selection, post-mitotic neurons isolated from E19.5 cortices were evaluated by fluorescence in situ hybridization (FISH). Two probes against randomly-chosen chromosomes 11qE1 (red) and 2qH3 (green) were used; no current evidence suggests that either chromosome 11 or 2 would be preferentially lost or gained in drug-induced aneuploid cells. Monosomies and trisomies were detectable for each chromosome from each treatment group; representative aneusomic nuclei are shown here (**Fig. 3.5 A**). For all treatment groups, a significant increase in aneusomy for both chromosome 2 and chromosome 11 were detected (**Fig. 3.5 B & C**): chromosome 11 aneusomy increased from 3.6% in vehicle to 7.2% with ethanol exposure ($p<0.0001$), and to 5.7% with amphetamine treatment ($p< 0.001$);

chromosome 2 aneusomy increased from 4.0% in controls to 6.4% with ethanol and 5.3% with amphetamines ($p < 0.05$ for each comparison, Student's t-test).

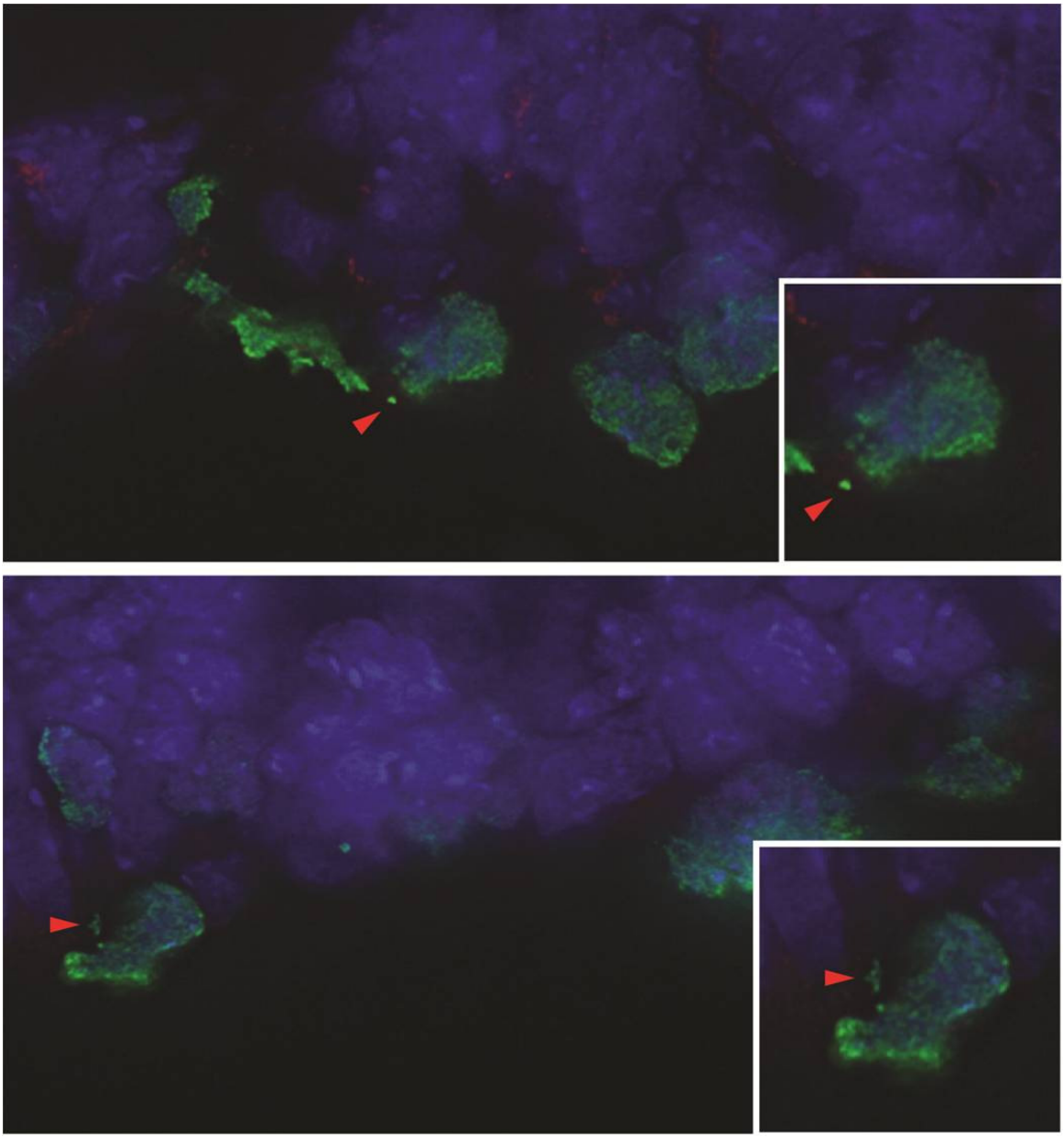

Figure 3.4. Ethanol and amphetamine-exposed mitotic neuroblasts show increases in lagging chromosomes. Representative images of lagging chromosomes from deconvolution microscopy analysis of mitotic neuroblasts in the E14.5 cortex. Mitotic neuroblasts in the ventricular zone are immunoreactive for phospho-H3 (green); counterstaining of nuclei with DAPI is shown in blue. Red arrowheads point to lagging chromosomes, determined by phospho-H3 immunoreactivity and positioning within one standard deviation of the average nuclear length.

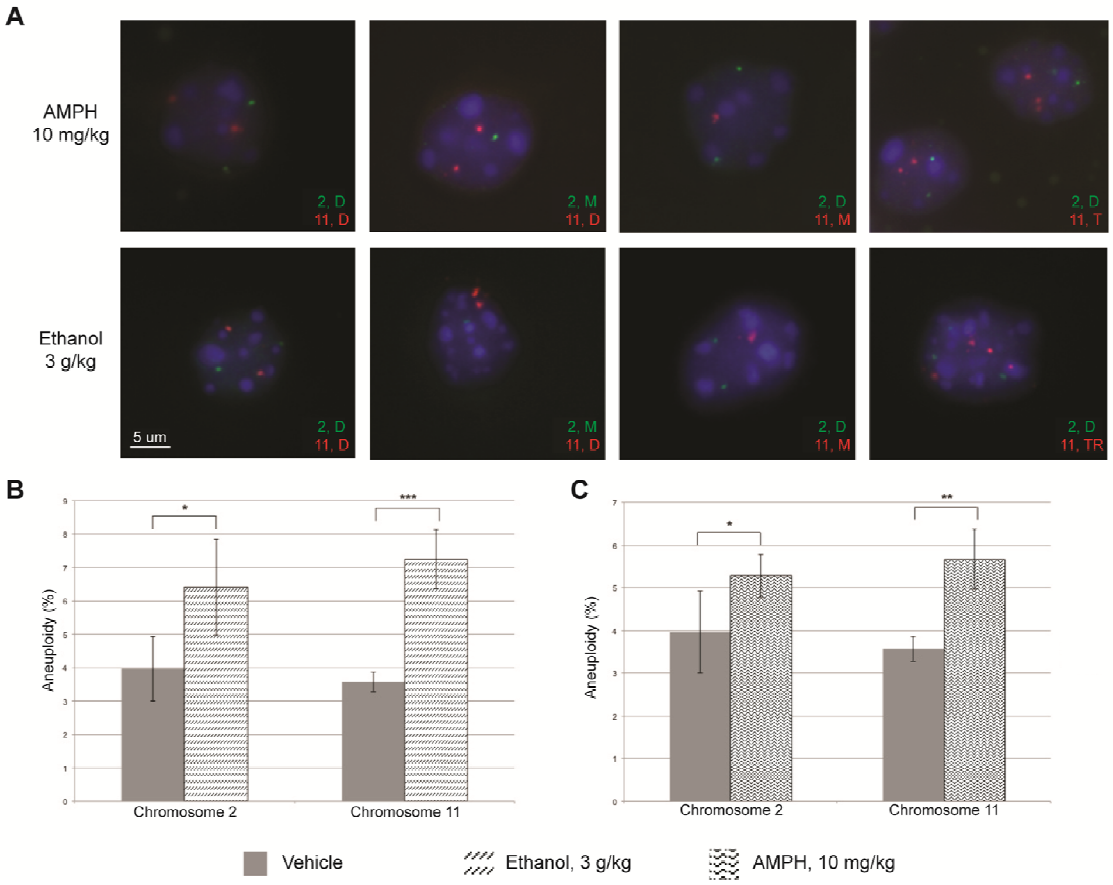

Figure 3.5. Post-mitotic neurons show increased levels of ethanol- and amphetamine-induced aneuploidy. **A**: Representative images of aneusomic nuclei analyzed by FISH at E19.5 using point probes against chromosomes 2 (green) and 11 (red). From each treatment group, nuclei monosomic, disomic, trisomic and tetrasomic for each probe were observed. **B & C**: Quantitative analysis of aneusomy rates for each probe reveals significant increases in aneusomy in embryos exposed to ethanol or d-amphetamine. Chromosome 2 aneuploidy increased to 6.4% for the 3 g/kg ethanol group (**B**) and 5.3% for the 10 mg/kg amphetamine group (**C**) from 4.0% seen in vehicle controls ($p<0.05$ for each comparison, Student's t-test). Chromosome 11 aneuploidy increased from 7.2% for the 3 g/kg ethanol group (**B**) and 5.7% for the 10 mg/kg amphetamine group (**C**) from 3.6% observed in vehicle controls ($p<0.0001$ and $p<0.001$, respectively, Student's t-test).

Discussion

Mosaic aneuploidy levels during cortical neurogenesis are dramatically altered in embryonic mice exposed to ethanol or amphetamines in a “binge” consumption paradigm. The major findings of this study are as follows: (i) the total incidence of aneuploidy in cortical neural progenitor cells from embryos treated with amphetamines or ethanol more than doubled compared to levels in embryos given saline, with hypoploidy more prevalent than hyperploidy; (ii) both severe forms of aneuploidy, with more than 5 chromosomes gained or lost, were preferentially increased to levels 3-4 times greater in treatment groups than in controls; (iii) lagging chromosomes were more frequent in drug and ethanol-exposed embryos, suggesting a mechanism through which altered levels of aneuploidy occur; (iv) drug-induced cortical aneuploidy persists through neurogenesis and concurrent programmed cell death into post-mitotic neurons.

This is the first study to examine the effects of alcohol or amphetamines on the genomic mosaicism of the brain, and these data are consistent with previous studies on the mechanisms of neurotoxicity. In particular, the role of oxidative stress is relevant for understanding drug-induced cellular outcomes, including DNA damage and cell death, as imbalances between the production and degradation of reactive oxygen species (ROS) increase DNA instability and damage [20]. For each drug, the original insult triggers a differential response in cellular signaling and subsequent ROS damage [21]. Amphetamines, sympathomimetics for dopamine and norepinephrine, are a substrate for the dopamine transport pathway and work to inhibit monoamine reuptake from nerve terminals; they also drive the release of dopamine and serotonin neurotransmitters from vesicular storage, increasing the cytoplasmic concentration of these monoamines [22, 23]. Metabolism of intraneuronal dopamine by monoamine oxidase produces H_2O_2 , which reacts with metals to form a hydroxyl radical (•OH) [24], and unusually high concentrations of dopamine that may overwhelm the ability of a cell to processes both DNA-damaging free radicals and toxic metabolites, including dopaquinone [22, 24, 25].

Ethanol, a known carcinogen, elicits cellular damage through both direct and indirect sources of oxidative stress. Direct mechanisms include the formation of free radicals such as the hydroxyethyl group ($CH_3C•HOH$) [26, 27], as well as the formation of reactive oxygen species from increased mitochondrial respiration (driven by metabolites including acetaldehyde and acetate), or increased cytochrome P450 activity in microsomes [28-30]. Indirectly, ethanol depletes antioxidant activity, including the critical cellular antioxidant protein glutathione (GSH) [28], leading to increased mitochondrial damage and activation of signaling cascades for cell death pathways or cell cycle disruption.

DNA lesions, characterized by altered bases like 7,8-dihydro-8-oxoguanine (8-oxo-G) [31] are a result of DNA damage via oxidative stress, and increased levels have been detected in the embryonic brains of mice exposed to methamphetamine *in utero* [11]. Normally, cells repair DNA lesions by non-homologous end joining (NHEJ) or homologous recombination repair [32-34], but the chromosomal instability resulting from failure or cellular inability to repair lesions can lead to asymmetrical chromosome rearrangement, end to end fusion, translocations and unequal segregation of chromosomes during mitosis, creating aneuploid daughter cells [35-39]. The level of oxidative damage induced in the fetal brain by one or more doses of alcohol or amphetamines, combined with the duration of the insult, could overwhelm the abilities of the cells to maintain genomic integrity, resulting in the levels of aneuploidy observed here.

Beyond causing DNA lesions, H_2O_2 and the free radicals it forms are also implicated in aberrant cell cycle progression. *In vitro* studies demonstrate the effects of H_2O_2 on cell cycle-arrested cell populations, demonstrating that oxidative stress can override the spindle assembly checkpoint preventing the continuation of anaphase by driving ubiquitin-mediated degradation of the anaphase inhibitor securin [37]. Without this spindle regulation, cell cycle continuation may increase chromosomal instability and aneuploidy in daughter cells. H_2O_2 can also cause hyperamplification of centrosomes, resulting in multipolar spindle formation [40] and potentially leading to micronuclei formation. Ethanol exposure *in vitro* increases the frequency of micronuclei, which, along with lagging chromosomes, are a marker of heightened genomic

instability during anaphase [35]; our data confirm an *in vivo* increase in drug-induced lagging chromosomes. The lagging chromosomes we observed in mitotic cortical neuroblasts are thought to arise through improper kinetochore-microtubule attachments, again implicating the spindle checkpoint [41]. Interestingly, the lagging chromosomes themselves are often integrated back into the nucleus [42]; erroneous segregation of sister chromatids occurs without evidence of lagging [41]. Additional mechanisms for increased genomic instability are also likely, especially given the extremely high levels of aneuploidy we observed following a single dose of either ethanol or amphetamine.

As examined in the previous chapter, a period of programmed cell death (PCD) within the ventricular zone of the cerebral cortex correlates with neurogenesis [17, 18, 43]; during this phase, aneuploid cells with extreme karyotypes are preferentially eliminated [19]. An increase in karyotype-specific cell death might account for the differences in aneuploidy between ethanol treatment groups. Complementary to this, an increase in oxidative stress corresponding to a higher ethanol dose could drive cell death as well – as cellular mechanisms for DNA damage and free radical elimination are overwhelmed, apoptotic pathways may be triggered. A previous study in mice exposed to ethanol from E6.5 to E11 characterized cell death patterns throughout the nervous system and craniofacial region, finding excessive apoptosis in stage-specific PCD sites [44], suggesting that ethanol neurotoxicity targets particular vulnerable cell populations. However, our data also show increased aneuploidy in post-mitotic neurons from the E19 cortex, after the periods of neurogenesis and PCD have concluded. If aneuploid neurons survive into the adult brain they may be integrated into the neural circuitry [45], and tracking ethanol- or amphetamine-induced aneuploidy into the mature cortex with BrdU birth dating and FISH approaches would allow for this type of examination. Analyses of neuronal signaling in these cells could also offer information on impaired function relevant to understanding the cognitive deficits associated with fetal drug and alcohol exposure.

Equally interesting and important would be cytogenetic studies to determine if there are specific genomic rearrangements, translocations, deletions or duplications associated with

alcohol or amphetamine use. The precedent for this has been set in yeast, as chronic oxidative DNA damage revealed a “hot spot” for genomic rearrangements on chromosome II [38]; well-developed techniques including SKY and CGH would facilitate such studies. The identification of sites susceptible to consistent genomic instability and the identification of the genes therein could also provide a deeper understanding of the cognitive and behavioral consequences of drug use. Preventative measures and potential remedies for genomic alterations induced by alcohol or amphetamine exposure are also being explored, with a current focus on oxidative damage. Antioxidants including flavenoids, α-tocopherol (Vitamin E), folic acid and β-carotene [27] would be worth assessing for their protective affects in reducing the genomic instability associated with *in utero* drug and alcohol exposure.

Chapter 3, in full, is currently being prepared for submission for publication of this material. The dissertation author was the primary investigator and author of this material. Hope Mirendil assisted with the design of the project, performed animal injections and tissue isolation, and assisted with metaphase chromosome spread counts and deconvolution microscopy sample preparation. Sidney Perez assisted with metaphase chromosome spread quantitation and deconvolution microscopy sample preparation, and performed all lagging chromosome data collection. Claudia Martinez assisted with metaphase chromosome spread quantitation. Jerold Chun supervised the project and provided advice.

References

[1] Ganapathy VV, Prasad PD, Ganapathy ME, Leibach FH. Drugs of abuse and placental transport. Adv Drug Deliv Rev 1999;38:99-110.

[2] Lindsay MK, Burnett E. The use of narcotics and street drugs during pregnancy. Clin Obstet Gynecol 2013;56:133-41.

[3] Ho E, Karimi-Tabesh L, Koren G. Characteristics of pregnant women who use ecstasy (3, 4-methylenedioxymethamphetamine). Neurotoxicol Teratol 2001;23:561-7.

[4] Acuff-Smith KD, Schilling MA, Fisher JE, Vorhees CV. Stage-specific effects of prenatal d-methamphetamine exposure on behavioral and eye development in rats. Neurotoxicol Teratol 1996;18:199-215.

[5] O'Leary CM. Fetal alcohol syndrome: diagnosis, epidemiology, and developmental outcomes. J Paediatr Child Health 2004;40:2-7.

[6] Ornoy A, Ergaz Z. Alcohol abuse in pregnant women: effects on the fetus and newborn, mode of action and maternal treatment. Int J Environ Res Public Health 2010;7:364-79.

[7] Finlay BL, Darlington RB. Linked regularities in the development and evolution of mammalian brains. Science 1995;268:1578-84.

[8] Guerri C. Neuroanatomical and neurophysiological mechanisms involved in central nervous system dysfunctions induced by prenatal alcohol exposure. Alcohol Clin Exp Res 1998;22:304-12.

[9] Miller MW. Limited ethanol exposure selectively alters the proliferation of precursor cells in the cerebral cortex. Alcohol Clin Exp Res 1996;20:139-43.

[10] Kido R, Sato I, Tsuda S. Detection of in vivo DNA damage induced by ethanol in multiple organs of pregnant mice using the alkaline single cell gel electrophoresis (Comet) assay. J Vet Med Sci 2006;68:41-7.

[11] Jeng W, Wong AW, Ting AKR, Wells PG. Methamphetamine-enhanced embryonic oxidative DNA damage and neurodevelopmental deficits. Free Radical Biol Med 2005;39:317-26.

[12] Abraham J, Balbo S, Crabb D, Brooks PJ. Alcohol metabolism in human cells causes DNA damage and activates the Fanconi anemia-breast cancer susceptibility (FA-BRCA) DNA damage response network. Alcohol Clin Exp Res 2011;35:2113-20.

[13] Koch OR, Pani G, Borrello S, Colavitti R, Cravero A, Farre S, et al. Oxidative stress and antioxidant defenses in ethanol-induced cell injury. Mol Aspects Med 2004;25:191-8.

[14] Wong AW, McCallum GP, Jeng W, Wells PG. Oxoguanine glycosylase 1 protects against methamphetamine-enhanced fetal brain oxidative DNA damage and neurodevelopmental deficits. J Neurosci 2008;28:9047-54.

[15] Rehen SK, McConnell MJ, Kaushal D, Kingsbury MA, Yang AH, Chun J. Chromosomal variation in neurons of the developing and adult mammalian nervous system. Proc Natl Acad Sci U S A 2001;98:13361-6.

[16] Barch MJ, Knutsen, T. & Spurbeck, J. L. The AGT Cytogenetics Laboratory Manual. Philadelphia: Lippincott; 1997.

[17] Blaschke AJ, Staley K, Chun J. Widespread programmed cell death in proliferative and postmitotic regions of the fetal cerebral cortex. Development 1996;122:1165-74.

[18] Blaschke AJ, Weiner JA, Chun J. Programmed cell death is a universal feature of embryonic and postnatal neuroproliferative regions throughout the central nervous system. J Comp Neurol 1998;396:39-50.

[19] Peterson SE, Yang AH, Bushman DM, Westra JW, Yung YC, Barral S, et al. Aneuploid cells are differentially susceptible to caspase-mediated death during embryonic cerebral cortical development. J Neurosci 2012;32:16213-22.

[20] Mani RS, Chinnaiyan AM. Triggers for genomic rearrangements: insights into genomic, cellular and environmental influences. Nat Rev Genet 2010;11:819-29.

[21] Maher P, Schubert D. Signaling by reactive oxygen species in the nervous system. Cell Mol Life Sci 2000;57:1287-305.

[22] Fleckenstein AE, Volz TJ, Riddle EL, Gibb JW, Hanson GR. New insights into the mechanism of action of amphetamines. Annu Rev Pharmacol Toxicol 2007;47:681-98.

[23] Yamamoto BK, Moszczynska A, Gudelsky GA. Amphetamine toxicities: classical and emerging mechanisms. Ann N Y Acad Sci 2010;1187:101-21.

[24] Cadet JL, Brannock C. Free radicals and the pathobiology of brain dopamine systems. Neurochem Int 1998;32:117-31.

[25] Cubells JF, Rayport S, Rajendran G, Sulzer D. Methamphetamine neurotoxicity involves vacuolation of endocytic organelles and dopamine-dependent intracellular oxidative stress. J Neurosci 1994;14:2260-71.

[26] Albano E. Alcohol, oxidative stress and free radical damage. Proc Nutr Soc 2006;65:278-90.

[27] Cohen-Kerem R, Koren G. Antioxidants and fetal protection against ethanol teratogenicity. I. Review of the experimental data and implications to humans. Neurotoxicol Teratol 2003;25:1-9.

[28] Das SK, Vasudevan DM. Alcohol-induced oxidative stress. Life Sci 2007;81:177-87.

[29] Kayani MA, Parry JM. The in vitro genotoxicity of ethanol and acetaldehyde. Toxicol In Vitro 2010;24:56-60.

[30] Wu D, Zhai Q, Shi X. Alcohol-induced oxidative stress and cell responses. J Gastroenterol Hepatol 2006;21 Suppl 3:S26-9.

[31] Cardozo-Pelaez F, Brooks PJ, Stedeford T, Song S, Sanchez-Ramos J. DNA damage, repair, and antioxidant systems in brain regions: a correlative study. Free Radical Biol Med 2000;28:779-85.

[32] Chun J, Schatz DG. Rearranging views on neurogenesis: neuronal death in the absence of DNA end-joining proteins. Neuron 1999;22:7-10.

[33] Gu Y, Sekiguchi J, Gao Y, Dikkes P, Frank K, Ferguson D, et al. Defective embryonic neurogenesis in Ku-deficient but not DNA-dependent protein kinase catalytic subunit-deficient mice. Proc Natl Acad Sci U S A 2000;97:2668-73.

[34] Obe G, Pfeiffer P, Savage JR, Johannes C, Goedecke W, Jeppesen P, et al. Chromosomal aberrations: formation, identification and distribution. Mutat Res 2002;504:17-36.

[35] Benassi-Evans B, Fenech M. Chronic alcohol exposure induces genome damage measured using the cytokinesis-block micronucleus cytome assay and aneuploidy in human B lymphoblastoid cell lines. Mutagenesis 2011;26:421-9.

[36] Cooke MS, Evans MD, Dizdaroglu M, Lunec J. Oxidative DNA damage: mechanisms, mutation, and disease. FASEB J 2003;17:1195-214.

[37] D'Angiolella V, Santarpia C, Grieco D. Oxidative stress overrides the spindle checkpoint. Cell Cycle 2007;6:576-9.

[38] Degtyareva NP, Chen L, Mieczkowski P, Petes TD, Doetsch PW. Chronic oxidative DNA damage due to DNA repair defects causes chromosomal instability in Saccharomyces cerevisiae. Mol Cell Biol 2008;28:5432-45.

[39] Samper E, Nicholls DG, Melov S. Mitochondrial oxidative stress causes chromosomal instability of mouse embryonic fibroblasts. Aging Cell 2003;2:277-85.

[40] Chae S, Yun C, Um H, Lee JH, Cho H. Centrosome amplification and multinuclear phenotypes are Induced by hydrogen peroxide. Exp Mol Med 2005;37:482-7.

[41] Thompson SL, Compton DA. Chromosome missegregation in human cells arises through specific types of kinetochore-microtubule attachment errors. Proc Natl Acad Sci U S A 2011;108:17974-8.

[42] Huang Y, Jiang L, Yi Q, Lv L, Wang Z, Zhao X, et al. Lagging chromosomes entrapped in micronuclei are not 'lost' by cells. Cell Res 2012;22:932-5.

[43] Thomaidou D, Mione MC, Cavanagh JF, Parnavelas JG. Apoptosis and its relation to the cell cycle in the developing cerebral cortex. J Neurosci 1997;17:1075-85.

[44] Dunty WC, Jr., Chen SY, Zucker RM, Dehart DB, Sulik KK. Selective vulnerability of embryonic cell populations to ethanol-induced apoptosis: implications for alcohol-related birth defects and neurodevelopmental disorder. Alcohol Clin Exp Res 2001;25:1523-35.

[45] Kingsbury MA, Friedman B, McConnell MJ, Rehen SK, Yang AH, Kaushal D, et al. Aneuploid neurons are functionally active and integrated into brain circuitry. Proc Natl Acad Sci U S A 2005;102:6143-7.